2013

Scanning Probe Investigations of the Surface Self-Assembly of Organothiols and Organosilanes Using Nanoscale Lithography

Tian Tian
Louisiana State University and Agricultural and Mechanical College, ttian2@lsu.edu

SCANNING PROBE INVESTIGATIONS OF THE SURFACE SELF-ASSEMBLY OF ORGANOTHIOLS AND ORGANOSILANES USING NANOSCALE LITHOGRAPHY

A Dissertation

Submitted to the Graduate Faculty of the
Louisiana State University and
Agricultural and Mechanical College
in partial fulfillment of the
requirements for the degree of
Doctor of Philosophy

in

The Department of Chemistry

by
Tian Tian
B.S., Peking University, 2003
M.S., Southeastern Louisiana University, 2009
May 2013

I would like to dedicate this work to my parents, Youlong Qi and Mei Wang; and to my husband Peng Zhao for their undying patience and support.

ACKNOWLEDGEMENTS

I would like to thank my research advisor, Dr. Jayne Garno for giving me the chance to be in her group. All of her help, support and guidance towards experimental, written and communication skills through my graduate career will be appreciated forever. I am grateful to Dr. Kermit Murray, Dr. Donghui Zhang, Dr. Juana Moreno and Dr. Ram Devireddy for serving on my committee. I would like to extend my gratitude to Dr. Kimberly Briggman and Dr. Daniel Stark at National Institute of Standard and Technology (NIST) for the internship, as well as former and current students in Garno research group for helpful discussions. My sincere gratitude goes to my student mentor, Dr. Zorabel Lejeune and my partner, Lauren Englade-Franklin for all the support, assistance and company inside and outside the laboratories. My special thanks goes to my friend Daisy Miller for all the fun and challenges that helped me accomplish my graduate studies within 4 years.

TABLE OF CONTENTS

LIST OF TABLES

LIST OF FIGURES

LIST OF ABBREVIATIONS

Abbreviation	Name
AFM	atomic force microscopy
APDES	aminopropyldiethoxysilane
bps	base pairs
BSA	bovine serum albumin
CAM	computer-assisted manufacturing
C10	decanethiol
C12	dodecanethiol
C18	octadecanethiol
C8DMS	octyldimethylmonochlorosilane
CMPS	chloromethylphenyltrichlorosilane
CP-AFM	conductive probe microscopy
DMS	octadecyldimethylmonochlorosilane
DNA	deoxyribonucleic acid
DPN	dip-pen nanolithography
DPP	5,10-diphenyl-15,20-di-pyridin-4-yl-porphyrin
dsDNA	double-stranded DNA
EDC	1-ethyl-3-(3-dimethylaminopropyl) carbodiimide hydrochloride
EG	ethylene glycol
GIXD	grazing incidence X-ray diffraction
HOPG	highly oriented pyrolytic graphite
IgG	immunoglobulin G
ITO	Indium doped tin oxide
LFM	lateral force microscopy
MAC	magnetic AC
MBP	maltose binding protein
MCH	6-mercaptohexan-1-ol
MFM	magnetic force microscopy
16-MHA	16-mercaptohexadecanoic acid
MHP	*n*-(6-mercapto hexyl) pyridinium bromide
MPA	3-mercaptopropionic acid
MSM	magnetic sample microscopy
11-MUA	11-mercaptoundecanoic acid
11-MUD	11-mercaptoundecanol
MWCNT	multi-wall carbon nanotube
NEXAFS	near-edge X-ray absorption fine structure spectroscopy
NHS	N-hydroxysuccinimide
NPRW	nanopen reader and writer

ODT	octadecanethiol
OTS	octadecyltrichlorosilane
PSD	position sensitive photodetector
SAMs	self-assembled monolayers
SFM	scanning force microscopy
SpA	staphylococcal protein A
SPL	scanning probe lithography
SPM	scanning probe microscopy
ssDNA	single-stranded DNA
STM	scanning tunneling microscopy
SWCNT	single-wall carbon nanotube
TMMH	1,1,1-tris(mercaptomethyl)heptadecane

ABSTRACT

Particle lithography and scanning probe lithography were applied to study the kinetics and mechanisms of surface self-assembly processes. Organothiols on Au(111) and organosilane on Si(111) were chosen as model systems for investigations at the nanoscale using atomic force microscopy (AFM). Fundamental insight of structure/property interrelationships and understanding the properties of novel materials are critical for developments with molecular devices.

Methods using an AFM probe for nanofabrication have been applied successfully to prepare sophisticated molecular architectures with high reproducibility and spatial precision. The established capabilities of AFM-based nanografting were reviewed for inscribing patterns of diverse composition, to generate complicated surface designs with well-defined chemistries. Nanografting provides a versatile tool for generating nanostructures of organic and biological molecules, as well as nanoparticles. Protocols of nanografting are accomplished in liquid media, providing a mechanism for introducing new reagents for successive *in situ* steps for 3-D fabrication of designed nanopatterns. Because so many chemical reactions can be accomplished in solution, there are rich possibilities for chemists to design studies of other surface reactions.

Surface assembly and self-polymerization of chloromethylphenyltrichlorosilane (CMPS) were investigated using test platforms of organosilanes fabricated with particle lithography. A thin film of octadecyltrichlorosilane (OTS) with well-defined nanopores was prepared on Si(111) to spatially confine the surface assembly of CMPS within nanopores of OTS. Time-dependent changes during the self-polymerization of CMPS were visualized *ex situ* using AFM. Molecular-level details of CMPS nanostructures were obtained from high resolution AFM images to track

the growth of organosilanes on Si(111). Measurements of the heights and diameters of CMPS nanostructures provided quantitative information of the kinetics of CMPS self-polymerization.

Scanning probe-based methods of nanolithography were applied to investigate the self-assembly of a tridentate organothiol, 1,1,1-tris(mercaptomethyl)heptadecane (TMMH). Multidentate adsorbates can address problems with long-term stability to oxidation observed with monothiolated *n*-alkylthiols. Multidentate thiol ligands demonstrate improved resistance to oxidation, thermal desorption and UV exposure. Progressive changes in surface morphology for TMMH assembly onto Au(111) was studied *in situ* with time-lapse AFM, monitoring changes in surface coverage at different time intervals. Nanoshaving and nanografting were used as molecular rulers to evaluate the thickness of films of TMMH.

CHAPTER 1. INTRODUCTION

The capability to investigate surface reactions and properties of materials at the nanoscale using scanning probe microscopy (SPM) offers rich opportunities for scientific research and discovery. Self-assembled monolayers (SAMs) of organothiols and organosilanes have become important building blocks for nanofabrication and provide excellent test platforms for surface studies. In basic science, questions can be addressed regarding topics such as how molecules arrange and interact with surfaces. The objectives of this dissertation were to achieve new fundamental insight about self-assembly processes on surfaces and to obtain useful information regarding chemical kinetics and mechanisms at the molecular level.

The experiments described in this dissertation applied nanolithography and SPM-based surface fabrication with SAMs combined with nontraditional approaches for surface characterizations at the nanoscale. There were several main goals for the research. First, test platforms of organothiol and organosilane were fabricated using nanolithography methods to provide well-defined test platforms for studies of surface reactions. Second, molecules of interest were investigated using the designed test platforms and the process of surface assembly was monitored by time-lapse AFM. Third, high resolution AFM images enabled measurements and analysis of the target molecules and provided insight at the molecular level for studies of surface reactions. A critical subject for the field of supramolecular chemistry is the study of intermolecular interactions and molecular self-assembly. Experiments were designed to acquire structural, functional and spectral information of designed organothiol films (e.g., adsorbates with multiple surface binding moieties) and supramolecular structures constructed from surface templates of nanopatterned thin films.

Numerous methods of nanoscale lithography have been developed to fabricate test platforms for investigations of chemical and biochemical surface reactions.[1-3] The scope of this dissertation encompasses studies with selected organothiols and organosilanes that were patterned using approaches with scanning probe-based nanolithography and particle lithography. Among the patterning techniques with organic thin films, particle lithography provides unprecedented capabilities for high throughput patterning, and scanning probe lithography (SPL) offers exquisite resolution. A detailed description and comparison of particle lithography and SPL approaches used in this dissertation is provided in Chapter 2. Approaches for surface characterization using atomic force microscopy imaging modes used for the experiments of this dissertation are reviewed and described in Chapter 2. Test platforms of organosilanes and organothiols prepared using nanolithography tools of particle lithography and scanning probe lithography were used as model surfaces for studies of surface self-assembly reactions.

A contemporary review of nanografting is provided in Chapter 3, a technique that is also used to study multidentate adsorbates in Chapter 5. Nanografting is a scanning probe-based technique which uses localized tip-surface contact to rapidly and reproducibly inscribe arrays of nanopatterns of thiol SAMs and other nanomaterials with nanometer-scale resolution. Scanning probe-based approaches for lithography such as nanografting with SAMs extend beyond simple fabrication of nanostructures to enable nanoscale control of the surface composition and chemical reactivity from the bottom-up. Commercial scanning probe instruments typically provide software to control the length, direction, speed and applied force of the scanning motion of a tip, analogous to a pen-plotter. Nanografting is accomplished by force-induced displacement of molecules of a matrix SAM, followed immediately by the surface self-assembly of *n*-alkanethiol *ink* molecules from solution. Desired surface chemistries can be patterned by

choosing SAMs of different lengths and terminal groups. By combining nanografting and designed spatial selectivity of *n* alkanethiols, *in situ* AFM protocols provide new capabilities for studies of nanoscale surface reactions with proteins, nanoparticles or chemical assembly. Methods to precisely arrange molecules on surfaces will contribute to development of molecular device architectures for future nanotechnologies.

A new approach for studying surface self-assembly reaction using test platforms of organosilanes nanostructures fabricated with particle lithography is described in Chapter 4. The self-polymerization of chloromethylphenyltrichlorosilane (CMPS) was chosen for studies because benzyl halide surfaces are ideal for nucleophilic substitution reactions. Particle lithography is a practical and highly reproducible method for nanoscale fabrication. Well-defined nanopores within a thin film of octadecyltrichlorosilane (OTS) was prepared to form a surface layer on Si(111). For these experiments, the surface assembly of CMPS was spatially confined within nanofabricated pores of OTS. Molecular-level details and growth of the nanostructures after steps of self-polymerization were obtained by high resolution AFM. The nanodots patterns of CMPS produced within bare areas of the surface formed pillars with different heights and diameters. Analysis of AFM images after progressive chemical exposure provided quantitative information for studying the kinetics and mechanisms of the surface reaction. The heights of CMPS nanostructures indicate multilayers have spontaneously formed by self-polymerization, with taller columns produced by longer immersion times. The diameter of the CMPS nanostructures corresponds to the initial sizes of the confined areas of Si(111). These investigations demonstrate intriguing new capabilities as a generic approach for nanoscale studies with ever more complex molecular architectures.

The self-assembly of multidentate organothiols onto Au(111) was studied using time-lapse AFM in Chapter 5. The way in which an adsorbate is bound to the surface, either through single or multiple thiolate attachments, or an alternative bonding mechanism, can impact the characteristics of the overlying thin film and its performance in coatings and/or nanoscale devices. Chemisorptive surface linkages of thiol SAMs are subject to damage from UV exposure, thermal desorption, and oxidation. The thickness, surface density, length of the alkyl chain, and composition of the surface films influence the rate of UV-induced damage of the coatings.[4] Multidentate thiols are shown to dramatically improve the etch selectivity and resist qualities of surface films. In comparison to SAMs derived from simple *n*-alkanethiols, studies with multidentate thiolated adsorbates have shown that films derived from multidentate thiol adsorbates benefit from the entropy-driven chelate effect, exhibiting improvements in thermal stability both in air and in the presence of a contacting solvent. In Chapter 5, progressive changes in surface coverage were disclosed as time progressed with time-lapse imaging of 1,1,1-tris(mercaptomethyl)heptadecane (TMMH). For regular *n*-alkanethiols, densely-packed monolayers typically are formed from dilute solutions within an hour or less; however, SAMs of bulkier multidentate thiols were found to assemble more slowly. A clean gold substrate was first imaged in ethanolic media. Next, a solution of multidentate thiol was injected into the liquid cell. As time progressed, molecular-level details of the surface changes at different time intervals were revealed by high resolution SPM images. Nanoshaving and nanografting protocols were used to investigate the orientation of adsorbed molecules. Since the dimensions of *n*-alkanethiols have been well-studied, the thickness of the multidentate thiol film was evaluated by referencing the known heights of *n*-alkanethiols as an *in situ* molecular ruler. Multidentate adsorbates attach to gold surfaces through multiple linkers which should provide greater stability and shelf-life for

prepared films as compared to monothiolated SAMs. Multidentate molecules provide a model surface that resists self-exchange and surface migration, to enable further steps of chemical reactions with high fidelity.

A summary and future prospectus of this research direction is provided in Chapter 6 of the dissertation. One may anticipate that controlling the selectivity and dimensions of surface sites for subsequently assembling supramolecular structures will provide information to elucidate mechanistic roles of intermolecular forces such as hydrogen bonding, van der Waals interactions, solvent effects as well as sulfur-metal chemisorption. From an applications perspective, generating interfaces of well-defined structure and composition are critical for emerging nanotechnologies based on molecularly thin organic films. To realize the full potential of patterning surfaces for iterative manufacturing processes to produce chemical, supramolecular, and biomolecular nanostructures on surfaces, challenges need to be addressed for designing surface coatings that resist damage and maximize edge resolution and patterning reproducibility. As an integral component of these investigations, new nanoscale protocols were developed with cutting-edge scientific instrumentation to achieve fundamental information of designed molecules.

CHAPTER 2. EXPERIMENTAL APPROACH: IMAGING PRINCIPLES AND MODES OF SCANNING PROBE MICROSCOPY (SPM)

2.1 Background and History of Atomic Force Microscopy

Scanning probe microscopy (SPM) represents a family of imaging and measurement techniques that provide unprecedented resolution for molecular level studies. Unlike optical microscopes, SPM measurements use a probe to "feel" and "view" the surface to provide molecular details of parameters such as topography, frictional forces, tip-sample adhesion, elastic properties and conductance. Therefore, the resolution of SPM is not limited by the wavelength of light. True atomic imaging has been achieved with SPM, providing real space images of the lattice arrangement, atomic vacancies and adatoms.[5, 6]

The first mode of SPM that was introduced is scanning tunneling microscopy (STM) invented in 1981 by Binnig and Rohrer.[7] The invention of STM earned the Nobel Prize in physics in 1986. The imaging principle of STM is based on electrons tunneling between the probe and sample over a short distance, less than one nanometer. Using STM, the electronic structure of surfaces can be viewed with atomic resolution for conductive or semi-conductive surfaces. The atomic force microscope (AFM) was invented in 1986 by Binnig, Quate and Gerber, which can be used for measurements with insulating surfaces.[8] The operating principle of AFM is based on atomic forces (e.g. attractive, repulsive) between the tip and sample, thus AFM is also commonly referred to as scanning force microscopy (SFM).

Over the past 27 years, AFM has been applied for fundamental studies of surface properties, chemical structures, and nanoscale patterning. Materials that have been studied by AFM include self-assembled monolayers (SAMs),[9] polymers,[10] metals,[11] nanoparticles,[12] quantum dots[13] and biological samples.[14] As a characterization tool, AFM has also been widely

used in applied research such as medical devices,[15, 16] molecular electronics[17, 18] and drug delivery.[19]

Table 2.1 Summary of several common modes of SPM imaging.

SPM imaging mode	Mode	What is measured	Type of tip	Feedback	Description	Ref.
Contact mode	contact	topography	Si/Si_3N_4	changes in tip deflection	the tip remains in contact with the surface	8
Force modulation AFM	contact	elasticity	Si/Si_3N_4	changes in tip deflection	measures the attractive/repulsive force of the tip	20
Lateral force microscopy (LFM)	contact	frictional forces	Si/Si_3N_4	changes in tip deflection	measures the torsion and twist of the tip	20
Tapping mode	intermittent contact	topography	Si/Si_3N_4	amplitude changes of tip oscillation	tip oscillates and periodically touches the surface	21
Magnetic AC mode (MAC)	intermittent contact	topography	magnetically coated cantilever	amplitude changes of tip oscillation	tip is driven by magnetic field	22
Non-contact mode	non-contact	topography	Si/Si_3N_4	changes in tip deflection	tip keeps a distance with the surface	23
Magnetic force microscopy (MFM)	interleave	magnetic dipoles	magnetically coated tip	changes in tip deflection	two pass technique where tip is lifted on 2^{nd} pass	24
Conductive probe AFM (CP-AFM)	contact	topography, conductivity	conductive tip	changes in tip deflection	a voltage is applied between tip and sample	25
Electrostatic force AFM	contact	electrostatic force	conductive tip	changes in tip deflection	a voltage is applied between tip and sample	26
Kelvin probe AFM	non-contact	electronic state	conductive tip	scan the surface at a constant height	tip scans at a constant height	27
Magnetic sample modulation (MSM)	contact	topography, vibrational response to magnetic field	Si/Si_3N_4 non-magnetic tip	changes in tip deflection	AC magnetic field drives sample actuation	28

Experiments with AFM can be accomplished in air, in liquid or in vacuum, for either conductive or insulating surfaces.[29] Samples do not require pretreatment, metal stains or coatings for AFM studies, however, the surface should be sufficiently flat to enable imaging at the scale of nanometers. Based on the nature of the samples and forces to be measured, a number of

operating modes have been introduced. Information such as elasticity, adhesion, sample conductance, magnetic forces and electronic properties can be acquired depending on the modes. A summary of AFM modes and brief description is presented in Table 2.1. The AFM imaging modes used primarily for investigations of this dissertation are contact mode, tapping-mode and SPM-based nanofabrication.

2.2 Basic Operating Principle of Contact Mode AFM

Various forces between the AFM probe and the surface can be measured with AFM.[8] The interactions between the tip and sample are detected and mapped point-by-point to form digital images. Surface morphology can be characterized at a scale from microns down to angstroms.

To acquire AFM images with the most commonly used deflection configuration, a laser beam is focused onto the back of a reflective cantilever and deflected to a position sensitive photodetector (PSD), as shown in Figure 2.1. The attractive or repulsive forces between the tip and different surfaces will cause the cantilever to bend, thus the position of the reflected laser beam on the PSD will change accordingly. This change will be compensated to maintain a user assigned setpoint by applying a voltage to the piezo scanner to adjust the position of the tip. The voltage changes are monitored in real time as the tip is raster scanned across the surface and translated into pixels to form a digital image. A true three-dimensional surface topography image can be generated with AFM. Other information such as lateral force and phase images can be obtained simultaneously in different channels with the topography images.

Tips for AFM, as shown in Figure 2.1, are commonly made of silicon or silicon nitride (Si_3N_4), and may be coated with magnetic or conductive metals for different operating modes. Tips can also be made of metals[30] or carbon nanotubes[31] to meet the needs of specific protocols. The apex of the tip is usually cone-shaped, with a diameter of 10-50 nm. Depending on the

sharpness of the tip, molecular resolution can be achieved with 0.1 nm in lateral dimension and 0.01 nm vertically for contact mode AFM. The tip is attached to the free end of a rectangular cantilever and which is affixed to the piezoceramic scanner. The cantilevers typically are either rectangular or V-shaped, with a reflective coating on the back. The movement of the cantilever is controlled by a piezoceramic scanner. Voltages can be applied to the piezoceramic scanner to precisely control the position of the cantilever in x, y and z directions.

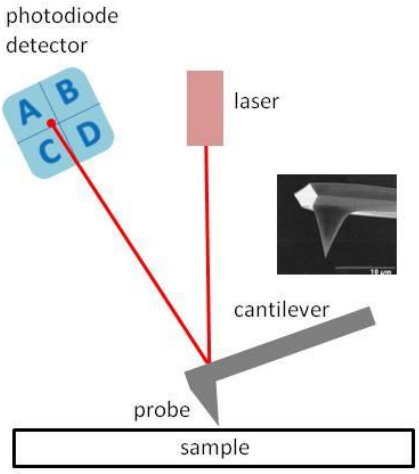

Figure 2.1 Basic operating principle of contact mode AFM.

Contact mode was the first imaging mode demonstrated for AFM.[8] Surface topography, deflection and lateral force images can be obtained simultaneously in different channels. An example is shown in Figure 2.2 for contact-mode images of a gold thin film deposited on a mica substrate. The topography frame (Figure 2.2A) is a map of heights of the surface, where brighter colors represent taller structures and correspondingly darker color indicates shorter features. The deflection image shows the raw data in volts that compensates for the changes of laser position controlled with the feedback loop, an example is shown in Figure 2.2B. Deflection images are particularly sensitive to revealing the edges of surface features but do not correlate with a physical property. The lateral force image (Figure 2.2C) provides useful information for

identifying difference in surface chemistry as well as edges of defined domains.[32] By subtracting left and right traces of lateral force images, measurements of frictional forces can be acquired.

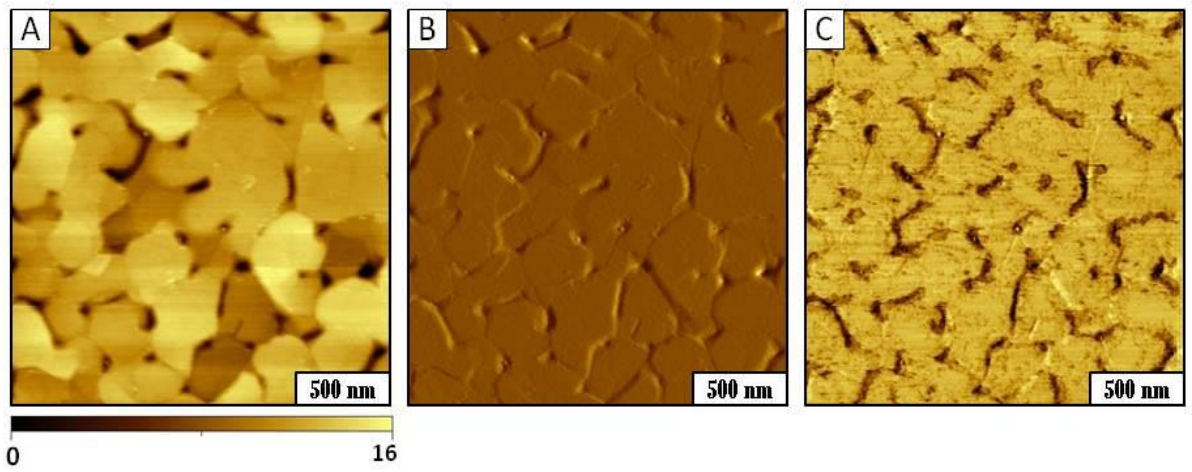

Figure 2.2 Examples of contact mode AFM images of a gold thin film formed on mica, acquired in ambient air. [A] Topography; [B] deflection; [C] lateral force frame.

Hysteresis refers to the directional difference between trace and retrace images due to the asymmetry of the AFM probe. As the tip scans the surface in a raster pattern, the "fast direction" refers to horizontal line scans and the "slow direction" refers to vertical motion between the line scans. The horizontal scans are sorted by directions to form trace (left to right) and retrace (right to left) images. In the absence of hysteresis, molecular friction measurements can be obtained by subtracting trace and retrace images.

As the tip is raster scanned across the surface, the interaction between tip and sample causes the cantilever to bend. Vertical changes resulting from the height differences of the surface structures will be processed to form topography images. Accordingly, horizontal changes from the torsion and twist of the tip will be converted to lateral force images. Voltages applied through the feedback loop to compensate both vertical and horizontal changes are referred to as "error signals" and are used to generate images.

There are two types of positional feedback mechanisms for contact mode: constant force and constant height. For constant force mode, the force between the tip and sample is held constant at a user assigned value. A voltage is applied through the feedback loop to maintain the deflection of the tip at a constant value. The main function of the feedback loop is to adjust the deflection of the tip according to the change between the initial force setpoint and the detected force. For constant height mode, the distance between the tip and sample is held constant and the force changes will be sensed. Constant height mode is not widely used because it requires the surface to be ultraflat at the scale of angstroms.

With time-lapse AFM, surface reactions can be monitored in real time by comparing the height difference in topography images before and after surface reactions. Lateral force images provide useful maps of local chemical differences of the surface, as the twisting of the tip over different terminal groups can be distinguished with high sensitivity.

2.3 Tapping-mode AFM

The AFM tip can be operated in contact, intermittent contact and non-contact configurations. In contact mode, the tip remains in continuous contact with the surface under a small pressure or setpoint force. Intermittent-contact mode, also referred to as tapping mode, describes a configuration where the tip oscillates and rapidly taps the surface. For non-contact mode, the tip is scanned over the surface at a certain distance and does not touch the sample. For conventional non-contact mode, Van der Waals' forces between the tip and sample can be detected and experiments are usually accomplished in vacuum.[33] Non-contact mode is also used for measurements of magnetic and electrostatic forces.[34]

A potential drawback of contact mode AFM is that the dragging force may damage or alter soft samples such as proteins or DNA. Tapping-mode was invented to reduce the shearing

forces between the AFM probe and the sample.[21] For tapping-mode, the cantilever is driven to oscillate and intermittently touch the surface instead of remaining in contact with the surface. Tapping-mode effectively eliminates frictional force and reduces the damage. Also the tip is drive to oscillate at high frequency. Information such as topography and phase images can be obtained concurrently with tapping-mode. Example images acquired with tapping-mode AFM in air are shown in Figure 2.3.

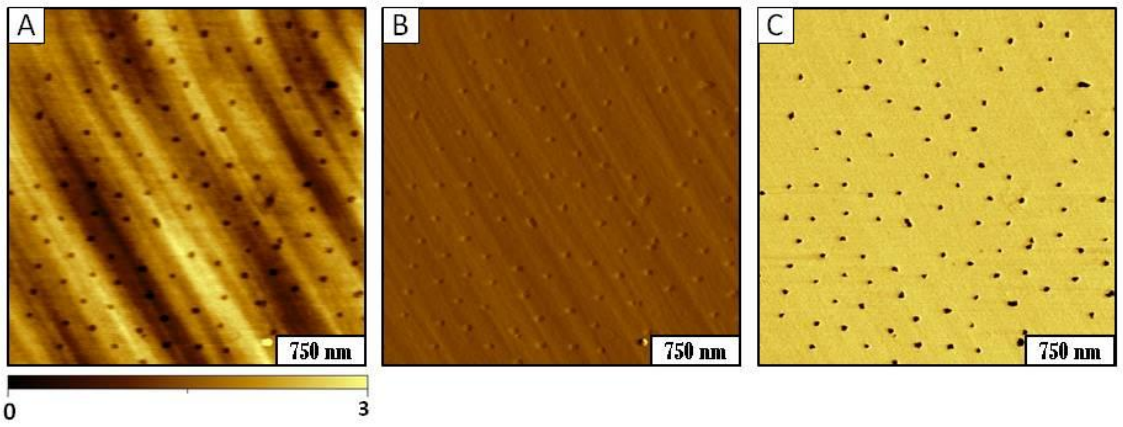

Figure 2.3 Tapping-mode images of nanoholes within a thin film of OTS on Si(111). [A] Topography; [B] amplitude, and [C] phase frames that were simultaneously acquired.

The feedback mechanism of tapping mode that is used for driving the tip position is quite different than that used for contact mode. As the tip oscillates, a voltage is applied to maintain constant amplitude through the feedback loop. The error signals resulting from the difference between amplitude setpoint and the detected value will be reconstructed to form an image. The phase image is obtained from the phase lag between the wave function of input AC and actual detected output of cantilever oscillation. Therefore, phase images provide sensitive maps of surface chemistry. Tapping mode has been widely used for AFM studies, especially soft samples. Table 2.2 provides examples of surfaces that have been characterized using tapping-mode AFM.

Table 2.2 Example samples characterized with tapping-mode AFM.

Sample	Substrate	Ref.
holoferritin	highly oriented pyrolytic graphite (HOPG)	[35]
ω-amine alkanethiols	gold	[36]
single-walled carbon nanotubes (SWCNTs)	gold	[37]
fetal bovine serum proteins	hard inorganic diamond substrates	[38]
lysozyme	alkanethiol SAMs on gold	[39]
tungsten oxide nanoparticles	mica and graphite	[40]
PtZn Nanoparticles	glassy carbon	[41]
Ag nanoparticles	Nb-doped conductive rutile TiO(100) single crystal	[42]
Au nanoparticles	Silicon	[43]
polyaniline (PAni)	silica, indium doped tin oxide (ITO)	[44]
silica nanoparticles	silicon	[45]
iron oxide (Fe_2O_3) nanoparticles	silicon	[46]
Au–Ag bimetallic layers	glass	[47]
Au/Pt/Pd	germanium	[48]
Zn	gold-coated quartz crystal	[49]
Guanosine (G)	mica	[50]
DNA wrapped multiwall carbon nanotube (MWCNTs)	HOPG	[51]
Hybrid nanostructure of polyamidoamine dendrimers and oligonucleotides	mica	[52]
DNA	Rutile(001) and *beta*-gallia rutile (BGR)	[53]

2.4 Chemistry of Self-Assembled Monolayers

Self-assembled monolayers (SAMs) are organized assemblies of molecules that formed on surfaces by spontaneous adsorption. In this dissertation, both organothiols and organosilanes were used for studies. A range of applications require SAMs, including surface modification,[54] fabrication of molecular devices,[55] biosensing,[56] lubrication,[57] and corrosion inhibition.[58] The properties of surfaces such as structure, adhesion, acidity and wetting can be exquisitely controlled by designs of the backbone, linker and terminal groups of SAMs.[61-63] The thickness of films can be tuned by choosing different chain lengths of SAMs.

2.4.1 Characteristics of Organothiol SAMs

The structure and surface arrangements of SAMs of *n*-alkanethiols have been studied and reviewed previously.[59-61] Well-ordered SAMs of alkanethiols are easy to prepare with high reproducibility by immersing gold substrates into dilute thiol solutions (typically 0.1 - 1.0 mM). Close-packed SAMs of *n*-alkanethiols form a commensurate ($\sqrt{3}x\sqrt{3}$)R30° lattice on Au(111) surface with a tilted chain oriented approximately 30° from surface normal, as shown representatively in Figure 2.4. The anchoring groups, sulfur atoms are considered to bind at the triple hollow sites of gold atoms, and both sulfur and gold atoms are hexagonally close-packed.

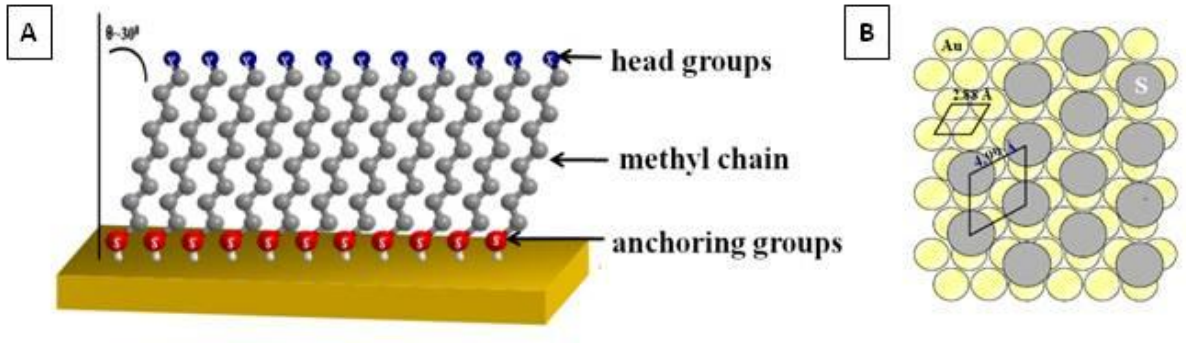

Figure 2.4 Model of *n*-alkanethiols SAMs. [A] Side-view; [B] top-view of the commensurate surface structure formed on Au(111).

Studies of the kinetics of the self-assembly of *n*-alkanethiols SAMs on gold from solution have been reported previously.[62] At first, alkanethiol molecules assemble on a gold surface with a parallel orientation in a "lying-down" configuration. As time proceeds, the molecules rearrange to "stand up" to form a dense monolayer with the backbone tilted 30° from surface normal. Natural defects can be observed from high resolution AFM and STM images of *n*-alkanethiols SAMs, such as domain boundaries, etch pits, pinholes, missing atoms, dislocations and gold steps, provided atomic resolution has been achieved.[63] The height of gold steps is 0.25 nm, which can be used for instrument z calibration.

Well-ordered structures of *n*-alkanethiol SAMs provide controllable surface chemistry with diverse functionality of terminal groups such as alkyls, hydroxyl, carboxyl, amides, esters, etc. Headgroups that provide active sites for protein binding can be selected according to requirements for binding specific protein molecules for biosensing applications, whereas the surrounding matrix SAMs provide a resist to minimize nonspecific adsorption. Nanografting is the primary AFM-based fabrication method used with alkanethiol SAMs in this dissertation, which will be described in detail in Chapter 3.

2.4.2 Thin Films of Organosilanes

The self-assembly process of organosilane SAMs is more complicated than for *n*-alkanethiol SAMs. Silane molecules consist of a silicon tetrahedron bond and can bind to the surfaces (such as silicon oxide, mica, glass, etc.) as well as adjacent molecules through Si-O covalent bonds. Ideally, *n*-alkylsilane can form a monolayer with the backbones almost perpendicular to surface normal, as shown in Figure 2.5. However, self-polymerization occurs and multilayers are often formed with reactive head groups. The quality of the films of organosilane SAMs depends on parameters such as the amount of water, the type of alkylsilane molecules, temperature, solvent, substrate and reaction time. Therefore, careful control of the reaction conditions is needed for reproducibility.

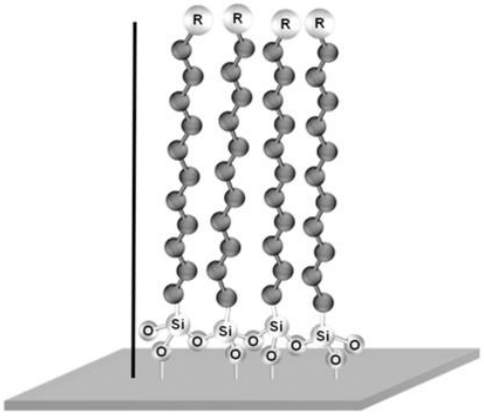

Figure 2.5 Idealized model of the structure of *n*-alkylsilane SAMs.

The nanostructure of organosilane reflects local interactions of silanol groups, substrates and trace amount of water. Since discovered by Sagiv[64] in 1980 that nanoscopic water is needed to initiate the surface assembly reaction for octadecyltrichlorosilane (OTS), the mechanism of the self-assembly process of tricholorosilane is still under investigation. Due to the nature of covalent bonds between silane and substrates, particle lithography has been widely used to generate nanostructures of organosilanes, such as rings, pores and dots.[65] Nanoshaving has also been applied to shave SAMs of octadecyldimethylmonochlorosilane (C_{18} DMS)[66] and 1-alkenes[67] on silicon substrates.

2.5 Nanofabrication Techniques: Nanografting and Particle Lithography

Lithography methods that can regulate the distribution of functional groups on surfaces have potential applications towards nanoscience and nanotechnology.[68] Evaluations of lithography methods at the nanoscale include resolution, reliability, reproducibility, throughput, cost, speed and ease of operation. A comparison of the two methods used in this dissertation is shown in Table 2.3.

Table 2.3 Comparison of SPL and particle lithography.

	SPL	**Particle Lithgraphy**
Resolution achievable	0.1 nm	100 nm
Throughput	Low, patterns are written individually in serial process	High, billions of patterns are generated simultaneously
Speed	minutes	a few hours
Ease of protocols	An SPM tip is used to inscribe patterns	Conventional bench chemistry (mixing, rinsing, drying)
Geometry of patterns	exquisitely controlled	Pores, rings, dots

An SPM tip is used as the tool for fabrication with SPL. The tip is analogous to a pen for writing nanopatterns, whereas the surface is serves as a piece of "paper" for SPL. A key

advantage of SPL is that the shape, size, spacing and arrangement of the patterns can be exquisitely controlled through computer automation.

Particle lithography has also been referred to as nanosphere lithography[69, 70] and colloidal lithography.[71, 72] Particle lithography was originally developed in 1982 by Deckman and Dunsmuir.[73] For particle lithography, mesospheres are used as a template to direct the self-assembly of nanomaterials such as SAMs,[74] polymers,[75] metals[76] and inorganic materials.[77] The close-packed arrangement of mesospheres provides a well-ordered mask to guide the adsorption of various materials. The center-to-center spacing between the patterns corresponds to the diameter of the particles used. A key advantage of particle lithography is high throughput, billions of nanostructures can be fabricated simultaneously within a few hours.

2.6 Experimental Design: Molecular-level Studies of Chemical Reactions with AFM

Test platforms of organothiol and organosilane SAMs can be fabricated for fundamental studies of surface assembly and surface reactions using SPL and particle lithography.[78, 79] Time-lapse AFM enabled surface reactions to be monitored at the molecular level. High resolution images provide valuable information for understanding the kinetics and mechanisms of molecular self-assembly processes on surfaces.[80, 81]

Particle lithography combined with immersion was applied to fabricate nanopores within a thin film of octadecyltrichlorosilane (OTS).[82, 83] The nanopatterns offer spatial confinement for the deposition of other trichlorosilane molecules because the methyl terminal group of OTS provides an effective resist. The second silane molecules grow selectively inside the nanopores and self-polymerize to form taller and wider nanostructures over time.

Nanografting, an SPL method, was used to study the surface self-assembly of organothiol SAMs on gold.[84] Methyl-terminated *n*-alkanethiols were used as matrix to furnish a molecular

ruler for determining the height and orientation of the multidentate organothiol adsorbates. The multidentate SAMs can address the stability issues of monothiol SAMs such as oxidation and desorption from UV exposure and high temperature. Therefore, multidentate adsorbates provide a more robust thin film through multiple surface-binding linkers.

Nanografting experiments were accomplished in liquid media using a liquid cell, as shown in Figure 2.5. A gasket between the sample plate and liquid cell prevents leaking. The liquid environment enabled *in situ* investigations of surface reactions; new reactants can be introduced through plastic tubing connected to the liquid cell. The solvent is replenished during the experiment as it evaporates. Improved resolution of AFM liquid imaging can be achieved due to greatly reduced or eliminated capillary force between the tip and sample.[85] Less imaging force ($\leq$ 1 nN) can be applied in liquid environments compared to regular force of 1 to 10 nN when imaging in air. Liquid imaging was used in kinetics studies of multidentate thiols in Chapter 5.

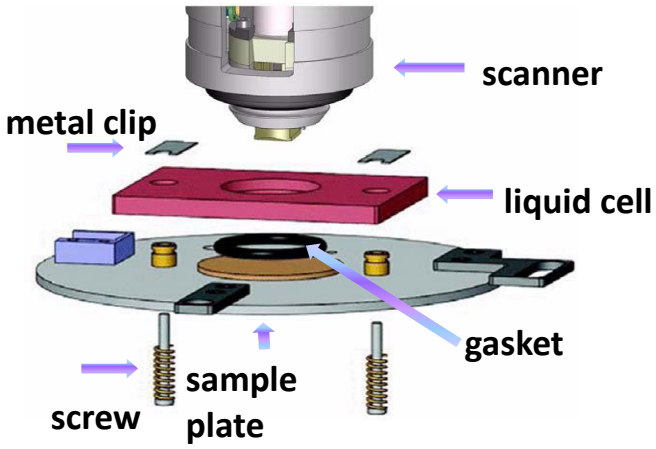

Figure 2.6 Components of the liquid cell used for nanografting experiments and AFM imaging.

CHAPTER 3. NANOGRAFTING: A METHOD FOR BOTTOM-UP FABRICATION OF DESIGNED NANOSTRUCTURES[84]

3.1 Introduction

Scanning probe lithography (SPL) enables bottom-up fabrication of nanostructures on surfaces for producing features with nanoscale dimensions. Methods using the probe of an atomic force microscope (AFM) have been used to fabricate sophisticated architectures at the molecular level with high spatial precision. A number of AFM-based approaches for SPL have been developed such as nanoshaving,[86-90] nanografting,[79, 91-93] dip-pen nanolithography (DPN),[17, 94] NanoPen Reader and Writer (NPRW), [95-97] catalytic probe lithography,[98-100] and bias-induced nanolithography.[101, 102] This chapter will focus specifically on the capabilities of nanografting for inscribing patterns of diverse composition from the bottom-up, to produce complicated surface designs with well-defined chemistries. Nanografting provides a versatile tool for generating nanostructures of organic and biological molecules, as well as nanoparticles. Protocols of nanografting are accomplished in liquid media, providing a mechanism for introducing new reagents for successive *in situ* steps for 3-D fabrication of complex nanostructures.

Nanografting was first introduced in 1997 by Xu, et al. and is accomplished by applying mechanical force to an AFM probe to generate nanostructures within a matrix film.[93] The molecules to be patterned are dissolved in the imaging media, and the substrates are precoated with a protective layer to prevent nonspecific adsorption of molecules throughout areas of the surface. When the tip is operated in liquid media under low force (less than 1 nN), high resolution characterizations of surfaces can be acquired *in situ*. When the force applied to the probe is increased to a certain displacement threshold the tip becomes a tool for surface

---

*Reproduced with permission from Springer.

fabrication. The exquisite resolution achieved with nanografting is mainly attributable to liquid imaging. When AFM experiments are conducted in liquid media, very low force can be used to accomplish imaging or nanofabrication. The geometry of the apex of the probe is preserved by operating at low forces, because liquid media serves to minimize the strong capillary forces of attraction that cause adhesion between the tip and sample.[103, 104]

3.1.1 General Procedure for Nanografting

The basic steps for nanografting are presented in Figure 3.1. In the first step, the surface of a self-assembled monolayer (SAM) prepared on a Au(111) substrate is imaged using low force in liquid media that contains the molecule or nanomaterial to be patterned. When the tip is operated at low force the surface is not damaged or altered by the scanning probe (Figure 3.1A).

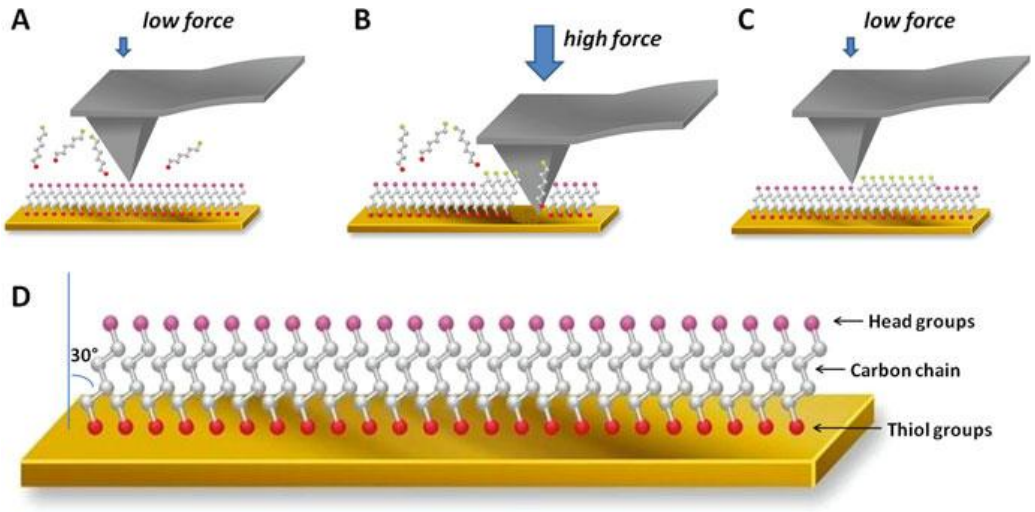

Figure 3.1 Steps for producing patterns of *n*-alkanethiols with nanografting by changing the mechanical force applied to the AFM probe. The process is accomplished under liquid imaging media containing the molecules to be patterned. [A] Characterization is accomplished when the tip is operated at low force; [B] patterns are nanografted when the force is increased to a certain displacement threshold; [C] returning to low force, the patterns are characterized in situ. [D] Model of an *n*-alkanethiol self-assembled monolayer.

A suitable flat area can be selected for inscribing patterns that has few defects or contaminants. Next, the tip is raster scanned across the surface using higher force to sweep away selected regions of the matrix SAM. During the fabrication step (Figure 3.1B), fresh molecules from solution bind to the exposed areas of the substrate immediately following the pathway of the scanning probe to produce nanopatterns. Finally, the pattern that was grafted can be characterized *in situ* by returning to a low force for nondestructive imaging (Figure 3.1C). Patterning and imaging are accomplished *in situ* with the same AFM tip, within a few minutes or less. The entire process can be automated to reproducibly write multiple patterns.[105, 106]

A key requirement for nanografting is to determine the necessary amount of force for cleanly removing local areas of the matrix monolayer without damaging the tip. To find the appropriate force, one can monitor surface changes *in situ* while successively increasing the load applied to the tip. As the force is gradually increased at small increments, images will clearly show changes in surface morphology at a certain threshold. The optimum force must be derived for each experiment for several reasons. At the nanoscale, the actual geometry of tips is never identical and thus the sharpness will vary from probe to probe. Also, different amounts of force are necessary for matrix layers of different thicknesses or compositions. The requisite force needed for imaging in various liquid media will change according to dissolution parameters, for example the forces required for nanografting in aqueous media are not the same as for ethanolic media. For each system, the amount of force to be applied for fabrication must be determined experimentally.

3.1.2 Applicability of Nanografting for In Situ Studies

Nanografting can achieve high spatial resolution. The length, size and shape of patterns can be controlled precisely, achieving an edge resolution of 1 nm and line widths of 10 nm or

less, depending on the dimensions of the probe. The head groups of grafted structures can be selected by choosing different molecules, such as aldehydes, carboxylates, thiols, amines, and others. The thickness of the patterns can be designed by choosing the carbon backbone of the matrix and nanografted molecules. Nanografting enables *in situ* reactions to be studied locally under dilute conditions.[107] Time-lapse AFM images can be acquired at selected intervals to view reaction kinetics for conditions that occur over time scales of minutes to hours. A range of different molecules and nanomaterials have been patterned with nanografting, examples will be described in this chapter for *n*-alkanethiol SAMs,[97, 108] metals,[11] nanoparticles,[109] porphyrins,[110] proteins[111-114] and DNA.[115]

Among the most significant contributions of scanning probe studies with nanografting are the possibilities for studying step-wise surface reactions in real time with a molecular-level view. Imaging in liquid media provides a means for exchanging liquids to introduce new reagents in successive steps to build nanostructures from the bottom-up. To date, the primary examples that have been reported demonstrate nanografted patterns of *n*-alkanethiol SAMs, often as a foundation for attaching other molecules and nanomaterials. Further chemistries for nanografting experiments are likely to be extended to other types of surface binding motifs, such as phosphonic acids on metal substrates;[116] siloxane binding, pyridyl-[110] or thiol- [117] functionalized porphyrins, thiolated proteins,[118, 119] thiolated DNA[115] or peptides and other types of surface linkers.

3.2 Patterning *n*-Alkanethiol Self-Assembled Monolayers (SAMs) by Nanografting

As a starting point, SAMs of *n*-alkanethiols prepared on gold substrates provide a model system for nanografting experiments. Thiol end groups furnish a functional handle for surface attachment, mediated by sulfur-gold chemisorption. The self-assembly process and surface

structures of *n*-alkanethiols on Au(111) have been previously described.[120, 121] The carbon backbones of the molecules consist of tilted alkane chains (Figure 3.1D), the lengths of which can be designed to define the thickness of the matrix areas and nanografted patterns. For *n*-alkanethiol SAMs, chain lengths ranging from 2 to 37 carbons have been nanografted successfully. The head groups of *n*-alkanethiols provide a way to attach other molecules and nanomaterials with spatial selectivity; for example, experiments can be designed to define patterned sites for specific adsorption of proteins, nanoparticles or DNA, within a matrix monolayer that resists binding of molecules or nanomaterials.

Nanopatterns of octadecanethiol (18 carbon backbone or C18) were nanografted side-by-side within a matrix SAM of decanethiol (10-carbon backbone or C10) as shown in Figure 3.2A.[93] The square patterns measured 0.88 nm taller than the matrix. The dimensions of the smaller feature are 3 nm × 5 nm, in which approximately 60 thiol molecules were grafted. The size of the larger nanopattern is 50 × 50 nm^2. Zoom-in views of both the nanografted pattern of C18 and the C10 matrix are shown by *in situ* AFM topography images in Figures 3.2B, C, respectively. The molecularly resolved images show that molecules within the nanopatterns display a periodic ($\sqrt{3} \times \sqrt{3}$) R30° lattice, thus the packing arrangement of thiols is preserved for alkanethiol nanostructures produced by nanografting.

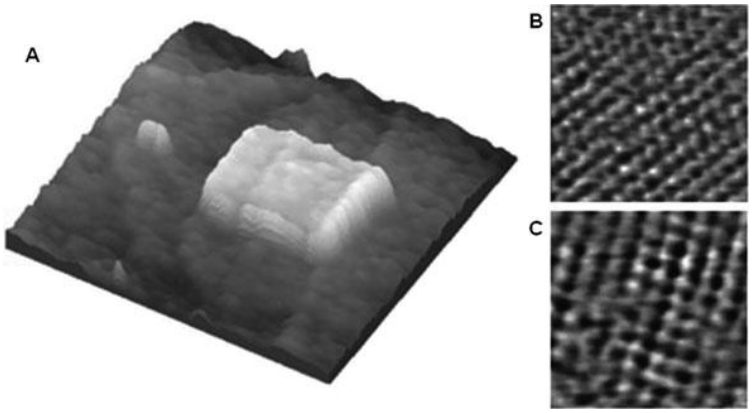

Figure 3.2 Patterns of *n*-octadecanethiol were nanografted within a matrix monolayer of decanethiol. [A] AFM topography view (130 × 130 nm^2); [B] zoom-in view of the pattern surface (5 × 5 nm^2); [C] Zoom view from an area of the C10 matrix (5 × 5 nm^2). (Reprinted with permission from Ref.[93]. Copyright © American Chemical Society.)

Nanografted structures can be erased and rewritten *in situ* by exchanging the imaging media with different molecular adsorbates for patterning. Results for writing two parallel line patterns of octadecanethiol within a decanethiol matrix with a distance of 20 nm between patterns were shown by Xu and others.[79] One of the lines was erased by replacing the liquid imaging media with a solution of decanethiol and scanning at high force over one of the C18 patterns to replace the previous nanostructure with C10 molecules. After the line pattern was "erased" the imaging media was exchanged again to introduce a fresh solution of C18SH molecules to graft a line pattern spaced 65 nm from the previous pattern. Accomplishing this experiment required a scanning probe microscope with high stability, however this clearly demonstrates the flexibility for introducing and exchanging reagent solutions for multiple synthetic steps when imaging with AFM in liquids.

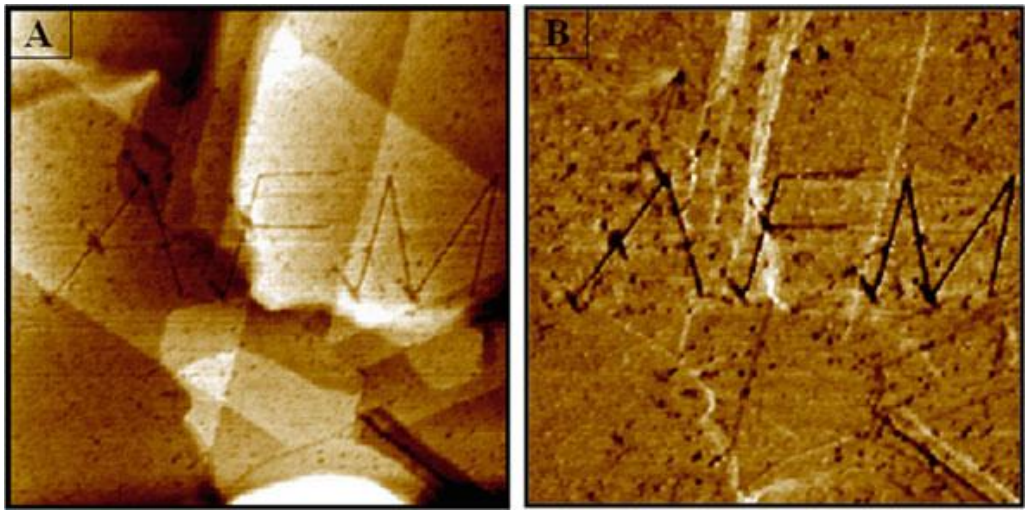

Figure 3.3 Nanografted letters of 3-mercaptopropionic acid written within a decanethiol matrix SAM. [A] Topographic image (600 × 600 nm^2); [B] concurrent lateral force image of the same area

Different shapes and molecular components can be patterned by nanografting. Several letter patterns that spell the acronym "AFM" are shown in Figure 3.3 that are terminated with carboxyl head groups. The line widths of the letter patterns are less than 10 nm, indicating that the very sharp AFM probe was not damaged by the physical process of scanning with the tip under high force. Although the AFM images of the patterns were captured after the writing process, we can still resolve the ultra-fine distinctive features of the matrix monolayer of decanethiol, resolving the characteristic details of an alkanethiol SAM landscape such as pinholes, scars, molecular island vacancies[122] and overlapping gold terrace steps. The patterns are composed of 3-mercaptopropionic acid written within a decanethiol matrix. The difference in terminal chemistry is clearly distinguishable in the simultaneously acquired lateral force AFM image of Figure 3.3B. Lateral force images do not show changes in height, instead the image contrast reveals nanoscopic differences in frictional and adhesive forces between the tip and surface. In this example, the tip-surface interactions are markedly different for the dark areas of the nanografted letters which are terminated with thiol head groups, as compared to the brighter areas of the surrounding methyl-terminated matrix SAM.

The simplicity of SAM preparation is another benefit of nanografting protocols. A matrix monolayer can be prepared by simply immersing a clean substrate into a dilute solution of *n*-alkanethiol in ethanol or sec-butanol for one or more hours. After a SAM film is formed on the metal substrate, the sample can be stored for several weeks in a solution of clean solvent, and often can be recycled and used for several experiments. Nanografted patterns can be engineered to incorporate diverse head group chemistries, such as methyl, alcohol, glycol, aldehyde, amide and carboxylate. Table 3.1 lists examples of thiol self-assembled monolayers which have been patterned using nanografting. Methyl-terminated SAMs of decanethiol or octadecanethiol have

been commonly used as matrix monolayers for nanografting. Either ethanol or 2-butanol are most frequently used as solvents for liquid imaging. Patterns of diverse shapes, such as squares, rectangles and rings have been reported ranging up to 500 nm in size, with the dimensions of the smallest pattern measuring 3 nm × 5 nm.

Table 3.1 Examples of thiol SAMs that have been successfully nanografted

Nanografted molecule	**Pattern dimensions**	**Matrix film**	**Liquid media**	**References**
1-hexanethiol	5.2 nm × 5.2 nm	Thiolated biotin SAMs	Ethanol	[114]
1-octadecanethiol	3 nm × 5 nm 50 nm × 60 nm	1-decanethiol	2-butanol	[93]
1-decanedithiol	100 nm × 100 nm	1-decanethiol	2-butanol	[123]
Dodecanethiol	300 nm × 300 nm	1,9-nonanedithiol	Ethanol	[124]
1-octadecanethiol Docosanethiol 2-mercaptoethanol 16-mercapto-hexadecanoic acid	20 nm × 60 nm 25 nm × 60 nm 75 nm × 100 nm 70 nm × 300 nm	1-decanethiol or 1-octadecanethiol	2-butanol	[79]
3-mercapto- 1-propanoic acid	400 nm × 400 nm	$C_{11}(EG)_6$	Water	[125]
11-mercapto- 1-undecanal	50 nm × 50 nm 100 nm × 100 nm	1-octadecanethiol	Decahydro-naphthalene	[78]
11-mercapto-undecanoic acid	Rings with diameter of 100 nm	1-octadecanethiol	Ethanol	[126]
1,8-octanedithiol	500 nm × 500 nm	Hexanethiol	Ethanol	[124]
6-mercaptohexan-1-ol	400 nm × 400 nm	$C_{11}(EG)_6$	Water	[125]
Biphenyl 4,4’-dithiol	100 nm × 100 nm	1-decanethiol	2-butanol	[123]
Mixed-n-alkanethiols	200 nm × 200 nm	1-decanethiol: 1-octadecanethiol =10:1	Ethanol or 2-butanol	[127]
10:1 ODT:decanethiol $CF_3(CF_2)_9(CH_2)_2SH$	200 nm × 200 nm 15 nm × 15 nm 300 nm × 300 nm	Hexanethiol Dodecanol Mixed SAM matrices	Ethanol, 2-butanol or poly-α-olefin oil	[127]
1-octadecanethiol	70 nm × 50 nm 175 nm × 225 nm 20, 50, 100, 200 nm	Decanethiol Mixed SAMs	Ethanol, 2-butanol or hexadecane	[128]

3.2.1 Automated Nanografting

Beyond simple patterns of lines or rectangles, nanografting can be used to fabricate complicated designs with modern computer automation. The William Blake quotation “What is

now proved was once only imagined" was nanografted with mercaptohexadecanoic acid by Cruchon-Dupeyrat, et al., using computer-assisted manufacturing (CAM) software.[106] The entire quotation was written in less than 20 seconds, inscribed within a 1.85 × 0.9 μm^2 area. Arrays of circles, squares, lines and even mouse ear designs were produced by automated nanografting of different functionalized alkanethiols by Ngunjiri and others.[105] A sophisticated example was demonstrated by Maozi Liu, et al. for nanografting the design of the University of California at Davis' seal with a 10 nm line resolution using an aldehyde terminated alkanethiol within a decanethiol SAM.[108] The design was patterned inside an 8 × 8 μm^2 area and was completed in 10 minutes.

The speed and ease of nanografting for AFM experiments has been greatly improved by advances in software for commercial instruments. Louisiana State University implemented nanografting experiments in physical chemistry laboratories starting in 2005 to teach and showcase the concepts of chemistry and nanoscience to undergraduate students.[129] Nanografted patterns can be produced within a few minutes and thus are an excellent venue for providing hands-on training for students. At present, scanning probe-based lithography is primarily used for laboratory research rather than as a tool for industry. Knowledge and experience in modern methods of surface measurements and analysis will be pivotal to the eventual transfer of the technology gained with academic nanoscience research to benefit industry. The latest advances in automation of scanning probe instruments enable new possibilities for educational modules for engaging students with modern and compelling course activities, such as with nanografting studies.

3.2.2 Evaluating the Tip Geometry with Nanografting

For both imaging and nanofabrication with an AFM probe, the shape of the apex of the tip is critical for high resolution. Nanografting provides a way to evaluate the shape of an AFM tip, to help discern if images show artifacts or represent the true shape of surface structures.[130] Line patterns of alkanethiol SAMs are first fabricated using nanografting with a single scan, and then imaged using the same tip. The tip size and tip-surface contact area can be derived from the cursor profile in the AFM topography viewsThe shape of the apex of the tip can be reconstructed by imaging small surface features of nanografted SAMs with known dimensions.When the tip is engaged for a sweeping a single line pattern, the width of the trench or pattern provides a reliable estimate of the tip-surface contact area. Tips with multiple asperities produce multiple nanopatterns. This approach is especially helpful for identifying tips with multiple asperities that are difficult to characterize by other techniques.

3.2.3 Nanografted Patterns of n-Alkanethiols Furnish a Molecular Ruler

Since the dimensions of methyl-terminated *n*-alkanethiols have been well-established, the height and orientation of other molecules can be evaluated by nanografting experiments, by referencing the thickness of *n*-alkanethiols as an *in situ* molecular ruler. Methyl-terminated *n*-alkanethiols can be prepared reproducibly with predictable, well-defined surface structures, thus nanografted patterns furnish a reliable height reference for nanoscale measurements of film thickness. Self–assembled monolayers of *n*-alkanethiols spontaneously form hexagonally-packed crystalline layers upon adsorption to metal surfaces, with an intermolecular spacing of ~ 0.5 nm.[131] The well-ordered packing of *n*-alkanethiol SAMs results from a strong affinity to the substrate through chemisorptive binding to produce a commensurate structure, and also from intermolecular chain-chain interactions of Van der Waals forces between the carbon backbones. Methyl-terminated *n*-alkanethiols form SAMs with a single thiol end group chemisorbed to

Au(111) oriented in an upright configuration, with all-trans carbon chains. Studies conducted using IR, near-edge X-ray absorption fine structure (NEXAFS) spectroscopy, and grazing incidence X-ray diffraction (GIXD) indicate that the alkyl chains of SAMs are tilted ~30^{o} with respect to surface normal.[132-135] The consistency for preparing reproducible molecular structures of *n*-alkanethiols provides predictable dimensions as a means to study structures of other patterned molecules using side-by-side local measurements of height differences with AFM-based nanografting protocols.[95, 136, 137]

By labeling the DNA 3' end with a fluorophore and immobilizing it onto a gold surface through thiol modification of the 5' end, a pH-driven DNA nanoswitch can be reversibly actuated. By cycling the solution pH between 4.5 and 9, a conformational change is produced between a four-stranded and a double-stranded DNA structure which either elongates or shortens the separation distance between the 5' and 3' ends of the DNA. The nanoscale motion of the DNA produces mechanical work to lift up and bring down the fluorophore from the gold surface by at least 2.5 nm and transduces this motion into an optical "on-and-off" nanoswitch. Nanografting was used to measure the thickness of the monolayers of thiolated "motor" DNA under changing pH conditions by Dongsheng Liu, et al.[138] Before nanografting, a DNA SAM prepared on template-stripped gold surface was first imaged under low force (0.2-0.5 nN) in phosphate buffered saline (pH 4.5) containing 1 mM of 2-mercaptoethanol. The area for nanografting was repeatedly scanned at 4-5 Hz under higher forces (~30 nN) to scratch away the DNA SAM, creating a freshly exposed gold surface that was immediately grafted with a SAM of 2-mercaptoethanol. After nanografting, a wider scan area was characterized under low force. Changes in the thickness of the DNA film measured at pH 4.5 and 9 were attributed to differences in the electrostatic interactions between the tip and the DNA layer.

3.2.4 Evaluating Properties such as Friction, Elastic Compliance or Conductivity of Nanografted Pattern

Friction mapping can be accomplished with AFM to provide useful information about the composition and chemical properties of a surface with nanoscale sensitivity. A systematic study of differences in molecular friction was accomplished *in situ* for nanografted patterns of different ω-functionalized *n*-alkanethiols by Joost te Riet et al.[32, 139] Trace and retrace lateral force images were subtracted to reveal the net frictional forces to obtain quantitative frictional force measurements at the nanoscale. Images of nanografted patterns with fluorocarbon-, hydroxyl-, thiol-, amine- and acid- terminated head groups were obtained in 2-butanol under common conditions of load force and scan speed. The same cantilever was used for nanografting patterns and acquiring *in situ* images in liquid media. In each case, they observed that the friction of the nanografted patches was lower than that of the surrounding matrix SAM. However, nanografted patterns with functional head groups showed statistically higher friction values than nanografted patterns with methyl groups. These observations were attributed to differences in topographical roughness of the nanografted patches, the amount of disorder and defects within the patterns, as well as surface composition.

Changes in molecular-level packing, molecule chain lengths, domain boundaries, and surface chemical functionalities in nanografted SAM nanopatterns can be sensitively characterized using force modulation imaging.[140] Size-dependent changes in elasticity were detected for test platforms of nanografted SAM patterns by Price, et al.[141] Surface patterns of octadecanethiol (ODT) of designed sizes and shapes were nanografted into *n*-alkanethiol SAMs for studies of the local mechanical properties using force modulation imaging. Certain surface features such as the edges of the domains and nanostructures or desired chemical functionalities can be selectively enhanced in the amplitude images when the driving frequency of sample

modulation is tuned to the resonance frequency of the tip-surface contact.[140] By means of tuning the driving frequency of sample modulation to the certain frequencies, the resonances at the tip-surface contact are activated to sensitively reveal characteristic contrast for surface changes in molecular-level packing, molecule chain lengths, domain boundaries, and surface chemical functionalities of SAM nanopatterns. These studies demonstrated that the resonance frequency of the tip surface contact varied according to dimensions of the nanostructures. Frequency spectra of the tip surface contacts were acquired for nanografted ODT structures, from which Young's modulus was calculated using continuum mechanics models.

An approach to study metal-molecule-metal junctions based on combining approaches for nanografting and conductive probe AFM was demonstrated by Scaini, et al.[142] Patterns of alkanethiol molecules were nanografted within a SAM of alkanethiol molecules of different chain lengths for local measurements of charge transport at the molecular level. The approach enables relative determination of the differential resistance between two molecular layers in ambient conditions; however absolute transport measurements also depend on the nature of the AFM tip-molecule contact. The tunneling decay constants of alkanethiols were measured as a function of chain lengths for octanethiol, nonanethiol and decanethiol nanopatterns relative to a matrix SAM of octadecanethiol/Au(111).

3.3 Spatially Confined Self-Assembly Mechanism of Nanografting

Both the assembly mechanism and kinetics of certain surface reactions can be sterically changed by spatial confinement with nanografting. Nanografted patterns of *n*-alkanethiols exhibit higher coverage and two-dimensional crystallinity than the matrix SAMs.[143] During the process of nanografting, thiolated molecules self-assemble within a spatially confined environment. A transient nanoscopic area of the surface is exposed by the scanning probe, which

is confined by the surrounding matrix and the probe. During the nanografting process, thiol molecules present in the solution rapidly assemble onto the exposed nanometer-size area of gold substrate that is confined by the scanning tip and surrounding matrix SAM. Spatial confinement is considered to alter the pathway for the self-assembly process causing the initially adsorbed thiols to adopt a standing-up configuration directly within a nano-sized environment. The mechanism for conventional solution self-assembly occurs through a two-step process when bare gold substrates are immersed in thiol solutions, because the assembly of thiols takes place in unconstrained conditions. Initially a "lying-down" phase is spontaneously formed which subsequently transitions over time by rearrangement to a standing-up orientation.[120] In contrast, with nanografting the "lying-down" configuration is not possible because the area of the surface exposed is smaller than the molecular length, therefore the molecules assemble directly into an upright or standing orientation.[144] Self-assembly within the constrained areas proceeds with a faster reaction rate because the time lapse for a phase transition from lying-down to an upright configuration is bypassed. Thus, the kinetics of SAMs formed with nanografting occur more rapidly than during natural growth on unconstrained surfaces. The spatially confined environment was found to reduce the amount of disorder present in the resulting nanografted patterns, to produce SAMs which exhibit fewer scars or defects.[139, 143]

3.3.1 Studies with Binary Mixtures of SAMs

A nanoengineering approach to regulate the lateral heterogeneity of mixed self-assembled monolayers was reported using nanografting and self-assembly chemistry.[32] Formation of segregated domains in mixed SAMs results from the interplay between reaction kinetics and thermodynamics. Considerable effort has been directed to investigate the impact of either reacting agents or surface reaction conditions such as concentration, temperature, thiol species

and molar ratio of mixed components for achieving control of the resulting local domain structures. For example, kinetics-driven products for mixed SAMs with a near molecular-level mixing were favored during coadsorption of thiol mixtures at high concentration with elevated temperature.[145] Thermodynamics-driven layers of large segregated domains were observed after long immersion in dilute solutions and/or when the adsorbate chain length and termini were sufficiently different.[146] Nanografting provides additional control of the reaction mechanism for thiol self-assembly on gold, and thus affects the local domain structures that are produced from solutions of mixed SAMs.

The heterogeneity of mixed solutions of SAMs can be regulated by changing the speed of nanografting.[144] This was demonstrated both theoretically[147] and experimentally.[148] Monte Carlo simulations of nanografting were found to reproduce experimental observations concerning the variation of SAM heterogeneity with the speed of an AFM tip. Simulations by Ryu, et al. demonstrated that the faster the AFM tip displaced adsorbed molecules in a monolayer, the monolayers formed behind the tip became more heterogeneous, according to the amount of space and time available for the formation of phase-segregated domains. By varying fabrication parameters of nanografting, the lateral heterogeneity can be adjusted to produce near molecular mixing or to form segregated domains ranging from several to tens of nanometers.[32]

3.4 *In Situ* Studies of Polymerization Reactions via Nanografting

Beyond preparing monolayer patterns of ω-functionalized *n*-alkanethiols, multilayer nanostructures can also be generated by nanografting. Depending on the concentration of thiols in the imaging media, patterns with the thickness of a bilayer were shown to form spontaneously by nanografting SAMs of certain head group chemistries.[95, 149] This is mediated by self-polymerization of molecules which have reactive groups through coupling of headgroups. Under

certain conditions of high concentration, the intermolecular interactions between molecules in solution predominate, to direct the vertical self-assembly of certain α,ω-alkanedithiols to produce bilayer patterns. For SAM patterns with methyl, hydroxyl, thiol, or carboxylic acid head groups, monolayer patterns were generated when nanografting in dilute ethanol or aqueous solutions. However, as the solution concentration was increased beyond a certain threshold, nanografted patterns were formed with thicknesses corresponding to a double layer for molecules with carboxylic acid head groups or with α,ω-alkanedithiols, as reported by Kelley, et al.[95] Nanografted patterns with methyl or hydroxyl head groups were observed to exclusively form monolayer structures for a fairly wide range of concentrations that were tested.

Designed functional groups of *n*-alkanethiols were used to attach additional organic molecules to enable site-selective surface reactions for studies of polymerization reactions at the nanoscale.[78] In the first step, nanografting was used to produce 2D nanopatterns of methyl head groups in a matrix SAM with hydroxyl head groups. The nanopatterns were then used to further construct 3D nanostructures by successive steps of an *in situ* reaction with organosilanes. Jun-Fu Liu et al. demonstrated transfer of 2D nanopatterns to chemically distinct 3D nanostructures with different head groups. The scheme and results for pattern transfer are shown in Figure 3.4. A nanografted rectangular frame of octadecanethiol was inscribed within a matrix SAM of mercaptoundecanol on a gold substrate. The pattern of a frame in Figure 3.4b measured 0.7±0.2 nm taller than the matrix monolayer, in agreement with the expected theoretical dimensions. After nanografting, the AFM liquid cell was rinsed three times with decahydronaphthalene to remove any residual thiols, then a solution of octadecyltrichlorosilane ($CH_3(CH_2)_{17}SiCl_3$ or OTS) was injected into the cell for several minutes. The trichlorosilanes from the liquid media reacted with the hydroxyl terminal groups of the surrounding matrix SAM of mercaptoundecanol to form

a thicker layer. However, the frame patterns did not react with OTS since the nanografted pattern with methyl head groups provided an effective resist, as shown in Figure 3.4c. After reaction with OTS the nanografted frame is shorter than the surrounding matrix film. The height changes at each step of the *in situ* reaction are shown with representative cursor profiles in Figure 3.4d. The process was completed within a few minutes and the time duration for immersion in OTS was found to influence the height of siloxane structures.

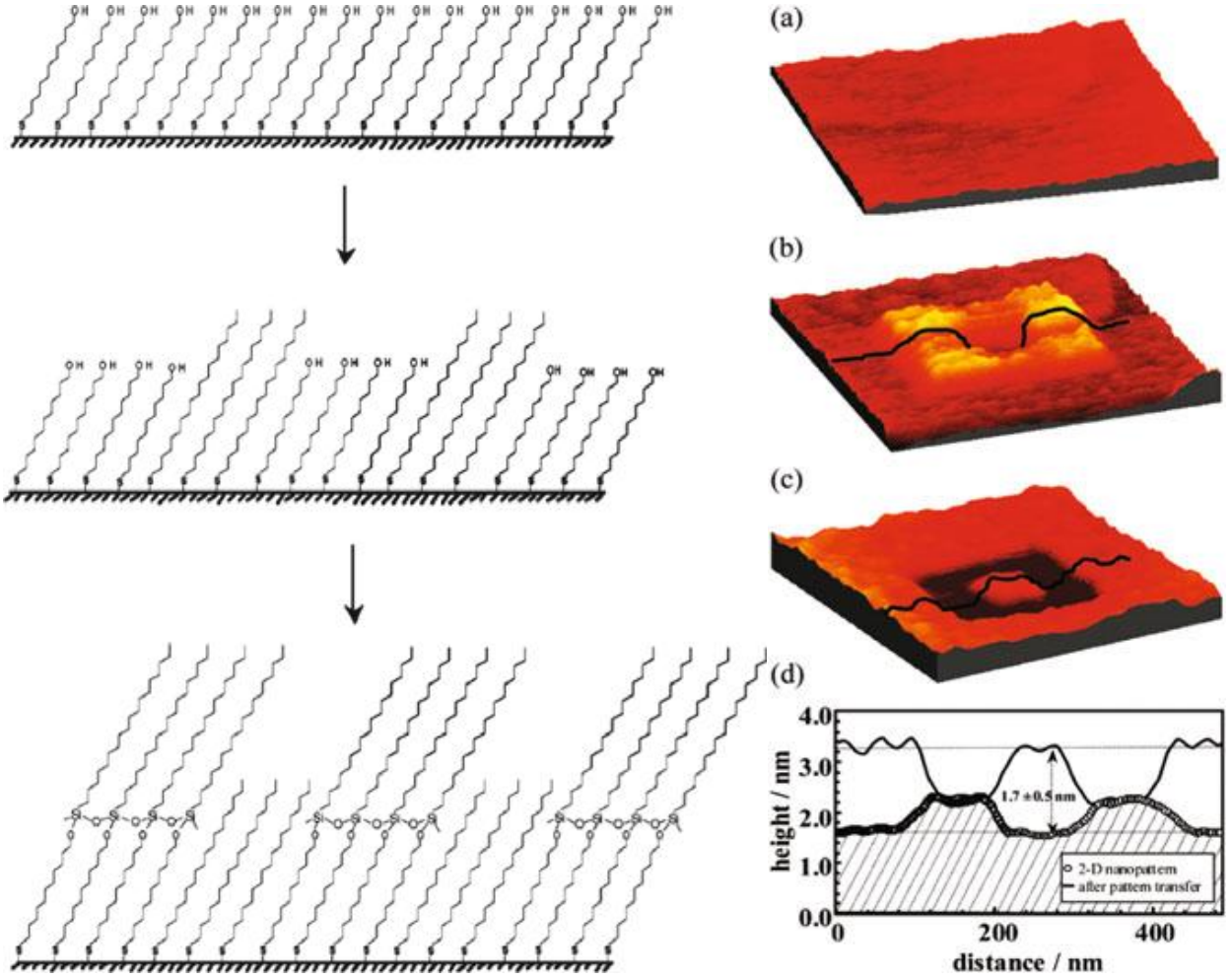

Figure 3.4 Snapshots showing bottom-up assembly accomplished in situ with a polymerization reaction for attaching organosilanes to a hydroxyl-terminated SAM. [A] Initial view of a mercaptoundecanol monolayer formed on Au(111); [B] Nanografted frame of ODT; [C] Pattern is shorter than the matrix SAM after reaction with OTS; [D] representative cursor profile for lines in [B] and [C]. (Reprinted with permission from Ref. [78]. Copyright © American Chemical Society)

Nanografting enables a critical first step for developing further protocols for designed surface reactions to construct hierarchical nanostructures with desired spacer lengths, composition and functionalities. The 2D patterns produced by nanografting provide a surface template for spatially directing the selective adsorption or binding of other molecules or nanomaterials in subsequent steps. Further examples will be presented in the next sections. The desired interfacial properties, such as lubricity, protein adhesion or resistance, and electron transfer, may be designed from the bottom-up by selection of various functional groups and designated architectures of the nanografted structures of metals, nanoparticles, protein or DNA.

3.5 Generating Patterns of Metals and Nanoparticles with Nanografting

Certain systems of metals and nanoparticles have been patterned successfully with AFM-based lithography. Nanopatterns of thiol-coated gold nanoparticles were prepared within a decanethiol SAM on Au(111) by scanning probe lithography[109] To attach nanoparticles to gold surfaces via sulfur-gold chemisorption, surface-active gold nanoparticles were prepared with a shell of a mixed monolayer comprised of alkanethiol and alkanedithiol molecules. Local regions of a decanethiol SAM were shaved using an AFM tip under high force to expose the substrate in a solution containing nanoparticles. Unlike nanografting where surface assembly is immediate, the kinetics of larger nanomaterials such as gold nanoparticles were found to be slower and took place over longer time scales. Depending on the concentration, thiolated nanoparticles adsorbed onto the exposed areas uncovered by the AFM tip after several hours, and particles were not observed to bind to the surrounding matrix areas of the methyl-terminated decanethiol SAM. Gold nanoparticles attached to the gold substrate via sulfur-gold chemisorption. The outer shell of the nanoparticles was encapsulated with mixed thiol groups of hexanethiol and hexanedithiol molecules. Cursor measurements of the nanoparticles revealed sizes ranged from 3 to 5 nm in

diameter, and patterns were formed with a single layer of nanoparticles. The slower adsorption of the nanoparticles on shaved areas of the substrate compared to nanografting of molecular patterns was attributable to differences in mobility and concentration.

3.5.1 Electroless Deposition of Metals on Nanografted SAM Pattern

Site specific reactions for electroless deposition of metals were accomplished using nanografting. Copper nanostructures formed selectively on carboxylic acid terminated SAM patterns that were nanografted within a hydroxyl-terminated resist monolayer, using electroless plating without a catalyst.[11] To accomplish *in situ* studies, the AFM cantilevers were coated with silane to prevent copper deposition on the probe. An example showing selective growth of copper nanostructures on nanografted patterns of 16-mercaptohexadecanoic acid (16-MHA) is displayed in Figure 3.5. A computer script was designed to automate the nanografting process to generate patterns of different line densities within a matrix SAM of 11-mercaptoundecanol (11-MUD), which resists copper deposition. The parameters of the tip trajectory during nanografting can be used to define the thickness of copper according to the density of grafted molecules. Lower density of carboxylic acid groups resulted in differences along the gradients for deposition of copper. Changes in the surface density of 16-MHA were systematically varied by designing the probe trajectory to advance either at the edges or centers of the patterns. The difference in the molecular gradients of 16-MHA nanopatterns was evaluated by introducing a copper solution. Metal ions (Cu^{2+}) deposited selectively in the reduced form as Cu^{0} via an autocatalytic reaction on regions patterned with 16-MHA. For patterns written with lower density, less copper was observed to deposit. When the probe was traced only once (top rows) less copper deposition occurred compared to the bottom rows where the tip was swept twice along a linescan.

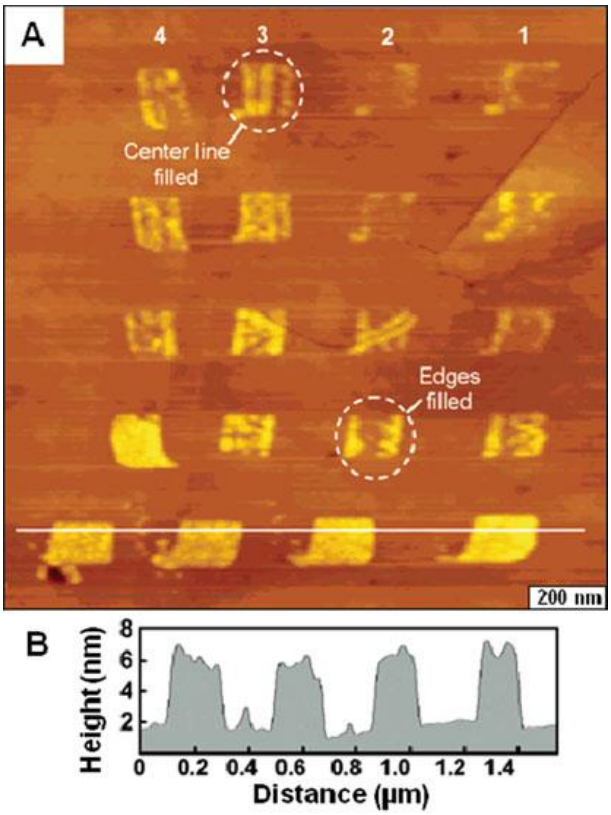

Figure 3.5 Nanografted patterns of carboxylic acid terminated SAMs were generated with different densities for electroless deposition of copper. [A] View of copper nanopatterns grown on nanografted patterns written with different line densities; [B] cursor plot for copper structures of the bottom row. (Reprinted with permission from Ref. [11]. Copyright © American Chemical Society)

Systematically engineering the writing parameters for arrays of nanopatterns generated by automated nanografting offers a further useful strategy for controlling reaction conditions for bottom-up surface assembly. Essentially, the surface density of reactive moieties can be defined to further control spatial parameters of surface reactions. In addition, the writing path itself was shown to influence the initial stages of metal deposition. The general approach for patterning metals with electroless deposition could readily be extended to other metals such as platinum or nickel for construction of a range of metal structures and nanoscale metal junctions.

3.6 Nanografting with Porphyrins

An obstacle for producing patterns with nanografting has been the limitation of using thiol-based chemistries. New directions are being developed for expanding beyond preliminary model systems of chemisorbed *n*-alkanethiols on gold substrates to other chemical linkers. Porphyrins and metalloporphyrins have a macrocyclic tetrapyrrole structure, which may be functionalized with various substituents. The choice of focusing research efforts on model systems of porphyrins is highly practical, because of the associated electrical, optical and chemical properties of this functional class of molecules. More complex surface structures could be achieved with nanografting by using porphryins with thiolated substituents[117] or pyridyl functional groups.[110] Modifications of the macrocycle, peripheral groups or bound metal ions can generate a range of electrical, photoemissive or magnetic properties. The orientation of porphyrins on surfaces is determined by factors such as the nature of the peripheral substituents and their position on the macrocycle. The resulting surface structures influence the photonic and electronic properties of the systems. Also, different properties result when different metals are coordinated to the macrocycle. Porphyrin and metalloporphyrin systems are excellent materials for surface studies, due to their diverse structural motifs and associated electrical, optical and chemical properties, and thermal stability.[150, 151] The rigid planar structures and π-conjugated backbone of porphyrins convey robust electrical properties for potential molecular electronic devices.

Scanning probe studies of nanografted patterns of dipyridyl porphyrins were used to provide insight for the molecular orientation and surface assembly of porphyrins from mixed solvent media, with studies by LeJeune, et al.[152] *In-situ* AFM furnished local views of the assembly of porphryins with pyridyl-substituents on surfaces of Au(111). Experiments were

accomplished for nanografting *n*-alkanethiols within a matrix film of 5,10-diphenyl-15,20-di-pyridin-4-yl-porphyrin (DPP) as well as for nanografting patterns of DPP within different matrix SAMs of *n*-alkanethiols. The solubility of porphyrins in ethanol, butanol or water are problematic for accomplishing *in situ* AFM studies, therefore a solvent mixture was used for nanografting. First the porphyrin was dissolved in a parent solution of dichloromethane, and then further diluted 100-fold in ethanol. Examples of nanografted porphyrin patterns are displayed in Figure 3.6. Dodecanethiol (C12) was used as a matrix SAM for writing nanostructures of DPP in a solution containing 1% dichloromethane in ethanol. The overall final concentration of DPP used for nanografting was 1 micromolar.

A mosaic design of 20 oval patterns was produced by nanografting DPP within a C12 SAM, as shown in the AFM topograph of Figure 3.6A. The patterns were produced by tracing the probe in a circular trajectory four times, so that the centers of the rings were not disturbed. The patterns were produced within 5 minutes using a scan speed of 0.1 μm/s. The dimensions of the oval structures of DPP measure 77 ± 3 nm from side to side, and 99 ± 6 nm from top to bottom. The dodecanethiol islands in the middle of the rings that are surrounded by a ring of DPP have an average diameter of 58 ±10 nm and furnish a convenient height reference for evaluating the depth of the DPP patterns. The distance between patterns ranged between 53 and 115 nm in the vertical direction and between 44 to 200 nm horizontally. A force of 2.3 nN was applied to write patterns of porphyrins within dodecanethiol while imaging in liquid media of mixed solvents. Characteristics of the underlying Au(111) substrate such as etch pits and scar defects are apparent in the 700 × 700 nm^2 topograph, indicating that after nanografting multiple patterns the probe still maintains a sharp geometry for accomplishing high-resolution imaging. The lateral force image (Figure 3.6B) exhibits distinct contrast because of the different head

groups of the C12 matrix and DPP nanopatterns. A zoom-in view of six ring nanopatterns is presented in Figure 3.6C showing the fine details of the pattern shapes and height differences. The difference in height for the matrix dodecanethiol and DPP measures 0.5 ± 0.2 nm as shown by a representative line profile in Figure 3.6D. This height difference corresponds to an upright configuration of DPP for a perpendicular orientation on Au(111) as shown by the molecular model of Figure 3.6E.

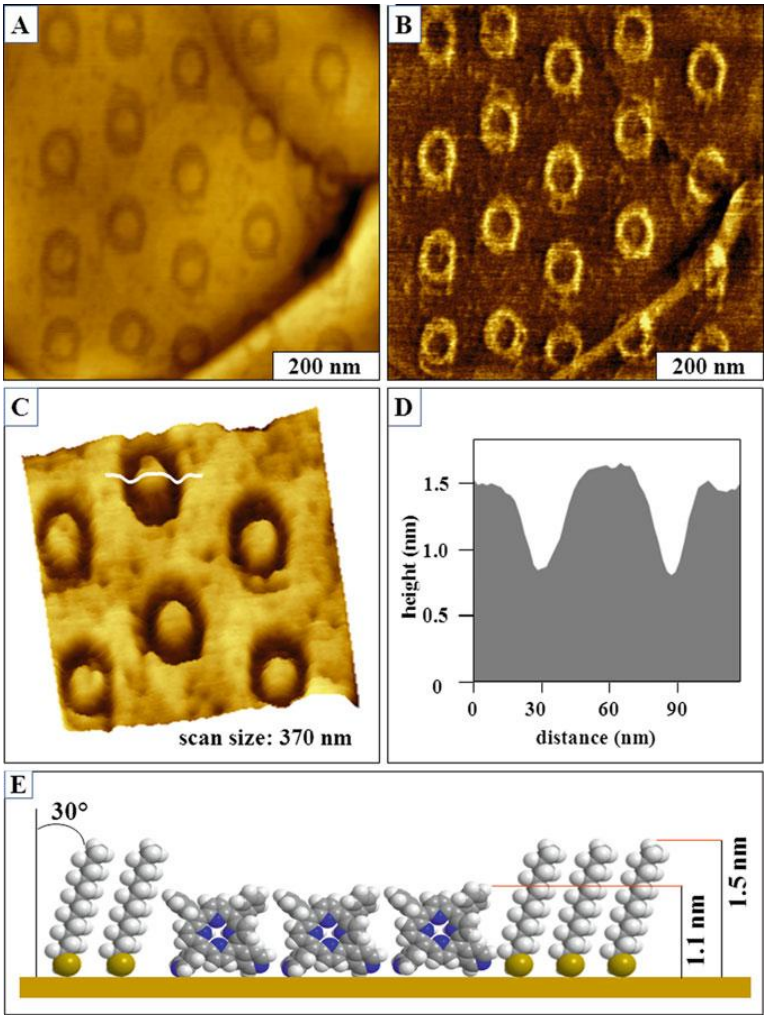

Figure 3.6 Nanopatterns of diphenyl-dipyridyl porphyrin nanografted within dodecanethiol [A] Mosaic design of 20 ring nanostructures viewed by an AFM topograph; [B] simultaneously acquired lateral force image; [C] magnified view; [D] cursor profile across one of the patterns traced in [C]; [E] height model

For nanografted patterns of DPP, the heights measured from cursor profiles indicate that molecules assemble with an upright configuration with the porphyrin macrocycle oriented perpendicular to the substrate. As previously shown for nanografted molecules of *n*-alkanethiols which have a rod-like shape, planar macrocycles of DPP likewise are confined during nanografting. Constrained conditions prevent molecules of DPP from adopting a coplanar orientation on the surface to directly generate an upright configuration. The mechanical process of nanografting alters the assembly pathway providing a means to control molecular orientation of nanopatterned porphyrins on surfaces.

3.7 Nanografted Pattern of Proteins

Methods for nanoscale fabrication are becoming important for biochemical investigations, supplying tools for basic research concerning protein-protein interactions and protein function. Protein patterning is essential for the integration of biological molecules into miniature bioelectronic and sensing devices. Often, fabrication of functional nanodevices for biochemical assays requires that biomolecules be attached to surfaces with retention of structure and function. Nanoscale studies can facilitate the development of new and better approaches for immobilization and bioconjugation chemistries, which are key technologies in manufacturing surface platforms for biosensors. Nanografting provides a way to spatially control the deposition of proteins on well-defined, local areas of patterned surfaces for accomplishing *in situ* studies of biochemical reactions. The ability to define the chemical functionalities of nanografted patterns at nanometer length scales offers new possibilities for studies of biochemical reactions in controlled environments. Capturing AFM images *in situ* throughout the progressive steps of nanografting and surface patterning can disclose reaction details at a molecular level, providing direct visualization of biochemical reactions.

An overview of the different proteins that have been patterned with nanografting is summarized in Table 3.2, with spatial dimensions reaching the level of single molecule detection with protein monolayers. Spatially well-defined regions of surfaces can be nanografted with reactive or adhesive terminal groups for the attachment of biomolecules. The dimensions of many proteins are on the order of tens to hundreds of nanometers, therefore nanografting provides a way to generate patterns with appropriate sizes for defining the placement of individual proteins on surfaces. The terminal moieties of SAMs mediate the nature of protein binding, such as through electrostatic interactions, covalent binding, molecular recognition or through specific interactions such as streptavidin-biotin recognition. The chemistry of SAM surfaces can be engineered to avoid non-specific protein adsorption for surrounding matrix monolayers, yet make specific interactions with selected proteins to be immobilized on nanografted patterns. Very few surfaces resist protein adsorption, and efforts have been directed to understand the mechanisms that contribute to protein resistance or adhesion to surfaces. Systematic studies of functionalized SAMs have been reported which evaluated the molecular characteristics that impart resistance to protein adsorption.[153-158] Depending on the protein of interest and buffer conditions, methyl-, hydroxyl- or glycol-terminated SAMs have been used effectively as matrices that resist non-specific protein adsorption.

The typical general steps of an *in situ* protein binding experiment with nanografting are to first graft nanopatterns of adhesive *n*-alkanethiols within a resistive matrix, then rinse the liquid cell and inject a solution of proteins to bind to the SAM nanopatterns. In a final step, the activity of the immobilized proteins can be tested by introducing an antibody or protein which binds specifically to the surface-bound protein. With nanografting the same tips that are used to produce patterns are also used to characterize the morphology of nanopatterns after successive

steps of protein adsorption. Unlike electron microscopy methods which require high vacuum chambers and conductive coatings for specimens, *in situ* AFM experiments can be accomplished under near-physiological conditions in aqueous buffered environments.

Table 3.2 Protein studies accomplished in situ with nanografted patterns of SAMs

Biomolecule	**Nanografted molecule**	**Pattern dimensions**	**Matrix SAM**	**Liquid media**	**Binding motifs**	**References**
Antibiotin IgG	1-hexanethiol	5.2 nm × 5.2 nm	Thiolated biotin SAMs	Ethanol	Specific biotinylation	[114]
Gal	Thiolated Gal	130 nm × 110 nm	Octanethiol	Ethanol	S-Au carbohydrate ligand	[81]
GalCer	Thiolated GalCer	150 nm × 150 nm	1-decanethiol	Ethanol	S-Au carbohydrate ligand	[81]
De novo 4-helix bundle protein S-824-C	S-824-C protein	100 nm × 100 nm 200 nm × 200 nm	Octadecanethiol	Mixed aqueous buffer	S-Au single cysteine thiol	[159]
De novo maltose binding protein (MBP)	MBP	50 nm × 100 nm 100 nm × 200 nm	Undecanethiol triethylene glycol	Mixed aqueous buffer	S-Au double cysteine residues at C terminus	[160]
Lysozyme	$HS(CH_2)_2COOH$	10 nm × 150 nm 100 nm × 150 nm	Decanethiol	2-butanol	Electrostatic	[81]
Staphylococcal protein A (SpA)	Mercapto-hexadecanoic acid	100 nm × 100 nm	Octadecanethiol	Ethanol water EDC/NHS	Covalent activation chemistry	[126]
Bovine carbonic anhydrase	3-mercapto-1-propanoic acid 6-mercaptohexanol	400 nm × 400 nm	$C_{11}(EG)_6$	Water	Electrostatic	[125]
Rabbit IgG	11-mercapto-undecanoic acid	5,000 nm × 5,000 nm	Octanethiol	Buffer	Covalent	[161]
Bovine serum albumin	3-mercapto-1-propanal	200 nm × 250 nm	Hexanethiol	Buffer	Covalent	[162]
Rabbit IgG mouse anti-rabbit IgG	11-mercapto-undecanal	300 nm × 300 nm	Octadecanethiol	Buffer	Covalent	[163]
Acetylcholine esterase (AChE)	$HS(CH_2)_{11}$-$(OCH_2CH_2)_3OH$	∼150 nm × 150 nm	$HS(CH_2)_{11}(OCH_2CH_2)_6O(CH_2)_{11}$-$CH(OH)CH_2OH$	Ethanol	Covalent	[164]
Insulin	$HS(CH_2)_{11}$-$(OCH_2CH_2)_3OH$	∼150 nm × 150 nm	$HS(CH_2)_{11}(OCH_2CH_2)_6O(CH_2)_{11}$-$CH(OH)CH_2OH$	Ethanol	Covalent	[164]
Anti-mouse IgG	Mouse IgG	400 nm × 400 nm	Octadecanethiol	Ethanol	Antigen-antibody recognition	[165]
Three-helix bundle metalloproteins	C-terminal thiolated protein	NA	Octadecanethiol	Trifluoro-ethanol	S-Au	[160]
Maltose binding protein (MBP)	MBP with a double cysteine	NA	Undecanethiol triethylene glycol	Buffer	S-Au double cysteine thiol	[166]

With *in situ* nanografting, the protein patterns are not exposed to air or dried, and remain in a carefully controlled liquid environment by rinsing and exchanging solutions within the liquid cell. Sequential real time AFM images can disclose reaction details at a molecular level, revealing information about the adsorption kinetics and configurations of protein binding.

The first studies using nanografting to immobilize proteins were conducted in 1999 by Gang-Yu Liu and co-workers using protocols with either electrostatic or covalent interactions to immobilize lysozyme, rabbit immunoglobulin G (IgG) and bovine serum albumin (BSA) on SAM nanopatterns.[113] In these initial investigations, functionalized alkanethiol SAMs of carboxylic acid head groups or aldehydes were nanografted to mediate either electrostatic or covalent binding of IgG and lysozyme. Proteins were sustained on patterns despite steps of washing with buffer and surfactant solutions and were stable for at least 40 hours of AFM imaging. The smallest protein feature yet produced by nanografting is a 10×150 nm^2 line pattern containing three proteins.[113]

3.7.1 Studies with Antigen-Antibody Binding Accomplished with Nanografting

The first successful AFM experiment reported that applied nanografting to study antigen-antibody binding *in situ* was conducted by Wadu-Mesthrige, et al.[112] The activity of rabbit IgG immobilized covalently on an aldehyde-terminated pattern produced by nanografting was tested for reactivity toward monoclonal mouse anti-rabbit IgG. Six aldehyde-terminated nanopatterns of different sizes and arrangement were first grafted within a dodecanethiol SAM matrix (Figure 3.7A). After injecting rabbit IgG and rinsing with a surfactant solution, selective adsorption of IgG was observed on all six nanopatterns (Figure 3.7B). In the next step, mouse anti-rabbit IgG was introduced (Figure 3.7C) revealing further increases in the heights of patterns. The changes in the height of nanopatterns before and after secondary IgG binding could be monitored *in situ*

(cursor profiles, Figures 3.7D-F), exhibiting thicknesses which correspond to the different surface configurations of IgG (Figure 3.7G).

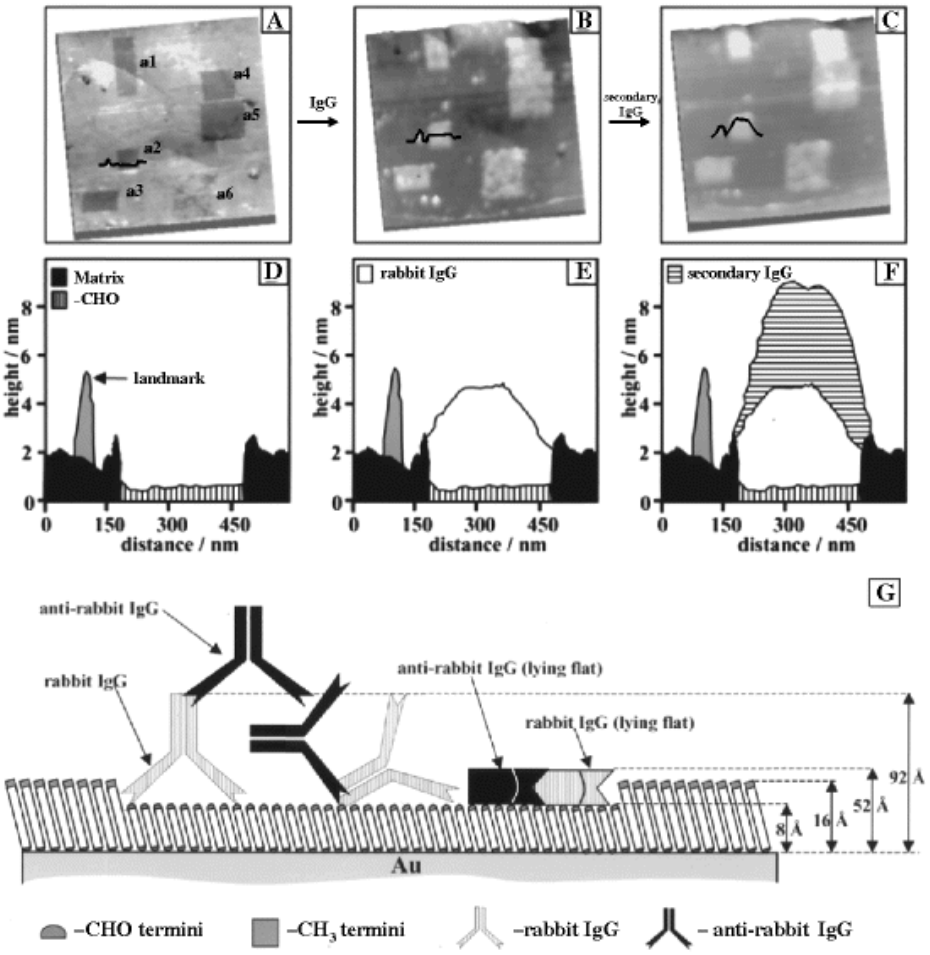

Figure 3.7 The steps of protein binding and molecular recognition with nanografted patterns captured by AFM topographic images. [A] Five nanopatterns of 3-mercapto-1-propanal were written in a dodecanethiol SAM. [B] The image contrast changed after rabbit IgG bound covalently to the aldehyde-terminated nanopatterns. [C] After introducing mouse anti-rabbit IgG, the patterns display further height changes, indicating the antibody binds specifically to the protein nanopatterns. Cursor traces across pattern a2 indicate the height changes [D] after nanografting; [E] after injecting IgG; [F] after introducing anti-rabbit IgG. [G] Map for understanding the evolution of molecular height changes during the steps of this in situ experiment. (Reprinted with permission from Ref. [162])

Changes in pattern heights were used to assess whether the immobilization chemistry resulted in a side-on or an end-on orientation for IgG molecules. The reactivity and stability of protein

nanopatterns was studied in further reports, with investigations of the retention of specific activity of the immobilized proteins for binding antibodies.[112, 167]

3.7.2 Protein Binding on Activated SAM Patterns

Chemical activation of carboxylic acid terminated SAMs was accomplished for nanografted patterns of staphylococcal protein A (SpA) through covalent linkage by Ngunjiri, et al.[111] The carboxylic acid head groups of SAMs were activated using 1-ethyl-3-(3-dimethylaminopropyl) carbodiimide hydrochloride (EDC) and N-hydroxysuccinimide (NHS) coupling chemistries.[168] The activation of carboxylic acid groups of nanografted patterns of 11-mercaptoundecanoic acid (11-MUA) was accomplished by immersing the substrate in an aqueous 1:1 mixture of NHS/EDC for 30 min to generate an activated complex with a stable reactive intermediate (N-succinimidyl ester). The resulting NHS ester interacts by a nucleophilic substitution reaction with accessible α-amine groups present on the N-termini of proteins or with ε-amines on lysine residues. The proteins bind covalently to nanografted patterns by forming a Schiff's base linkage to make complexes with the carboxylic acid groups of 11-MUA. For the *in situ* protein patterning experiment with SpA, 16 square nanopatterns (100 × 100 nm^2) of 11-MUA were written within a matrix octadecanethiol (ODT) SAM arranged in a 4 × 4 array (Figures 3.8a-c). The nanopatterns were spaced 50 nm apart within each row, and the rows were spaced at 100 nm intervals. After nanografting, a 1:1 aqueous solution of 0.2 M EDC and 0.05 M NHS was introduced into the AFM cell to react for 30 min. The cell was then rinsed twice with phosphate-buffered saline, and a solution of 0.05 mg/mL SpA solution was introduced and incubated for 30 min. Finally, the cell was rinsed with water and ethanol to completely remove any unreacted protein. After chemical activation and protein immobilization, the same array of nanostructures was imaged in ethanol with AFM (Figures 3.8d-f). All of the steps of

nanografting, NHS/EDC activation of carboxylate groups, and protein adsorption were accomplished *in situ* with the same tip, and the entire experiment was completed in ~3 hours. The SpA molecules were shown to bind selectively to the 11-MUA nanopatterns, forming a single layer of protein attached to nanopatterns of 11-MUA.

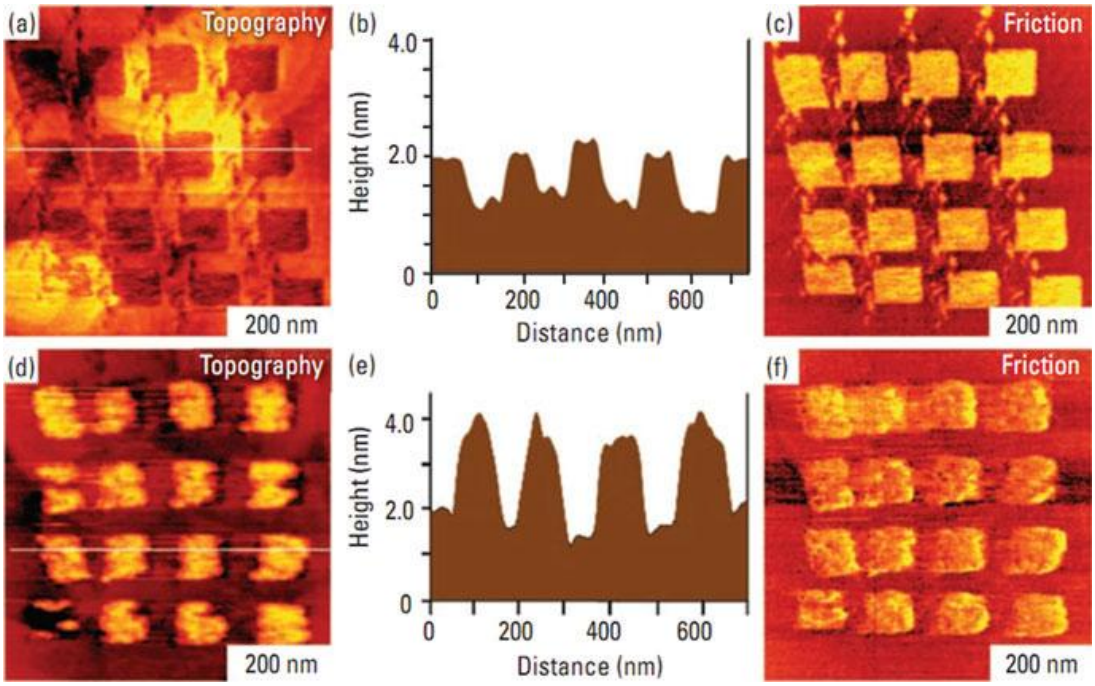

Figure 3.8 Nanoscale protein assay of the adsorption of SpA on nanografted patterns. [A] An array of 11-MUA squares written in an ODT matrix SAM, [B] cursor plot along the white line; [C] corresponding lateral force image for [A]; [D] same area after EDC/NHS activation and subsequent adsorption of SpA; [E] cursor plot along the white line in [D]; [F] simultaneously acquired lateral force image for [D]. (Reprinted with permission from Ref. [126], Copyright © American Chemical Society)

For *in situ* studies of biochemical reactions using nanografting, the most suitable immobilization chemistries for nanoscale experiments should proceed under aqueous conditions to preserve protein activity. Also, investigations should be completed using very dilute protein and reagent solutions to slow the reaction rate so that the reaction transpires over time intervals of 20–30 minutes. A potential technical detail is that the motion and force of the scanning tip can sweep away adsorbates or perturb the reaction environment. To address this concern, the

immobilization chemistry selected for patterning must be sufficiently robust to enable continuous imaging and scanning by the tip. Imaging in liquids enables using small imaging forces (0.005–0.2 nN) because the adhesive interactions between the tip and sample are minimized. An intrinsic advantage for these protocols is that small forces in the range of piconewtons to nanonewtons can be precisely controlled with AFM instruments.

3.7.3 In Situ Studies of Protein Adsorption on Nanografted Patterns

Nanografting has been applied by several investigators to write nanopatterns for studies of protein immobilization and reactivity. Zhou et al. evaluated protein adsorption at the nanoscale by comparing differently functionalized SAMs side-by-side using nanografting.[88, 125] Protein adsorption on three differently charged linkers nanografted within a hexa(ethylene glycol) terminated alkanethiol resist SAM, was monitored *in situ* by AFM at different pH conditions. The adsorption of proteins onto nanografted patches of 6-mercaptohexan-1-ol (MCH), *n*-(6-mercapto hexyl) pyridinium bromide (MHP), and 3-mercaptopropionic acid (MPA), was studied with lysozyme, IgG and carbonic anhydrase II. They concluded that the overall charge of protein molecules as well as the charge of local domains of the proteins plays a role in immobilization. In the same report, nanografting was applied to assemble multilayered protein G/IgG/anti-IgG nanostructures through electrostatic interactions, as an approach to orient IgG molecules for antibody-based biosensor surfaces.

Using SPL methods of nanografting and nanoshaving, Kenseth, et al. compared three approaches for protein patterning.[161] Nanografting was successfully combined with immobilization of IgG through EDC activation of 11-MUA acid and also through chemisorption of a disulfide coupling agent, dithiobis(succinimidyl undecanoate). Insulin and acetylcholinase esterase were immobilized on nanografted 1,2-diols which were activated by sodium periodate to

produce aldehyde groups, reported by Jang, et al.[169] Retention of catalytic activity was demonstrated for nanografted patterns of enzymes.

3.7.4 Direct Nanografting of Proteins Modified with Thiol Residues

Nanografting was applied to directly pattern designed metalloproteins by Au-S chemisorption by Case, et al.[118] A 3-helix bundle protein structure with a 78 amino acid iron(II) complex was nanografted into an ethylene glycol-terminated SAM. The protein was designed to present the C-termini of three helices, terminated with D-cysteine residues for attachment to gold surfaces. The heights of nanografted patterns of this protein measured 5.3 nm, in good agreement with the dimensions predicted theoretically for the *de novo* protein to assemble in a upright orientation normal to the Au(111) substrate. A *de novo* 4-helix bundle protein was nanografted within an ODT matrix through a single cysteine thiol by Hu, et al.[119] The protein used for these studies was engineered to have a glycine-glycine-cysteine tag at its C-terminus for attachment to the gold surface through a single cysteine thiol.

Maltose Binding Protein (MBP) was successfully patterned using nanografting by Staii, et al.[170] The MBP protein was engineered to terminate with a double-cysteine residue for chemisorptive binding to gold surfaces. The biochemical activity of the substrate immobilized proteins was verified *in situ,* demonstrating that MBP function is not altered by either the immobilization process, the spatial confinement associated with the surrounding proteins, or protein-substrate interactions. The dependence of the frictional force upon the maltose concentration was used to extract the dissociation constant: k_d =1 ± 0.04 μM for this system, detecting maltose at the level of tens of attograms.

3.7.5 Reversal Nanografting

An approach for "reversal" nanografting was introduced for regulating surface heterogeneity to control protein binding.[114] As with nanografting, the reversal method also has three main steps of imaging, shaving-and-replacement, and imaging again. However, rather than directly nanografting desired termini for protein binding, the matrix SAMs are made of the binding termini, and nanografted thiols are used to isolate and separate well- defined areas of the matrix SAMs to generate ultra-small domains of protein binding sites. By controlling the shaving size and the spacing between the shaving lines, broad areas of arrays of regular nanostructures were rapidly fabricated, achieving dimensions of 5 to 30 nm for nanografted patterns. Reversal nanografting was demonstrated with an array of thiolated biotin nanostructures which were reacted with antibiotin IgG. Within a single experiment, reversal nanografting produced 1089 biotin nanostructures measuring with 5.2 nm × 5.2 nm; 288 nanostructures with dimension of 12.7 nm × 12.7 nm; and 144 nanopatterns with dimensions of 10.3 nm × 31.9 nm. Thus, by changing the dimension and separation of each element of nanografted arrays the coverage and orientation of protein molecules can be regulated at the molecular level.

Although not yet practical for high throughput applications and manufacturing, combining the *in situ* steps of nanografting with protein immobilization enables new approaches for directly investigating changes that occur on surfaces during biochemical reactions from the bottom-up. *In situ* AFM investigations of protein reactions are valuable for studying antigen-antibody binding at the nanometer scale, for assessing the specificity of protein-protein binding, and for evaluating the orientation of immobilized proteins and the corresponding accessibility of ligands for binding.

3.8 Patterns of DNA Produced by Nanografting

Surface platforms of arrays of DNA patterns are used for studies with gene mapping, drug discovery, DNA sequencing and disease diagnosis. Scanning probe-based experiments offer compelling advantages and opportunities for high sensitivity, label-free detection with studies of molecular-level phenomena. Initial studies have been advanced using nanografting to prepare patterns of DNA with successive steps of enzyme digestion,[115, 171] hybridization studies [172-174], as well as DNA-mediated binding of proteins.[175] A comparison of the different DNA systems and pattern dimensions produced by nanografting is provided in Table 3.

Table 3.3 Studies reported with nanografted patterns of DNA

System	Pattern sizes	Matrix film	Liquid media	Year	References
DNA-derivatized gold nanoparticles	100 nm × 50 μm lines	Octadecanethiol	Buffer: 1 M NaCl, 10 mM phosphate, pH 7	2001	[173]
Single stranded DNA (ssDNA) 5'-HS $(CH_2)_6$-CTAGCTCTAATCTGCTAG 5'-HS $(CH_2)_6$-AGAAGGCCTAGA	Dimensions in nm: 115 × 135; 190 × 255; 20 × 170; 15 × 150; 25 × 160	1-hexanethiol 1-decanethiol	Mixed solvent of 2-butanol/ water/ ethanol 6:1:1 (v/v/v) containing 40 μM ssDNA.	2002	[176]
Single stranded DNA 5'-HS-$(CH_2)_6(T)_{15}$ 3'-HS-$(CH_2)_6(T)_{25}$ 5'-HS-$(CH_2)_6(T)_{35}$ 5'-HS$(CH_2)_6$ ACTGCACATGGCGTG TTGCGGTGATT CGCGTTGGT	Dimensions in nm: 120 × 200; 100 × 380; 100 × 200; 250 × 250 80 × 220; 100 × 400; 180 × 250; 40 × 250; 150 × 75	1-decanethiol	Mixed solvent of water saturated with 2-butanol and ethanol (6:1)	2005	[177]
Nanografted patterns of mercaptoethanol were used to evaluate thickness of DNA SAMs	300 × 300 nm squares of 2-mercaptoethanol	HSC_6H_{12}-5'-CCCT AACCCTAACCCTAA CCC-3'-rhodamine gree 5'-GTGTTAGGT TTAGGGTTAGTG-3'	Phosphate buffered saline (pH 4.5)	2006	[178]
λ-DNA adsorbed to octadecyldimethylmonochloro -silane (C18DMS)	100 nm × 3 μm lines of (C18DMS)	Octadecyldimethyl monochlorosilane	Nanografted patterns were incubated with λ-DNA in TE buffer (pH 7.2)	2007	[66]
Thiolated ssDNA	300 nm × 300 nm to 1 μm × 1 μm	Oligo-ethyleneglycol modified thiols	1:1 mixture of buffer and ethanol	2008	[179]
ssDNA with 44 base pairs	1 μm × 1 μm	Top-oligo ethylene-glycol (EG) HS-(CH_2)11-$(EG)_3$-OH	Thiol-DNA containing 3:2 mixtures (v/v) of 1 M buffer and ethanol	2008	[180]

Table 3.3 continued

System	Pattern sizes	Matrix film	Liquid media	Year	References
ssDNA-mediated binding of proteins thiol modified oligonucleotides	200 nm × 200 nm to 1 μm × 1 μm	Ethylene glycol-terminated alkylthiols	1:1 mixture of buffer and ethanol	2009	[181]
94 basepair thiolated double stranded DNA attached to nanografted patterns	50 nm × 50 nm	Octadecanethiol	Mixture of 11-aminoundecane thiol with DNA (10,000:1) in Tris acetate EDTA (TAE)	2010	[182]
Thiol derivatized single-stranded oligonucleotide HS-C_6H_{12}-5'-AGA TCA GTG CGT CTG TAC TAG CAC A-3' and complementary sequence	0.5–1 μm	6-mercapto-1-hexanol	10 μM probe DNA in a 1:1 mixture (v/v) of STE-buffer and absolute ethanol	2010	[183]

Individual DNA molecules can be localized within mixed patterns by diluting DNA with another alkanethiol molecule. To achieve single-molecule precision, Josephs et al., nanografted thiolated double-stranded DNA (dsDNA) with 94 base pairs from a solution containing a ~10000:1 mixture of aminoundecanethiol and dsDNA.[184] By diluting DNA molecules with another alkanethiol molecule, DNA can be positioned on a chemically well-defined, atomically flat surface and be imaged *in situ*. One to four dsDNA molecules were localized confined within a nanografted area to provide high precision for positioning individual DNA molecules within biochemical structures.

3.8.1 In Situ Studies of Hybridization with Nanografted Patterns of DNA

Nanostructures of single stranded oligonucleotides or single stranded DNA (ssDNA) have been produced with nanografting for molecular-level studies of DNA hybridization.[171-174, 176] Label-free hybridization of ssDNA nanostructures was accomplished for nanografted patterns of ssDNA incubated with complementary segments of designed sequences.[172] To mediate attachment to gold surfaces for nanografting, the DNA molecules were designed to contain a short thiol linker at either the 3' or 5' end. These investigations provide information about the

specificity, kinetics and selectivity of surface-bound ssDNA for hybridization with complementary strands.

Label-free hybridization of nanostructures has proven to be highly selective and sensitive; as few as 50 molecules can be detected by *in situ* AFM studies.[172] The efficiency of the hybridization reaction at the nanometer scale depends sensitively on the packing density of DNA within the nanostructures.[171, 172, 174] The density of ssDNA molecules within nanografted patterns can be regulated by changing certain experimental parameters such as written line density and concentration. The structure of nanografted patterns and the relative surface orientation of the ssDNA molecules have been determined *in situ* using AFM to show that molecules of ssDNA adopt a standing upright orientation.

Nanopatterns of thiolated ssDNA were produced using nanografting by Maozi Liu, et al.[176] Thiolated ssDNA molecules adsorb chemically onto exposed areas of gold through the sulfur-gold chemisorption. The ssDNA molecules within nanopatterns adopt an upright, standing orientation on gold surfaces which were found to be accessible by enzymes. A ssDNA pattern (115×135 nm^2) of an 18-nucleotide oligomer (5'-HS-$(CH_2)_6$-CTAGCTCTAATCTGCTAG) was nanografted into a hexanethiol matrix, as shown in Figure 3.9A. Nanografting and imaging of the patterns were conducted in a mixed solvent of 2-butanol/water/ethanol with a (v/v/v) ratio of 6:1:1containing 40 μM ssDNA. The heights of the nanografted patterns were found to match well with the theoretical dimensions of an upright configuration of DNA, shown with cursor profiles. In Figure 3.9C, a second 12-mer ssDNA (5'-HS-$(CH_2)_6$-AGAAGGCCTAGA) was grafted into a dodecanethiol SAM. Line patterns of ssDNA as narrow as 10 nm were produced, as shown in Figure 3.9E. Three lines of the 12-nucleotide oligomer were nanografted within decanethiol.

Unlike natural, unconfined solution adsorption of thiolated DNA on gold surfaces, in which DNA oligomers tend to assemble with the backbone parallel to the substrate in a lying down configuration, nanografted patterns of ssDNA form a standing conformation, confined by the surrounding matrix monolayer to generate a fairly dense, close-packed structure of upright strands.[172, 176] The alkanethiol matrix SAM guides the adsorption of DNA to define the geometry and packing of grafted ssDNA molecules. Upright ssDNA molecules within the nanografted structures maintain their reactivity, as demonstrated by hybridization reactions with complementary DNA in solution. The hybridization and corresponding control experiments indicate that nanografted patterns of ssDNA exhibit high specificity and selectivity towards complementary strands.

3.8.2 Reactions with Restriction Enzymes Studied Using Nanografted Patterns of DNA

Time-dependent AFM images were acquired *in situ* for a nanografted pattern of the 18-nucleotide oligomer during digestion by the enzyme shown in Figure 3.9A. The RQ1 DNase I enzyme endonucleotically degrades DNA to produce oligonucleotide fragments at the 3' end with a hydroxyl terminal group. After nanografting steps, the ssDNA patterns were rinsed and the solvent was then replaced sequentially by ethanol, water, and finally buffer solution. Next, RQ1 DNase I was introduced and surface changes were captured *in situ* with high-resolution AFM images. The liquid cell experiment establishes that upright, densely-packed strands of DNA within nanografted patterns are accessible to enzyme digestion.

Studies with the cutting action of restriction enzymes were accomplished by Castronovo. et al. to better understand enzyme/DNA interactions.[171] An enzymatic reaction (*DpnII* restriction digestion) with DNA nanopatterns of variable density (surface coverage) was investigated to

understand the effect of molecular crowding on the accessibility of the DNA molecules to the restriction enzyme.

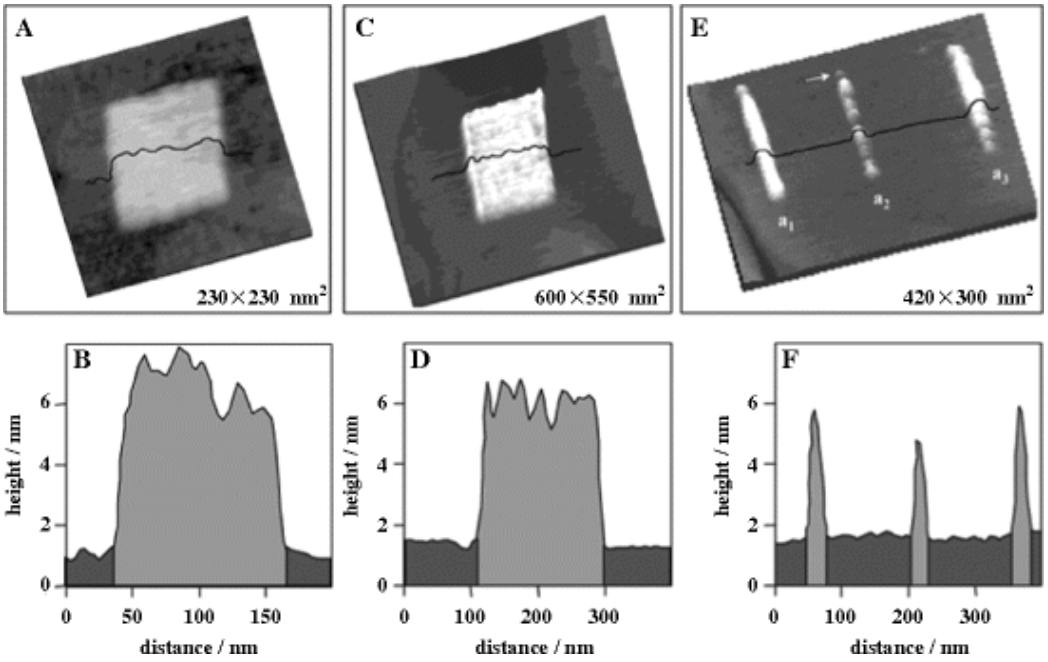

Figure 3.9 Patterns of single-stranded DNA were nanografted into an alkanethiol SAM matrix. [A] Topograph of an 18-nucleotide ssDNA nanografted into a hexanethiol SAM (115 × 135 nm2); [B] corresponding profile for the line in [A]. [C] Nanografted rectangle (190 × 255 nm2) of ssDNA with 12 nucleotides inscribed within a dodecanethiol matrix; [D] cursor profile for [C]. [E] Line patterns of the ssDNA 12-mer nanografted into decanethiol; [F] profile for [E]. The 18-mer and 12-mer ssDNA strands are 5'-HS-(CH2)6-CTAGCTCTAATCTGCTAG and 5'-HS-(CH2)6- AGAAGGCCTAGA, respectively. (Reproduced with permission from reference [176], Copyright © American Chemical Society)

Single-stranded DNA molecules containing 44 base pairs (bps) with a 4 base pair recognition sequence (specific to the *DpnII* restriction enzyme) in the middle were patterned by nanografting. The resulting nanostructures were then hybridized with a complementary ssDNA sequence of the same length to yield patterns of restriction-ready double stranded DNA. The surface density of the DNA nanostructures produced by nanografting can be tuned by changing the writing parameters or by changing the concentration of the DNA when grafting. The study demonstrates that the *DpnII* restriction enzyme is sensitive to the DNA packing density; the

enzymatic reaction is inhibited when the DNA density is higher than a certain threshold density within nanografted patterns.

3.8.3 Binding of Proteins to Nanografted Patterns of DNA

Hybrid nanostructures of DNA-protein conjugates can be produced for nanografted patterns of DNA oligomers with site-specific DNA-directed immobilization of proteins, as reported by Bano, et al.[175] In the first step, nanografted patches of thiolated ssDNA were generated within a monolayer of ethylene glycol-terminated alkylthiols ($HS\text{-}(CH_2)_{11}\text{-}(OCH_2CH_2)_3\text{-}OH$) on Au(111) substrates. In subsequent reaction steps, proteins covalently modified with cDNA sequences were immobilized onto the $1 \times 1\ \mu m^2$ nanografted patterns. A covalent conjugate of streptavidin tethered with a DNA oligomer was found to bind to the nanografted ssDNA pattern by sequence-specific DNA hybridization. The surface was carefully rinsed with phosphate buffered saline to remove any physically adsorbed molecules and imaged with AFM between successive biochemical reaction steps. Changes in heights of the patterns enabled label-free detection of protein binding between each step of the reactions, which were likewise accomplished in multiplex experiments with control samples of streptavidin that did not have the complementary DNA tethers. The nanopatterns of DNA-protein conjugates were then used for further studies of selected protein-protein interactions with an anti-streptavidin immunoglobulin G as well as with the biomedically relevant matrix of human serum. The fabrication of nanografted arrays of multiple proteins in this study demonstrates that the interactions of biomolecular recognition mediated by DNA-protein recognition are highly specific and that bound proteins retain activity for further selective binding of proteins.

3.8.4 Using Nanografted Patterns to Mediate Binding of DNA

Nanografted patterns of an aminopropyldiethoxysilane (APDES) SAM were used as sites for selective adsorption of DNA within matrices of octyldimethylmonochlorosilane (C8DMS) monolayers by Lee et al.[185] Line patterns of APDES that were 100 nm wide were nanografted in a C8DMS monolayer prepared on silicon dioxide substrates. After incubation in a 10 ng/μL solution of λ-DNA in buffer (pH 7.2) the heights of the nanopatterns was increased and revealed the shapes of individual DNA strands. The negatively charged DNA deposited on the positively charged amine-functionalized line patterns of aminosilanes. The negatively charged DNA molecules bound to nanografted patterns via electrostatic interactions with the positively charged amine groups of APDES, but did not bind to matrix areas terminated with methyl headgroups. These investigations provide a fundamental step toward sensitive DNA detection and construction of complex DNA architectures on surfaces.

Nanografting provides a useful protocol towards sensitive DNA detection and likely attains the most sensitive detection levels yet achievable for label-free assays. The DNA nanopatterning methodology provides a unique opportunity for engineering biostructures with nanometer precision, which benefits the advancement of technologies for DNA biosensors and biochips.

3.9 Limitations of AFM-Based Nanografting

Thus far, the capabilities of nanografting for molecular manipulation by nanografting have primarily been a tool for academic research. However one may anticipate that nanografting will eventually provide commercial value for chemical or biochemical sensing or for nanotechnology. A potential disadvantage for nanografting is that over time, molecular exchange reactions take place between solution molecules and the matrix SAM for certain

systems of alkanethiol matrices. Natural processes of self-exchange become an issue specifically when nanografting longer chain alkanethiols into a shorter chain matrix layer, thus it is important to use dilute (< 0.1 μM) solutions for nanografting. Depending on the nature and age of the matrix SAM, exchange reactions can be detected within 2-4 hours when molecules from solution adsorb onto defect sites and at step edges. Software addresses this problem by enabling rapid automation of the nanofabrication process. Hundreds of exquisitely regular patterns can be produced within an hour or less, leaving sufficient time to progress to further *in situ* steps of reactions before exchange reactions have occurred.

The serial nature of nanografting with a single probe may be a problem for applications that require higher throughput, such as at scales of millions of nanostructures. Prototype arrays of 1024 and 55,000 AFM probes have been developed for high-throughput nanopatterning.[186, 187] At this time, nanoscale studies with AFM enable new approaches to refine and optimize parameters used to link and organize proteins and other nanomaterials on surfaces. With *in situ* AFM characterizations, the orientation, reactivity, and stability of molecules adsorbed on SAM nanostructures can be monitored with successive time-lapse images using liquid AFM. These investigations provide the groundwork for advancing nanotechnology toward the nanoscale and furnish molecular-level information through the visualization of surface reactions.

3.10 Future Prospectus

Nanografting provides a practical tool to precisely control the arrangement of molecules on surfaces to enable bottom-up nanofabrication of structures through successive chemical reactions. *In situ* AFM studies with nanografting furnish opportunities for visualization, physical measurements and precise manipulation molecules at the nanometer scale. There are multiple advantages for nanografting, particularly because experiments are accomplished using liquid

media. Advantages are the ability to precisely produce nanometer-sized patterns of metals, polymers, proteins and DNA with the advantages of successively imaging and accomplishing fabrication within well-controlled environments. Because so many chemical reactions can be accomplished in solution, there are rich possibilities for studying other surface reactions, in ambient, cooled or heated conditions. The capabilities for capturing real time images throughout sequential steps of reactions offer intriguing possibilities for new studies, with directly viewing the role of temperature, reagents and solvents. Nanografting protocols provide an additional unique capability for defining spatial parameters for controlling surface coverage and confining reactions within defined boundaries. The challenge for future research directions will be to achieve greater complexity for experiments for building ever more sophisticated 3D architectures from the bottom-up.

CHAPTER 4. SURFACE-DIRECTED SELF-POLYMERIZATION OF 4-(CHLOROMETHYL) PHENYLTRICHLOROSILANE: SELF-ASSEMBLY WITHIN SPATIALLY-CONFINED SITES OF SI(111) VIEWED BY ATOMIC FORCE MICROSCOPY

4.1 Introduction

Model systems of *n*-alkanethiols have been well-studied, including the surface self-assembly mechanisms,[121] structures and growth.[188] Organosilane self-assembled monolayers (SAMs) were first introduced by Sagiv in 1980,[189] which offer the advantage of not requiring substrates comprised of expensive precious metals. In particular, organosilane SAMs can be formed on glass and transparent surfaces for sensing applications. The surface assembly of organosilanes is more complicated than *n*-alkanethiols and remains a target for investigation.[190] Organosilanes attach to oxidized surfaces mediated by steps of hydrolysis and condensation to form cross-linked films. Competitive reactions with adjacent molecules are difficult to control, generating multilayer films. From an applications perspective, generating interfaces of well-defined structure and composition is critical for emerging technologies based on molecularly thin organic films.

Aromatic organosilanes have previously been studied as surface layers for lithography protocols with deep UV photo irradiation,[191-194] near field scanning optical microscopy,[195] microcontact printing,[196] scanning tunneling microscopy reactive ion etching,[197] electron beam lithography[198] and x-ray lithography,[199] The benzyl halide surfaces of 4-chloromethylphenyltrichlorosilane (CMPS) furnish sites for nucleophilic substitution reactions,[200] furnishing ligands for binding DNA,[195] polymers,[201] peptide synthesis,[202] fluorescent binding assays[203] and chromophores.[204]

There are only a few methods of positioning molecules at a local scale of nanometers that will enable studies with AFM at the molecular-level. Methods of scanning probe–based lithography that have been used to create patterns of organosilanes include bias-induced lithography,[205] nanoshaving,[67] nanografting,[206] Dip-Pen nanolithography[207] and constructive nanolithography.[208] Although the size, shape and terminal group of the patterns can be exquisitely controlled with the scanning probe, each pattern is created or inscribed individually by a relatively slow, serial writing process. To scale up to produce millions of nanopatterns with high density, particle lithography methods have been developed. Particle lithography has also been referred to as nanosphere lithography[209] or colloidal lithography.[72]

Particle lithography has been used to pattern proteins,[210] metals,[211] polymers,[212] nanoparticles[213] and other inorganic materials.[214] For particle lithography, mesospheres are used as a surface mask to control the deposition of molecules or nanomaterials. Innovative protocols with particle lithography have recently been developed to pattern thiol[215-218] and organosilane[219, 220] SAMs, which enables exquisite control of the chemical functionalities presented at interfaces. The periodicity and density of SAM patterns can be precisely controlled by the diameters of mesospheres used for patterning.[221] By combining particle lithography with different deposition methods, patterns such as rings, pores or dot nanostructures can be produced.[222]

In this report, a protocol for particle lithography using immersion was applied to study the surface self-assembly of 4-(chloromethyl)phenyltrichlorosilane (CMPS) from solution. Over time, CMPS spontaneously forms multilayered surface structures through hydrolysis of Si-Cl bonds to form trisilanols which bridge into crosslinked Si-O-Si networks. Designed surface platforms with well-defined sizes of enclosed reaction sites enabled AFM characterizations of surface changes at the nanoscale for samples prepared *ex situ*. Typically, mesospheres detach

upon immersion in liquids. To address this problem, a strategy of annealing the masks of silica mesoparticles was developed to prepare nano-containers within a film of octadecyltrichlorosilane (OTS). The natural variations in the sizes of the containers provide a snapshot of the reaction progress at defined intervals up to 20 h after CMPS immersion, with fixed conditions of temperature, humidity and concentration. Controlling the selectivity and dimensions of surface sites for subsequently assembling supramolecular structures will provide information to elucidate mechanisms and kinetics of surface reactions.

4.2 Experimental Section

4.2.1 Atomic Force Microscopy (AFM)

Scanning probe microscope models 5500 and 5420 (Agilent Technologies, Chandler, AZ) were used for characterizing samples. The AFM images in Figures 2, 4, 5, and 6 were acquired with tapping mode in air using silicon nitride tips with a spring constant of 48 N/m and average resonant frequency of 176 kHz (Nanoscience Instruments, Phoenix, AZ). Figure 3 was obtained using contact mode imaging with silicon nitride tips with an average spring constant of 0.5 N/m (MSCT, Veeco Metrology, Santa Barbara, CA). Images were processed using Gwyddion.[223]

4.2.2 Nanoshaving

For nanoshaving, a higher force was applied to the AFM tip (ranging from 2 to 10 nN) to push the probe through the matrix film to make contact with the substrate. A nanoshaved pattern was generated by scanning over a small area several times, while applying a higher force than used for imaging. The local pressure at the area of contact produced sufficient shearing force to displace adsorbates during scanning, the area was swept 10 times in a raster pattern. Nanoshaving was accomplished in ethanol which enabled displaced molecules to be dissolved in

the surrounding liquid media. Afterwards, the same AFM probe was used to characterize the nanoshaved areas *in situ* by returning to a lower force setting.

4.2.3 Immersion Particle Lithography

The general procedure for particle lithography is outlined in Figure 1. Silicon wafers (Virginia Semiconductor, Frederickburg, VA) were cut into small pieces (1×1 cm^2) for use as substrates. Surfaces were cleaned by immersion in piranha solution for 30 min. Piranha is a mixture of sulfuric acid and hydrogen peroxide at a (v/v) ratio of 3:1. Caution: Piranha solution is highly corrosive and should be handled carefully. First, a drop of monodisperse silica mesospheres was deposited on Si(111) and dried (Figure 4.1A). To enable sustained immersion in solvent solutions with mesoparticle masks, a heating step was developed to solder the beads to the substrate. The samples were heated briefly to anneal the mesospheres to the surface (100°C for 15 min), before immersion into OTS solutions. The annealed films of mesospheres were used as masks for surface patterning. The samples were cooled to room temperature (25 °C), then immersed into 0.1% octadecyltrichlorosilane (Gelest, Morrisville, PA) in anhydrous toluene for 12 h. Silane molecules assembled on the substrate except in the areas where mesospheres were attached to the surface. Next, the samples were rinsed copiously with deionized water and sonicated with ethanol to remove the silica mesospheres (Figure 4.1B). The center-to-center spacing between the nanopores corresponds to the diameter of the mesosphere masks. In the final step, the nanopatterned samples were submerged into a 0.006 M solution of 4-chloromethylphenyltrichlorosilane (Gelest, Morrisville, PA) in anhydrous toluene (Figure 4.1C). Samples were removed at successive intervals to evaluate surface changes over time (30 min, 1 h, 20 h, 24 h). Samples were rinsed with acetone and chloroform with sonication and dried under

argon. The uncovered areas of Si(111) that had been masked by mesospheres provided well-defined surface sites for directing the subsequent attachment and growth of CMPS.

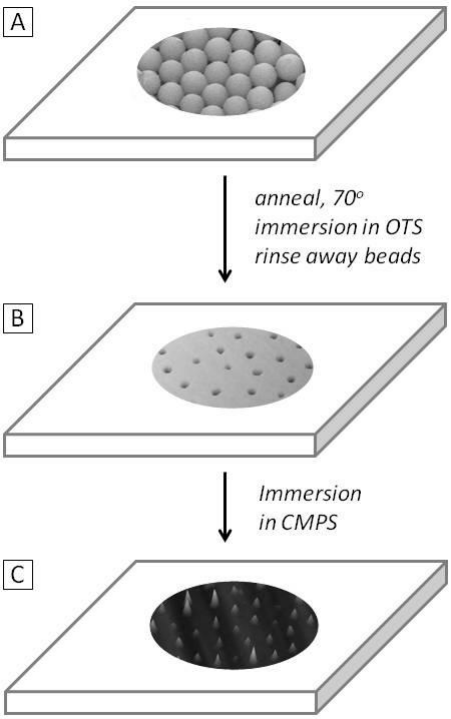

Figure 4.1 General steps for immersion particle lithography. [A] A mask of silica mesospheres was deposited on the surface of Si(111); [B] After rinsing away the mesospheres, a porous film of OTS was formed on the substrate; [C] The nanopores were backfilled with CMPS by an immersion step.

4.3 Results and Discussion

Studies of molecular self-assembly and intermolecular interactions are critical in the field of supramolecular chemistry. Our experimental strategy combines the local spatial resolution of particle lithography with molecular self-assembly to prepare arrays of nanostructures with designated periodicity. Millions of nearly regular nanopatterns can be generated using basic steps of particle lithography (mixing, rinsing, drying, heating, centrifuging and sonication) to enable exquisite nanoscale control of the geometry, density, and interfacial chemistry of surfaces. For

this study, nanopore structures produced within a film of OTS were used as nano-containers to designate sites for the growth of CMPS. Of course, at the nanoscale there are small variations in the geometry and sizes of the nano-containers that are produced. This provides an opportunity to evaluate the size-dependent spatial effects of confinement as a function of exposed surface area.

4.3.1 Confined Nano-Containers

Views of the nano-containers are shown in Figure 2. Nanopores or holes within an OTS thin film were generated on Si(111) using particle lithography combined with solution immersion. Within an area of 2×2 μm^2 there are 48 holes, measuring 1.2 ± 0.2 nm in depth (Figure 4.2A), with an average surface area of 0.003 ± 0.001 μm^2. The holes are the sites where the silica mesospheres were displaced from surface. The grooves in the background are due to the natural roughness of polished silicon wafers. The imperfections of the substrate influence the order and periodicity of the mesosphere masks, as well as the uniformity of the pore geometries. The simultaneously-acquired phase image (Figure 4.2B) more clearly defines the shape of the sites of uncovered substrate. A close-up view of three nanostructures (Figure 4.2C) reveals that the shapes of the nanoholes are not always circular. The center-to-center spacing of the holes measures 250 nm, which matches the diameter of the silica mesospheres used as a patterning mask. The shapes of the nano-containers are smaller in the phase image (Figure 4.2D) compared to the corresponding topography frame because the height images do not distinguish defined edges of the nanopatterns as clearly and measurements include convolution effects of the tip shape. Using the topography images, the surface coverage of uncovered sites measures 2.7%; whereas the lateral force image reveals that the area of the nanopores measures 1% of the surface. Cursor profiles across two of the nanopores indicate the local thickness of the OTS film

ranges from 1.5 to 1.7 nm (Figure 4.2E). A view of a single nanohole is presented in Figure 4.2F, revealing the surface texture of the surrounding OTS domains.

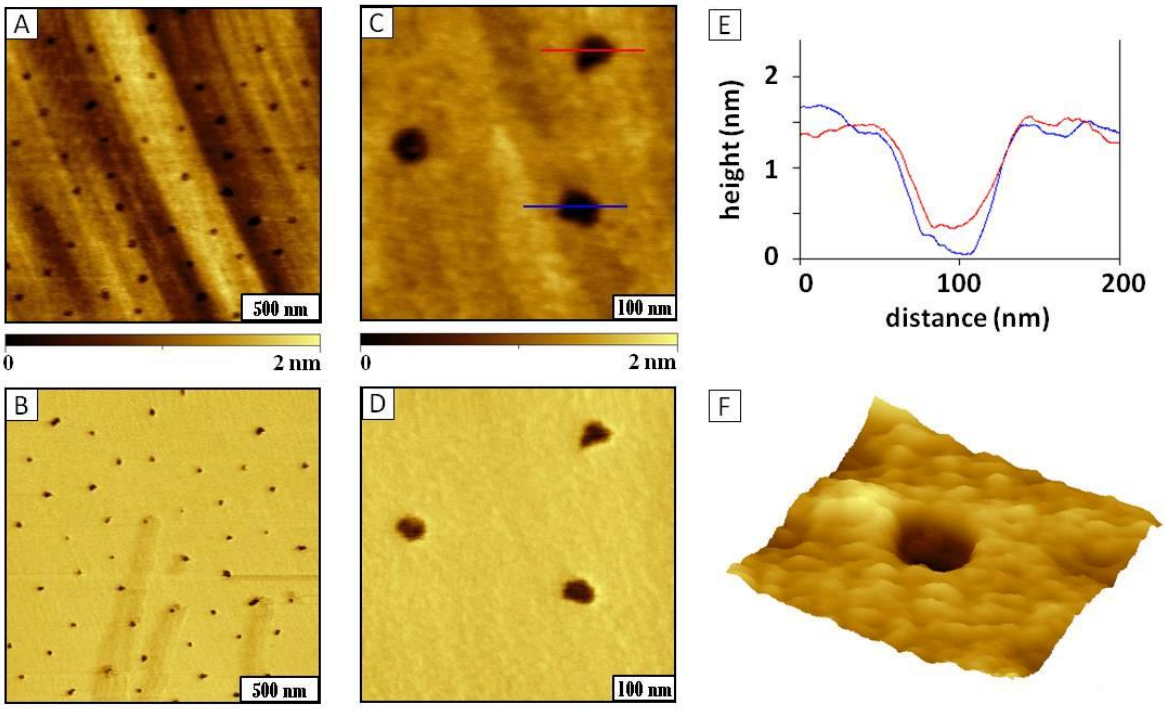

Figure 4.2 Nanopores within a film of OTS viewed by AFM. [A] Topography frame, 2×2 μm^2; [B] corresponding phase image; [C] higher magnification topograph, 0.5×0.5 μm^2; [D] phase image; [E] cursor profile across two patterns traced in ***C***; [F] view of a single nanopore.

To further evaluate the thickness of the OTS film, a protocol known as "nanoshaving" was accomplished by applying high mechanical force to the AFM tip to sweep away the OTS film from a selected area.[224] A square pattern was produced by nanoshaving in air as shown in Figure 4.3A. The pattern measures 500×500 nm^2 and has a depth that is similar to that of the nanopores, ~ 1.2 ± 0.2 nm, which is shorter than the value expected for a densely packed SAM of OTS. The depth of the pattern and holes are compared side-by-side with the cursor profile in Figure 4.3B.

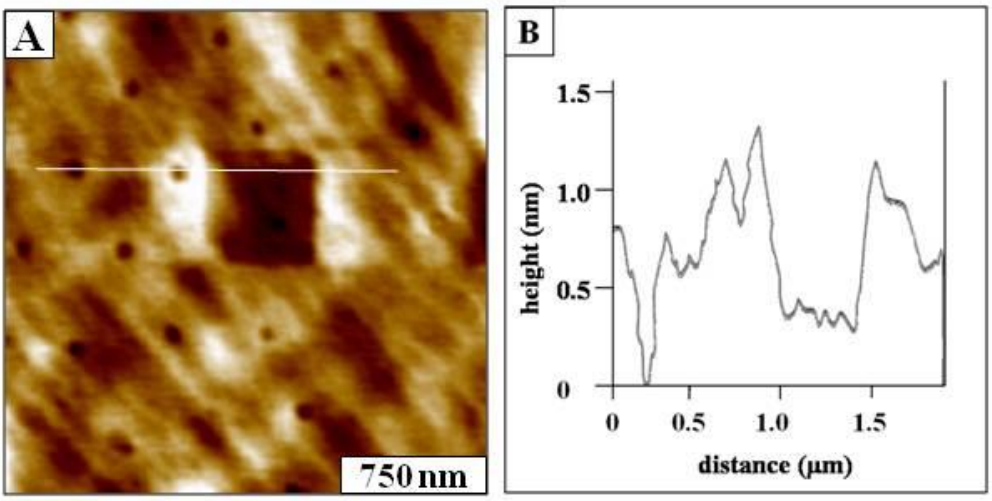

Figure 4.3 Square pattern nanoshaved within the OTS film with nanopores. [A] Topography, 2.5×2.5 μm^2; [B] cursor profile across the nanopores and nanoshaved area.

The thickness of OTS films from ellipsometry measurements have been reported to range from to 2.25 to 2.81 nm for densely-packed monolayers formed on silicon substrates.[225-227] In a dense arrangement, the alkyl chains of OTS adopt an all-trans configuration with tilt angles that range from 0 to 17°. The range of measured values can be attributed to changes in surface coverage as well as differences for the methods of sample preparation for OTS. Immersion of a substrate in solvents is the most common approach for preparing films of organothiols, and has produced the most consistent thickness of a monolayer.

4.3.2 Backfilling Nano-sized Containers with CMPS

By backfilling nanopores produced with particle lithography, exquisitely tiny spatially confined surface sites can be used for studying successive changes after further reaction steps. The combination of chemical synthesis combined with surface engineering likewise provides a unique opportunity for studying spatial confinement effects for surface-based chemical reactions at the molecular level within well-defined nanoscopic areas. Surface patterns of organic thin films can be used as confined nano-containers for building supramolecular structures through

sequential chemical reactions. Successive changes of the surface topography can be viewed after each reaction step.

The progressive surface changes during the growth of CMPS nanostructures were characterized with high-resolution AFM at different intervals of time to reveal molecular-level details of the surface assembly and self-polymerization of CMPS. The sample with nanopores within an OTS film on Si(111) was immersed in CMPS/toluene solution and removed after 30 min (Figure 4.4). The nanostructures of CMPS initially form small islands within the central areas of the nanopores and have a boundary surrounding the edges near the inner walls of OTS. Nearly all of the pores evidence growth of CMPS nanostructures (Figures 4.4A-C). After 30 min, the CMPS has not completely filled the nanopores; however the height of the CMPS structures corresponds to a multilayer which is taller than the initial height of the surrounding OTS film. The Si(111) substrate can no longer be distinguished to reference as a baseline for height measurements, therefore the OTS matrix is used as a height ruler. A representative cursor measurement across two CMPS nanostructures reveals the heights and lateral dimensions of backfilled CMPS (Figure 4.4D). The nanostructures are approximately 0.5 ± 0.2 nm taller than the OTS matrix; therefore the overall thickness would measure 2.1 ± 0.2 nm. Since the theoretical length of CMPS is 0.75 nm this corresponds to a trilayer of CMPS formed after 30 min.

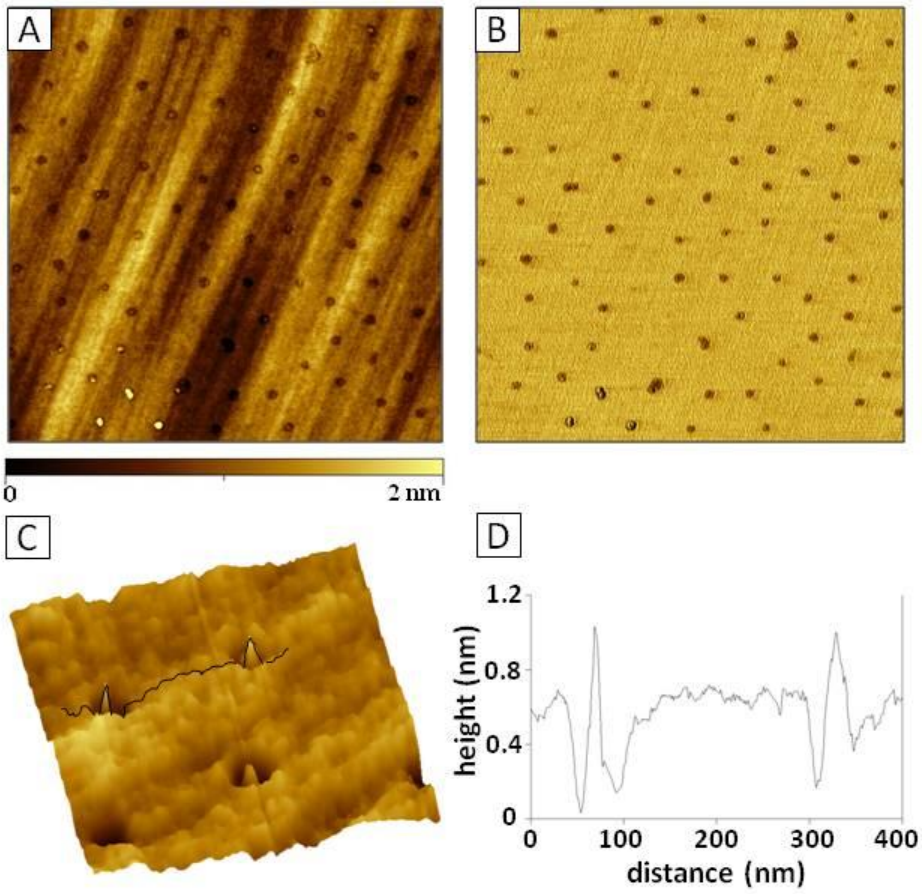

Figure 4.4 Nanostructures of CMPS after 30 min immersion. [A] Topography frame, 2.5×2.5 μm^2; [B] corresponding phase image; [C] Zoom-in view of CMPS nanostructures, 0.6×0.6 μm^2; [D] cursor profile for the line in ***C***.

After longer immersion, the nanostructures increased in height and width, as shown in Figure 4.5. A representative topography image (Figure 4.5A) after 1 h immersion reveals the periodic arrangement of 14 nanostructures of CMPS formed on Si(111) inside the OTS nano-containers. The heights of the nanostructures are not consistent, smaller nanopores appear to have formed smaller nanostructures. Details are more clearly viewed in Figure 4.5B for a single nanostructure of CMPS. There is a dark ring surrounding the CMPS nanostructure, indicating that the CMPS did not fully fill the nanoholes and avoided growth at the edges near OTS sidewalls. There are multiple tips at the apex of the nanostructure, resulting from additional

nucleation sites being formed during growth. A view of three nanostructures is presented in Figure 5C. The cursor profile (Figure 4.5D) discloses heights measuring 3 nm and 8 nm above the OTS matrix, corresponding to 4-10 layers of CMPS. The nanostructures became taller and wider in dimension, according to the initial size of surface sites.

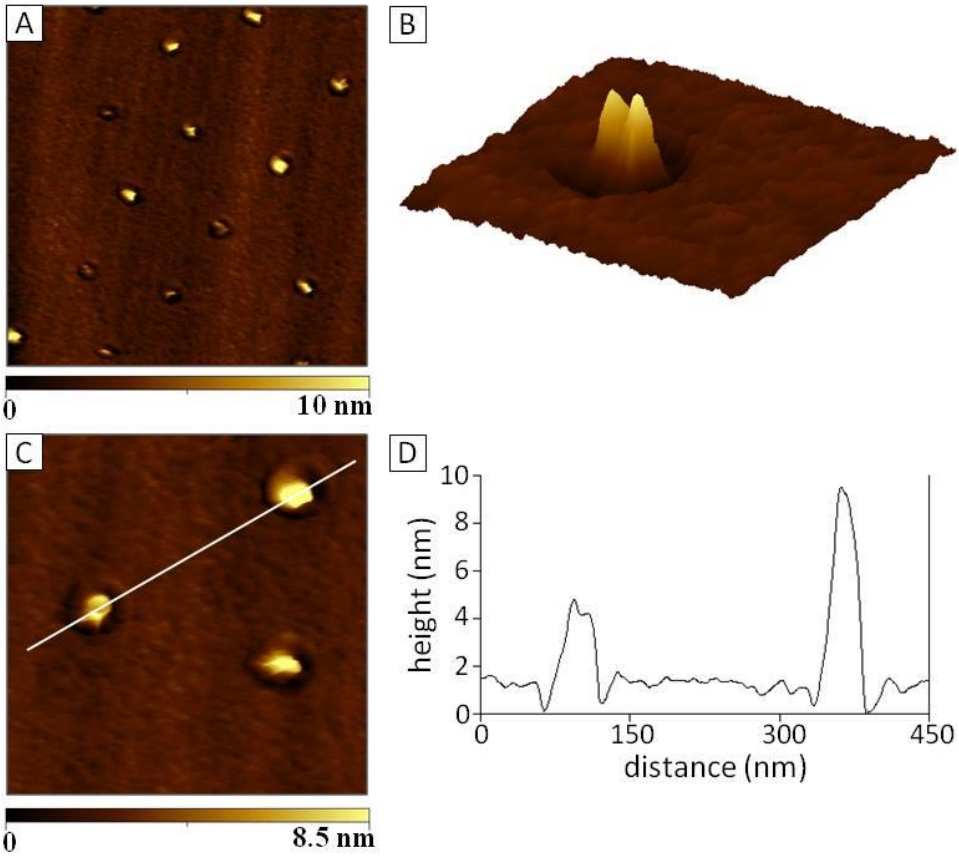

Figure 4.5 Surface changes after 1 h immersion in CMPS. [A] AFM topograph, 1×1 μm^2; [B] view of a single structure, 200×200 nm^2; [B] Topograph, 400×400 nm^2; [D] cursor profile across two patterns traced in ***C***.

To assess whether the self-polymerization of reactive chloro groups of CMPS continued with extended immersion, later timepoints were evaluated. After 20 h immersion in CMPS, the nanostructures were observed to increase further in length and width as shown in Figure 4.6. Larger cluster-shaped nanostructures are observed throughout the sample within the OTS nanopores. A representative topograph is presented in Figure 4.6A showing 14 nanostructures.

The growth of CMPS remains confined within the sites of the nanopores, and adsorption is not detected on surrounding matrix areas passivated with OTS. A single CMPS nanostructure is shown in Figure 4.6C, revealing that multiple nucleation sites were formed over time. The edges of the OTS can be clearly resolved, indicating that CMPS growth is directed in the vertical direction without branching in lateral directions beyond the borders of the nanopores. A view of three nanostructures in Figure 4.6C reveals that the structures have grown taller and slightly wider, to mostly fill the OTS nanopores. The heights of two of the nanostructures measure 18 and 20 nm (Figure 4.6D) which corresponds to 24-28 multilayers of CMPS.

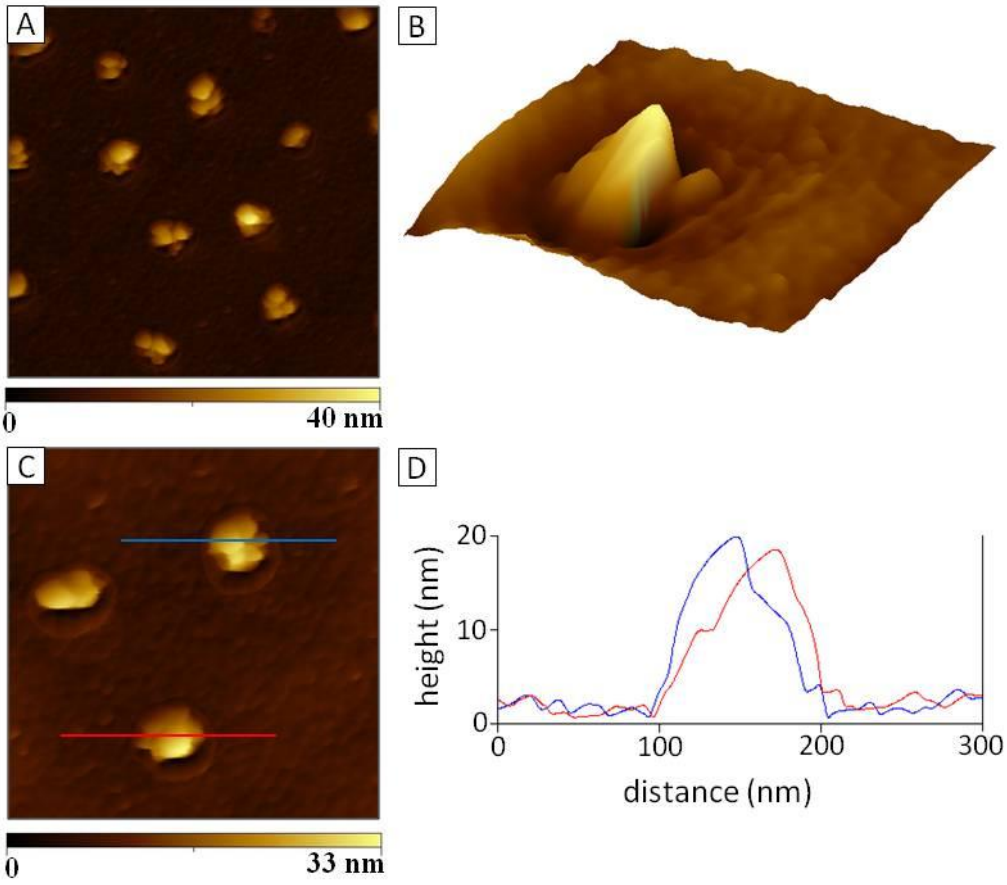

Figure 4.6 Spatially-contained nanostructures of CMPS formed after 20 h immersion. [A] Topograph, 1×1 μm^2; [B] close-up view of a single nanostructure; [C] topograph, 0.5×0.5 μm^2 [D] cursor profile across two patterns traced in ***C***.

4.3.3 Analysis of Size Changes for CMPS Nanostructures

Initially, CMPS molecules started to grow at nucleation sites near the center of the nanoholes, and a cross-linking reaction produced multilayers over time in a vertical direction. An approximate model of the self-polymerization scheme is shown in Figure 4.7, as previously proposed by Brandow, et al.[228] The CMPS nanostructures grow through hydrolysis of the Si-Cl groups to form silanols to produce a cross-linked network. A trace amount of water is needed to convert the chloro groups to hydroxyl groups. Our samples were prepared using anhydrous toluene to minimize the amount of water to that produced by ambient humidity.

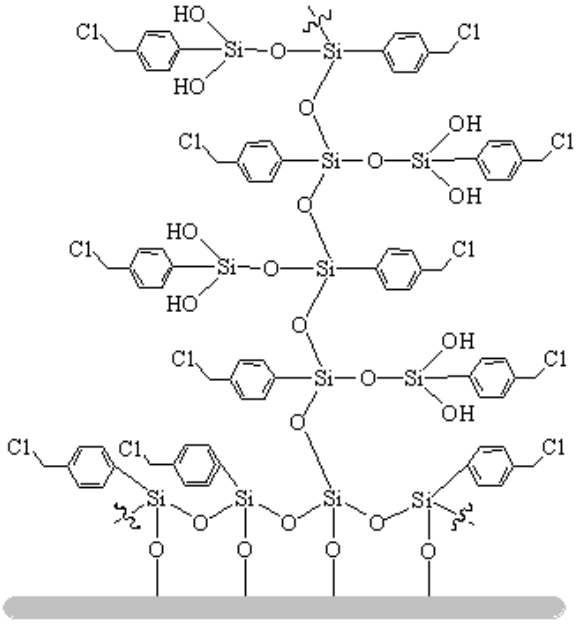

Figure 4.7 Model of the self-assembly of CMPS.

Measurements of the heights and surface area of CMPS nanostructures after different intervals of immersion are summarized in Table 4.1. Both the height and surface area increase as time progressed, however any polymer branching was constrained by the sides of the nano-containers. The heights indicate multilayers were formed over time, with taller structures

produced by longer immersion. Therefore, CMPS primarily increased in a vertical growth mode, and larger surface sites produced structures with wider diameters.

Table 4.1 Surface changes after different intervals of immersion in CMPS.

Immersion time (h)	Height (nm)	Height range (nm)	Average surface area (μm^2)	Surface area range (μm^2)
0.5	3.6 ± 1.1	1.9 – 5.1	0.0005 ± 0.0002	0.0004 – 0.001
1	7.4 ± 2.2	2.8 – 11	0.006 ± 0.002	0.001 – 0.008
10	10 ± 2.1	6.3 – 16	0.008 ± 0.001	0.001 – 0.01
20	20 ± 3.8	12 – 33	0.01 ± 0.002	0.007 –0.02

The correspondence of the nanostructure growth to the initial sizes of nanopores is shown more quantitatively in Figure 4.8. The maximum heights of CMPS nanostructures versus the surface area of the nanopores were plotted for immersion times of 1 h and 20 h. The trends indicate that larger surface sites produce taller structures, and correspondingly the growth of shorter structures was observed for smaller surface sites. As time progressed, CMPS nanostructures filled the areas within the holes but did not spread out beyond the edges of the OTS nano-containers. The methyl-terminated headgroups of OTS provided an effective surface mask to prevent non-specific adsorption of CMPS.

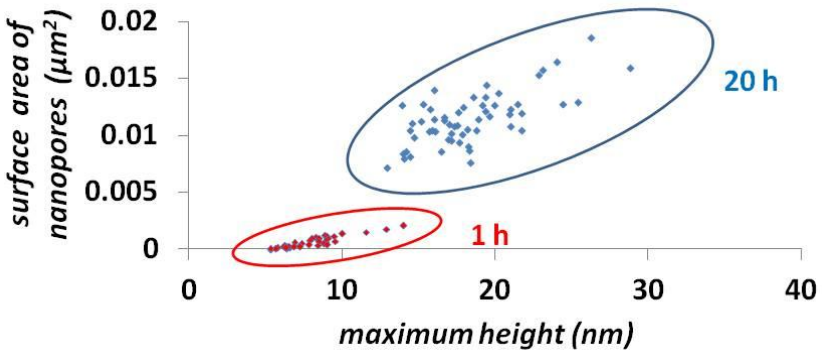

Figure 4.8 Correlation of the heights of CMPS nanostructures versus the surface area of OTS nanopores.

It is well-known that chemisorption of trichlorosilanes from solution onto oxide surfaces is influenced by factors such as the nature of the solvent and substrate, temperature, humidity, concentration and adsorption time.[219, 228, 229] For this study, the *ex situ* experiments primarily evaluated surface changes as a function of immersion time using fixed conditions of solvent, humidity, temperature and concentration.

4.4 Conclusion

An approach based on particle lithography was tested for nanoscale studies of CMPS surface reactions, using test platforms of well-defined nano-containers within a passivating OTS resist. Details of the surface assembly and subsequent self-polymerization of CMPS within confined, nanoscopic areas were studied *ex situ* using AFM. As time progressed, the heights of CMPS nanostructures increased according to the initial sizes of the surface sites of OTS nanoholes. Multilayers formed over time intervals of 0.5 to 20 h. Further directions for this research will be to study the assembly of different designs of organosilane molecules, to gain insight for the dynamics and mechanisms of self-assembly reactions on silicon surfaces.

4.5 Acknowledgements

This research was supported by the National Science Foundation Career program (CHE-0847291, PECASE award) and by the Dreyfus foundation, Camille Dreyfus Teacher-Scholar award.

CHAPTER 5. SURFACE ASSEMBLY OF 1,1,1-TRIS(MERCAPTOMETHYL)-HEPTADECANE ONTO AU(111) VIEWED WITH TIME-LAPSE AFM

5.1 Introduction

Multidentate adsorbates attach to gold surfaces through multiple linkers which provide greater stability compared to monothiolated self-assembled monolayers (SAMs) of *n*-alkanethiols. Although detailed investigations of monothiolated SAMs have been reported, relatively few studies have been accomplished for bidentate or tridentate thiol adsorbates. One may predict that bulkier geometries of multidentate SAMs would exhibit distinct changes for the kinetics, stability and surface organization in comparison to equivalent geometries of monothiolated *n*-alkanethiol SAMs. The synthesis of multidentate thiol-based adsorbates offers opportunities for generating interfaces of well-defined structure and composition designed to have either bidentate or tridentate thiol groups, a crosslinked junction, and tailgroups of tunable chemical composition. The nature of the headgroup, junctions, hydrocarbon backbone, and tailgroups enable designs of complex architectures for applications with surface patterns.

From an applications perspective, generating interfaces of well-defined structure and composition are critical for emerging nanotechnologies based on molecularly thin organic films. The stability of organosulfur-based adsorbates on noble metal surfaces is a consideration for applications of self-assembled monolayers (SAMs), which impacts the reliability and durability of the related products.[230-240] To realize the full potential of patterning surfaces for manufacturing processes, challenges need to be addressed for designing robust surface coatings that resist damage. Multidentate molecules provide a model surface that will resist self-exchange and surface migration, and enable further steps of chemical reactions with high fidelity. Degradation of alkanethiol SAMs on metal surfaces is caused by UV exposure, thermal desorption, and

oxidation. It has been reported that SAMs designed with longer chain lengths are more thermally stable than those with shorter chains.[241-244] Multidentate thiols have been investigated as a means to improve the overall stability of alkanethiol SAMs, by forming multiple bonds between a molecule and the surface.[245, 246] Several new classes of multidentate alkanethiols have been synthesized which have two or three legs and a binding group at each end of the legs.[238, 245, 247-249] By appropriate design of the anchoring point, multidentate alkanethiols bind to multiple sites on a noble metal surface. The trend in thermal stability is tridentate alkanethiol > bidentate alkanethiol > *n*-alkanethiol.[238] Multidentate adsorbates form stable films that resist desorption and exchange and also resist diffusion across the surface of gold, offering opportunities to generate robust surface nanopatterns.

Details of the surface self-assembly of tridentate alkanethiols on Au(111) have not yet been reported. Bulkier multidentate SAMs will exhibit differences for the kinetics, stability and surface organization in comparison to *n*-alkanethiols. Within a liquid environment studies of surface reactions can be accomplished using time-lapse atomic force microscopy (AFM) imaging. To better understand the surface structure and self-assembly process for multidentate thiols, we designed an *in situ* AFM study of a tridentate molecule, 1,1,1-tris(mercaptomethyl)-heptadecane (TMMH). The orientation of TMMH on the surface was investigated using approaches with liquid imaging and scanning probe lithography. Using a liquid sample cell, fresh reagents can be introduced to the system and step-wise changes of surfaces before and after nanofabrication can be captured *in situ*. Side-by-side comparisons of the surface structures of multidentate adsorbates versus *n*-alkanethiol SAMs were accomplished to give a local measurement of film thickness, referencing the well-known dimensions of *n*-alkanethiols as a baseline.

5.2 Experimental Section

5.2.1 Materials and Reagents

Octadecanethiol and dodecanethiol were purchased from Sigma Aldrich (St. Louis, MO) and used as received. The tridentate molecule 1,1,1-tris(mercaptomethyl) heptadecane (TMMH) was synthesized at the University of Houston, in Dr. T. Randall Lee's laboratory. Ethanol (200 proof) was obtained from AAper Alcohol and Chemical Co. (Shelbyville, KY). Flame-annealed gold films on mica substrates (150 nm thickness) were obtained from Agilent Technologies (Phoenix, AZ). Template-stripped gold films were prepared on glass slides using Epotek 377, as previously described by Wagner et al.[250]

5.2.2 Atomic Force Microscopy (AFM)

Either a model 5500 or 5420 scanning probe microscopes (Agilent Technologies, Chandler, AZ) equipped with PicoView v1.8 software were used for the AFM characterizations and scanning probe lithography. Images were acquired using contact mode in a liquid cell which can hold up to 1 mL of solution. Imaging and fabrication were accomplished with silicon nitride tips which had an average spring constant of 0.5 N/m (Bruker Instruments, Camarillo, CA). Digital images were processed and analyzed with Gwyddion v.2.25 software.[251] Analysis of surface coverage was accomplished by manually selecting a threshold value to convert images to black and white data sets, and counting pixels using the UTHSCSA *ImageTool* program (developed at the University of Texas Health Science Center at San Antonio, Texas and available from the Internet by anonymous FTP from maxrad6.uthscsa.edu).

5.2.3 AFM Study of the Self-Assembly of TMMH from Solution

A piece of template-stripped gold on glass was placed in the liquid cell and imaged continuously. Initially, the sample was imaged in ethanolic media to obtain a representative view

of the gold substrate. Next, a solution of TMMH (0.01 mM) in ethanol was injected into liquid cell to monitor the growth of TMMH *in situ.* After introducing TMMH solution into the sample cell, images were acquired every 15 min for 3 h for the same area. After 3 h, the tip was moved to image a new area to minimize the effects of perturbing the surface by the scanning probe and images were taken every 30 min.

5.2.4 Scanning Probe Lithography (Nanoshaving and Nanografting)

Nanoshaving experiments were accomplished by applying a high force (2-5 nN) to sweep a selected area ten times at 256 lines/frame in ethanol. The nanoshaved patterns could be imaged *in situ* using the same probe by returning to low force. Nanografting experiments were accomplished by sweeping an area under high force in a liquid cell containing an ethanolic solution of the molecule to be patterned. Solutions of either octadecanethiol or dodecanethiol solutions were prepared at a concentration of 1 mM for nanografting. A dodecanethiol SAM was prepared by immersing a piece of template stripped gold in a 1 mM ethanolic solution for 12 h. A monolayer film of TMMH was prepared by immersing a piece of template stripped gold in a 0.01 mM ethanolic solution for 72 h.

5.3 Results and Discussion

Liquid environments expand the capabilities for scanning probe protocols to provide insight for dynamic processes at the nanoscale. Liquid AFM imaging has advantages for studies, particularly for conducting *in situ* investigations of chemical or biochemical reactions.[252] Liquid media has benefits for improving resolution, since the amount of force applied between the tip and sample can be reduced.[253] Surface changes after immersion in different liquids can be investigated using time-lapse AFM imaging. Investigations of surface changes throughout the course of chemical self-assembly reactions have been monitored with AFM in liquid media.[254]

Further, by injecting new molecules into the sample cell, AFM-based nanofabrication can be accomplished using protocols of nanoshaving and nanografting.[79, 255] Of course, the solvents chosen for AFM liquid experiments should be optically transparent, and must have a relatively slow rate of evaporation, e.g. water, ethanol, butanol or hexadecane.

5.3.1 Surface Self-Assembly of TMMH

A liquid AFM study was accomplished using time-lapse imaging to investigate surface changes during the self-assembly of TMMH molecules on template-stripped gold (Figure 5.1). The surface was imaged in ethanol before injecting the TMMH solution (Figure 5.1A). The image reveals relatively flat domains bordered by several cracks and scars, the sites of the defects furnish reference landmarks for *in situ* imaging. After injecting a solution of TMMH in ethanol (0.01 mM) into the liquid cell, small changes were observed during the first hour. At this concentration, few adsorbates became apparent after 1 h (Figure 5.1B). Increases in surface coverage were readily detected as time progressed, time-lapse images after 2, 2.5 and 3 h are presented in Figures 5.1C-5.1E with a distinct arrangement of surface landmarks to anchor the location for acquiring successive images. However, as the surface coverage of TMMH increased the landmarks became indistinguishable. To continue the experiment, a square region was shaved clean to provide a reference location for further time points (Supplemental Figures 1 and 2). For nanoshaving, a higher force was applied to the AFM tip during scans to sweep away TMMH molecules from the gold surface (Figure 5.1E). The experiment was terminated after 6 h before the surface reached saturation coverage (Figure 5.1F).

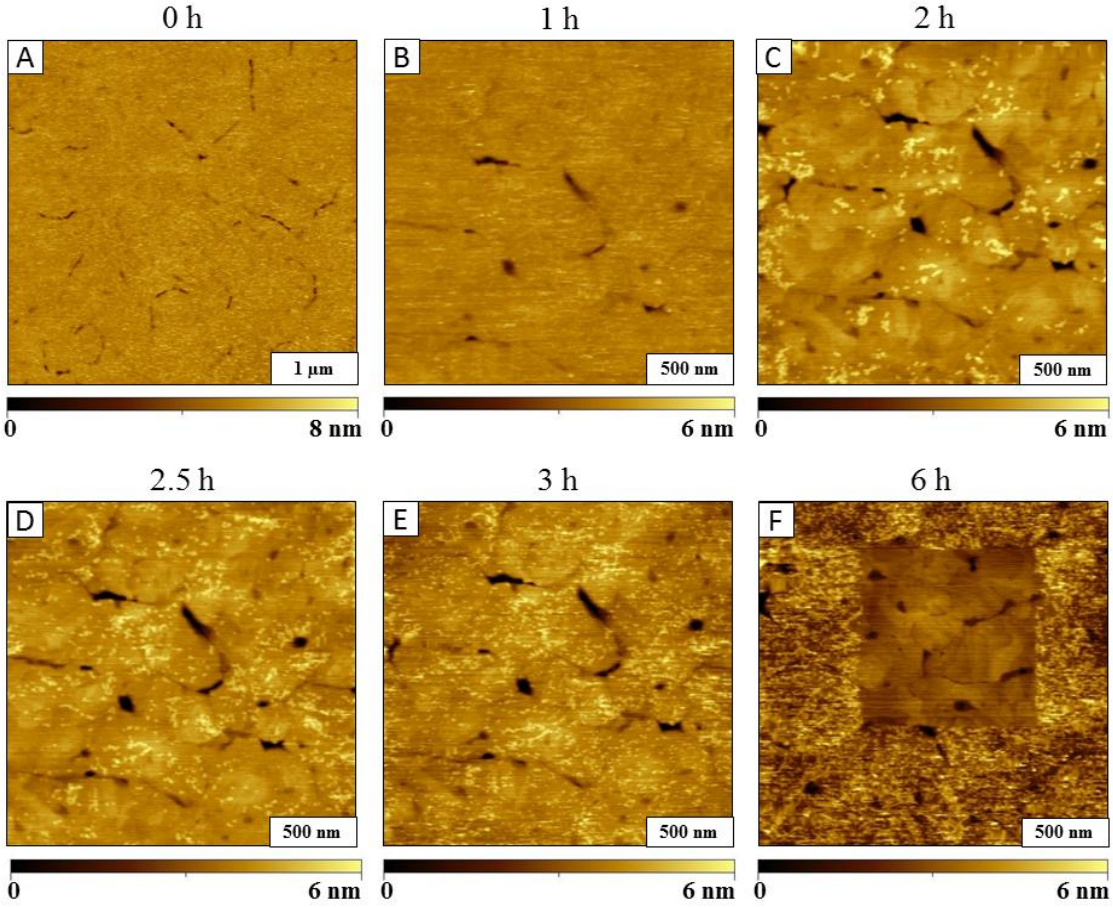

Figure 5.1 Solution self-assembly of TMMH on Au(111) viewed by time-lapse AFM. Topography images taken at [A] 0 h; [B] 2 h; [C] 2.5 h; [D] 3 h; [E] 6 h after injection of TMMH solution.

With higher magnification, the thickness of the adsorbates can be measured (Figure 5.2). The initial bright structures (Figure 5.2) appear to attach preferentially to the edges of gold terraces; however at this magnification it is difficult to be certain. Unfortunately, there are multiple overlapping terraces throughout the areas of the substrate, so the evidence is not conclusive. Several heights are apparent for the adsorbates ranging from 0.5 to 2.2 nm. The shortest structures correspond approximately to the thickness of an alkane chain, with a side-on orientation. This concurs with the height expected for a physisorbed phase, and is evidence that there is a phase transition from lying-down to an upright orientation. The tallest heights

measured are 2.2 nm, and this value corresponds to a standing upright configuration of the TMMH which has a theoretical length of 2.3 nm. However there seems to be rearrangement of the standing phase at later timepoints during the course of self-assembly to form a condensed film of shorter heights.

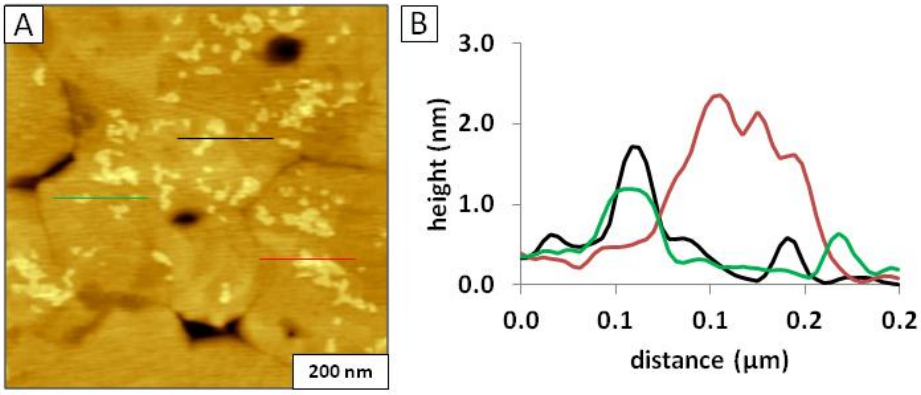

Figure 5.2 Representative cursor profiles of the side-on and standing phases of TMMH measured at 2.5 h.

Kinetic trends for the surface-assembly of the taller phase of TMMH are plotted in Figure 5.3. The binding of TMMH is relatively slow at this concentration as compared to regular *n*-alkanethiols, which evidence adsorption within minutes and typically form a monolayer within an hour or less. As shown by the surface coverage estimates in Figure 5.3, after 2 h, the rate of surface adsorption of TMMH increased. This suggests that intermolecular interactions influence the rate of surface attachment. After TMMH has bound to surface sites, molecules begin to associate and attach to the surface more quickly. These preliminary results achieved at a fixed low concentration corroborate our observations that greater time is required to form complete monolayer films of TMMH. Incomplete monolayers were observed for brief immersion steps, and mature SAMs required at least 24 h immersion. The initial studies with tridentate TMMH molecules evidence slower adsorption kinetics (> 6 h), in comparison to monothiolated SAMs, which typically form dense monolayers within an hour.

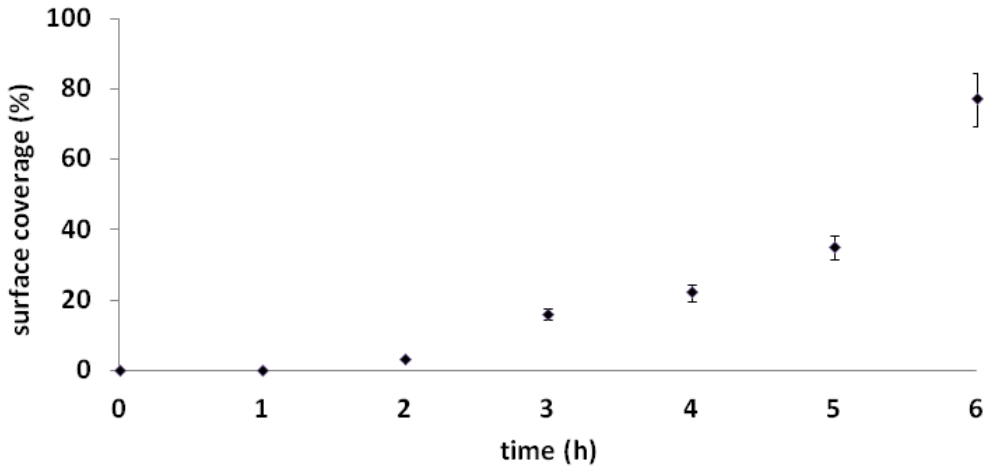

Figure 5.3 Gradual increase in surface coverage of the taller phase of TMMH as time progressed.

5.3.2 Nanoshaving of TMMH Film on Gold

A convenient way to locally measure the thickness of an organothiol film with liquid AFM is to shave away a small area of the surface by applying higher force to the AFM probe and sweeping. A nanoshaving example is shown in Figure 5.4 for a 200 × 200 nm^2 area of gold that was uncovered by the AFM tip. Some of the molecules are deposited at the left and right sides of the nanopattern, evidenced by the bright edges. However, most of the molecules dissolve in the liquid media or are swept away by the scanning action of the AFM tip. A possible concern when increasing force to the AFM tip is that the probe might become dull or break. However, the tip retains its sharpness because you can so clearly resolve the pinhole defects and contours of the step edges of the underlying gold beneath the SAM of TMMH (Figure 5.4A). In comparison to the example of nanoshaving in Figure 5.1, the SAM is more densely packed after 30 h immersion in TMMH for The example in Figure 5.4. The thickness of the SAM is 1 ± 0.2 nm measured at

the right edge of the nanopattern. The left side has a hill of adsorbate from the material scraped to the side by the nanoshaving process and is not as reliable for measurement of thickness.

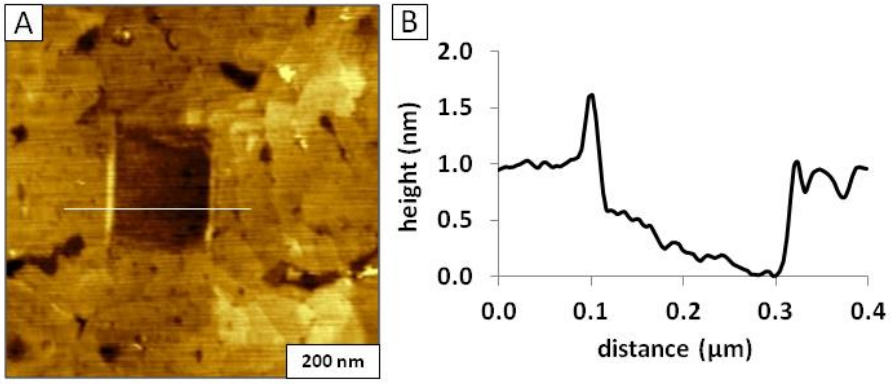

Figure 5.4 Nanoshaved square within a SAM of TMMH. [A] Topography image acquired in ethanol; [B] Line profile across the square pattern.

5.3.3 Nanografting of *n*-Alkanethiols within TMMH

By injecting new molecules into the sample cell, AFM-based nanofabrication can be accomplished using nanoshaving and nanografting protocols.[79, 255] Approaches with nanolithography enable side-by-side comparisons of the surface structures of multidentate adsorbates versus *n*-alkanethiol monolayers (i.e. film thickness, periodicity). Our experimental strategies rely on using a liquid sample cell for AFM studies, since fresh reagents can be introduced to the system and step-wise surface changes before and after nanofabrication can be monitored *in situ*. For experiments in liquid media, the method of surface nanografting developed by Xu, et al. was used to inscribe nanopatterns.[79] For these experiments *n*-alkanethiol SAMs provided an internal calibration tool. Essentially, the well-known dimensions of *n*-alkanethiol monolayers serve as a molecular ruler for local *in situ* measurements of the thickness of molecular films.[256-258]

Our protocols for nanografting used either dodecanethiol or TMMH as matrix SAMs which were prepared by immersion in ethanolic solutions. Areas of the matrix were selected for

nanoshaving or nanografting of patterns to enable a side-by-side comparison of molecular thickness. Experiments with nanoshaving and nanografting in liquid media provide advantages for *in situ* investigations, since the steps of characterization and writing are accomplished sequentially without the need for exchanging AFM tips. The successive changes of the surface topography can be viewed after each step: inscribing SAM patterns, rinsing, and introducing ink solutions.

A square pattern of octadecanethiol (ODT) was nanografted into a matrix of TMMH, as shown in Figure 5.5. The bright square consists of densely-packed alkanethiolates with methyl-terminated headgroups (Figure 5.5A). A darker contrast for the nanografted pattern compared to the matrix is revealed in the lateral force image of Figure 5.5B, even though TMMH and ODT are both terminated with methyl groups. This could be caused by differences in packing density: the nanografted pattern appears to be more densely-packed than the surrounding SAM of TMMH. The surrounding areas of the TMMH matrix are shorter than ODT. The expected thickness of an octadecanethiol SAM on gold is 2.2 nm, and octadecanethiol square is approximately 1 nm taller the TMMH matrix (Figure 5.5C). Thus the thickness of TMMH measures 1.2 ± 0.2 nm for this example.

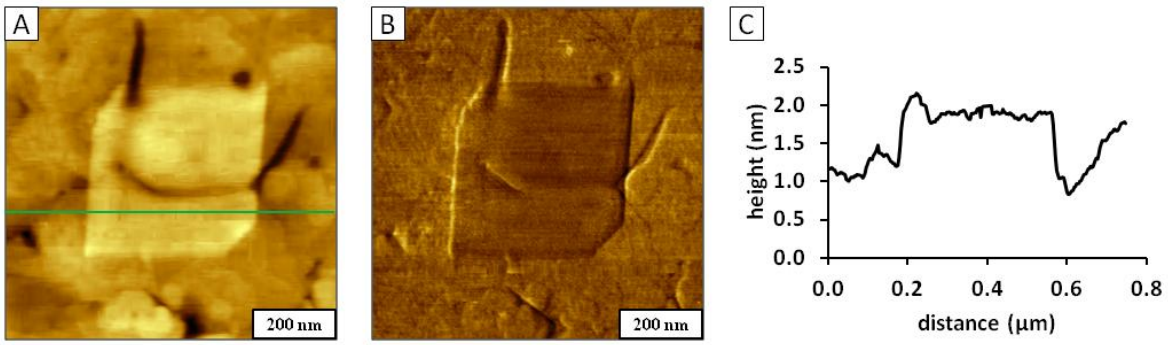

Figure 5.5 Nanografting of octadecanethiol within a densely-packed TMMH matrix. [A] Topography image acquired in contact mode; [B] corresponding lateral force image. [C] Height profile taken across the square pattern in ***A***.

To obtain further thickness measurements of TMMH, nanopatterns of 11-mercaptoundecanoic acid (MUA) were grafted within a matrix of TMMH (Figure 5.6A). Each of the patterns were inscribed by multiple sweeps across the same regions, which has been shown to produce a double layer for nanografting of carboxylic acid terminated SAMs.[95] The square nanopattern of MUA on the left side of the topography frame measures 200×200 nm^2, and reveals a two-tier design with single and double layers. Cursor lines were drawn across the top and bottom areas of the MUA nanopatterns (Figure 5.6B) measuring 0.5±0.2 and 2.0±0.2 nm above the TMMH matrix for the single and double layers, respectively. The profile across the monolayer region of the pattern (Figure 5.6B black line) measuring ~0.5 nm above the matrix indicates that TMMH is ~1 nm in thickness. The areas of the pattern with a double layer (Figure 5.6B red line) are 2±0.2 nm taller than the TMMH matrix. Since a double layer of MUA would be 3.0 nm thick, this likewise indicates a height of ~1 nm for TMMH.

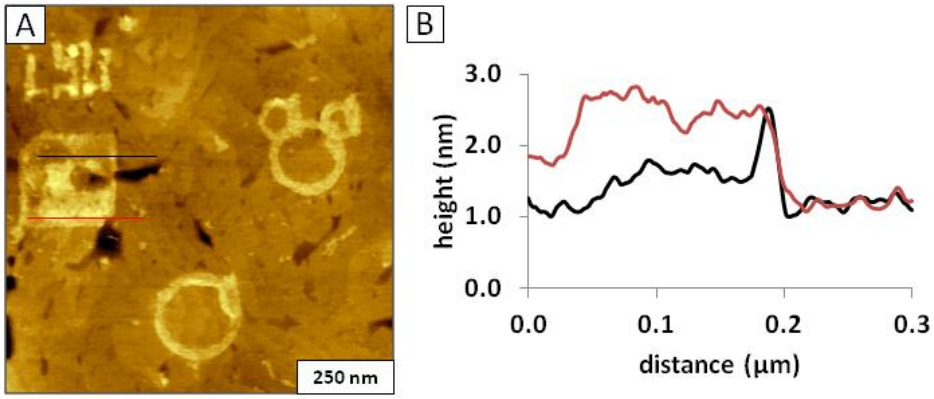

Figure 5.6 Nanografting of 11-mercaptoundecanoic acid within a matrix of TMMH. [A] Topography view of multiple nanografted patterns within a 800 ×800 nm^2 region. [B] Cursor profiles across the terraced square of ***A***.

Experiments were accomplished for grafting TMMH nanopatterns within a methyl-terminated dodecanethiol SAM (Figure 5.7). The expected thickness of a dodecanethiol SAM is 1.5 nm, which provides a reference measurement for evaluating the thickness of TMMH

nanostructures. Four patterns were written within the methyl-terminated SAM (Figures 5.7A-5.7B). The height of the TMMH squares is shorter than the surrounding matrix SAM of dodecanethiol. The difference in thickness ranges from 0.6-0.9 nm, which corresponds to a thickness of 0.7±0.3 nm for nanografted patterns of TMMH (Figure 5.7C).

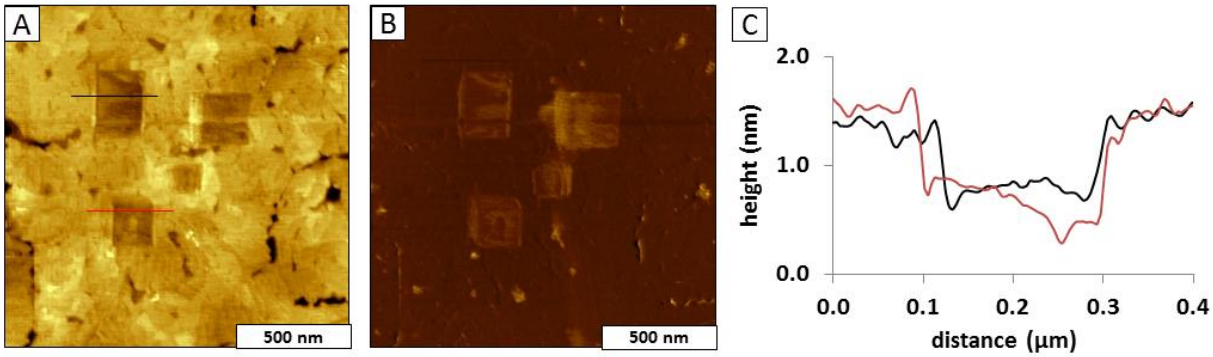

Figure 5.7 Nanografted patterns of TMMH within a dodecanethiol SAM. [A] Topograph of squares of TMMH (1.5 × 1.5 µm^2); [B] lateral force image for ***A***; [C] height profile across two TMMH nanopatterns in ***A***.

When nanografting *n*-alkanethiols, the molecules attach to gold surfaces directly in a standing-up configuration due to the effects of spatial confinement.[143] However, for tridentate molecules of TMMH, the molecules have a larger endgroup or foot. The packing density is influenced by the larger endgroup, and there are also differences in the overall molecular tilt of TMMH SAMs. The thickness values derived from each of the different AFM experiments are summarized in Table 1, and are in reasonable agreement for nanoscale measurements.

Table 5.1 Thickness measurements of TMMH on gold substrates.*

AFM Protocol	TMMH thickness	Example
Time-lapse AFM study, upright adsorbates on gold	1.0 ± 0.2 nm	Figure 2
Nanoshaving of mature SAM of TMMH	1.0 ± 0.2 nm	Figure 4
Nanografted ODT within TMMH matrix SAM	1.2 ± 0.2 nm	Figure 5
Nanografted MUA within TMMH matrix SAM	1.0 ± 0.2 nm	Figure 6
Nanografted TMMH within dodecanethiol SAM	0.7 ± 0.3 nm	Figure 7

*The error is estimated to be at least 0.2 nm from the thickness of a gold step.

Unlike our previous observations that several hours were required for TMMH to bind to gold surfaces to form a SAM, nanografting experiments reveal that TMMH attached immediately following the scanning track of the AFM tip (Figure 7). However, the shorter height suggests a less-dense packing arrangement for the nanografted patterns of TMMH with the bigger foot. Using the value of 1.0-1.2 nm as the thickness of a mature TMMH SAM, the heptadecane backbone would measure 59-64 degrees, compared to the well-known 30^{o} tilt of *n*-alkanethiol SAMs. Since tridentate TMMH binds to multiple sites on a gold surface, the intramolecular spacing would be greater which results in differences for the surface density and packing arrangement compared to monothiol SAMs.

5.4 Conclusion

Analysis of the changes in surface coverage with time-lapse AFM indicates that TMMH binds to surfaces more slowly (hours) compared to *n*-alkanethiols (minutes). Protocols of nanografting and nanoshaving were used to compare the heights of TMMH with *n*-alkanethiol SAMs with side-by-side AFM views. Differences in the packing density and tilt angle were observed for tridentate TMMH. Future directions for studies with TMMH will investigate the stability of multidentate films with exposure to oxidation, UV-irradiation and solvents.

5.5 Acknowledgements

This research was supported by the National Science Foundation (DMR-0906873), by the American Chemical Society Petroleum Research Fund New Directions Program, and the Camille Dreyfus Teacher-Scholar award.

CHAPTER 6. SUMMARY AND FUTURE PROSPECTUS

Results presented in this dissertation demonstrate the capabilities of scanning probe studies for monitoring surface reactions at the molecular level and builds a foundation for future research with engineering surface composition and reactivity. Visualization of the self-assembly process was demonstrated for model systems using both organosilanes and organothiols. Studies with high resolution atomic force microscopy (AFM) show promise for development of analytical methods for real-time measurements with even more complex molecular designs.

Molecular details of the surface assembly and self-polymerization of 4-chloromethylphenyltrichlorosilane (CMPS) within spatially-confined nanoholes on Si(111) were obtained *ex situ* from high resolution AFM images (Chapter 4). Progressive exposure of the nanoholes to solutions of CMPS provided quantitative information and details of the surface reaction. Further directions will be to study the self-assembly of other systems, such as organosilanes, porphyrins or multidentate adsorbates to gain insight for understanding the dynamics and mechanisms of self-assembly reactions on surfaces.

The solution self-assembly of 1,1,1-tris(mercaptomethyl)heptadecane (TMMH) was viewed by time-lapse AFM (Chapter 5). Side-by-side comparison of the surface structures of TMMH versus traditional *n*-alkanethiol monolayers were accomplished by scanning probe lithography procedures of nanoshaving and nanografting. Although monodentate *n*-alkanethiols have been widely investigated, thin films derived from bidentate or tridentate thiol adsorbates have not been studied in detail. Studies of multidentate adsorbates will provide benefits for applications of surface coatings because of the robust nature of films that attach to surfaces through multiple linkers. Future directions will be to investigate surface structures and properties of other multidentate adsorbates of organothiols or organosilanes. Experimental conditions (e.g.

changing concentration, pH or immersion time) will be optimized to improve the quality of the films. Studies of the stability of the films can be designed by aging samples or exposing patterned surfaces to UV irradiation or ozone.

Nanolithography enables fabrication of well-defined test platforms for molecular level investigations of surface reactions. Approaches with scanning probe lithography (SPL) provide exquisite control of the size, shape and surface chemistry of nanopatterns and fabrication can be accomplished within minutes using computer automation. Particle lithography offers high throughput capabilities to generate billions of reproducible nanopatterns simultaneously (Chapter 4). The choice of lithography methods can be tailored to achieve specific research goals.

To study the properties of thin film materials, the exceptional selectivity and sensitivity of SPL can provide rich information about molecular dimensions, molecular orientation, intermolecular interactions and surface chemistry. The spatial confinement of small areas surrounding an AFM probe achieved with nanografting affects the surface assembly of organothiol SAMs compared to natural solution self-assembly and therefore influences the molecular orientation. Molecules assemble on surfaces directly in an upright configuration with nanografting, whereas without spatial constraint *n*-alkanethiols assemble through a lying-down to standing phase transition.[80] By referencing well-studied model system of *n*-alkanethiol SAMs, the heights of other molecular systems can be measured *in situ* with liquid AFM for determining surface conformations.

To obtain quantitative measurements towards understanding the kinetics and mechanisms of molecular self-assembly, particle lithography enables fabrication of billions of nanostructures on the surface with exquisite control of periodicity.[65] Arrays of nano-containers used for studying surface reactions can be generated with traditional bench chemistry steps with high

reproducibility, as described in Chapter 4. The protocol of using nano-containers prepared by particle lithography is a first step for designing molecular-level studies of the processes of building supramolecular assemblies with more complex designs.

Nanofabrication methods are becoming indispensable not only for fundamental research, but also for commercial applications. Future innovations of nanolithography will very likely contribute to applications in technology for solar cells, molecular electronics, biosensors and material engineering. Development of inexpensive lithography methods for fabricating robust nanostructures on surfaces is essential for future applications of thin films in chemical and biological sensors. Understanding and controlling molecule arrangement at the nanoscale is a key step for surface engineering. Strategies demonstrated in this dissertation for surface investigations are a new direction for potential studies with other molecules.

The capability of investigating properties of molecules at the nanoscale is one of the greatest advantages for scanning probe microscopy (SPM). Beyond the protocols used in this dissertation, studies of surface properties such as conductance and magnetism using designed surface test platforms can be achieved using other SPM imaging modes. Future directions of SPM-based studies will continue to disclose mysteries of the “nano” frontier, and provide new insight of size-dependent phenomena that were previously inaccessible.

REFERENCES

1. Xia, Y. N.; Rogers, J. A.; Paul, K. E.; Whitesides, G. M., Unconventional methods for fabricating and patterning nanostructures. *Chem. Rev.* **1999,** *99,* 1823-1848.

2. Senaratne, W.; Andruzzi, L.; Ober, C. K., Self-assembled monolayers and polymer brushes in biotechnology: Current applications and future perspectives. *Biomacromolecules* **2005,** *6,* 2427-2448.

3. Chen, Y.; Pepin, A., Nanofabrication: Conventional and nonconventional methods. *Electrophoresis* **2001,** *22,* 187-207.

4. Tam-Chang, S.-W.; Biebuyck, H. A.; Whitesides, G. M.; Jeon, N.; Nuzzo, R. G., Self-Assembled Monolayers on Gold Generated from Alkanethiols with the Structure $RNCOCH_2SH$. *Langmuir* **1995,** *11,* 4371-4382.

5. Kautz, N. A.; Kandel, S. A., Alkanethiol Monolayers Contain Gold Adatoms, and Adatom Coverage Is Independent of Chain Length. *J. Phys. Chem. C* **2009,** *113,* 19286-19291.

6. O'Dwyer, C., In-situ examination of the selective etching of an alkanethiol monolayer covered Au{111} surface. *Mater. Lett.* **2007,** *61,* 3837-3841.

7. Binnig, G.; Rohrer, H., Scanning tunneling microscopy. *Helv. Phys. Acta* **1982,** *55,* 726-735.

8. Binnig, G.; Quate, C. F.; Gerber, C., Atomic force microscope. *Phys. Rev. Lett.* **1986,** *56,* 930-933.

9. Liu, G. Y.; Xu, S.; Qian, Y. L., Nanofabrication of self-assembled monolayers using scanning probe lithography. *Accounts Chem. Res.* **2000,** *33,* 457-466.

10. Asnachinda, E.; O'Haver, J. H.; Sabatini, D. A.; Khaodhiar, S., Atomic Force Microscopy and Contact Angle Studies of Polymerizable Gemini Surfactant Admicelles on Mica. *J. Appl. Polym. Sci.* **2010,** *115,* 1145-1152.

11. Garno, J. C.; Zangmeister, C. D.; Batteas, J. D., Directed electroless growth of metal nanostructures on patterned self-assembled monolayers. *Langmuir* **2007,** *23,* 7874-7879.

12. Garno, J. C.; Yang, Y. Y.; Amro, N. A.; Cruchon-Dupeyrat, S.; Chen, S. W.; Liu, G. Y., Precise positioning of nanoparticles on surfaces using scanning probe lithography. *Nano Lett.* **2003,** *3,* 389-395.

13. Bosacchi, A.; Frigeri, P.; Franchi, S.; Allegri, P.; Avanzini, V., InAs/GaAs self-assembled quantum dots grown by ALMBE and MBE. *J. Cryst. Growth* **1997,** *175*, 771-776.

14. Engel, A.; Lyubchenko, Y.; Muller, D., Atomic force microscopy: a powerful tool to observe biomolecules at work. *Trends Cell Biol.* **1999,** *9*, 77-80.

15. Banerjee, R.; Katsenovich, Y.; Lagos, L.; McIintosh, M.; Zhang, X.; Li, C. Z., Nanomedicine: Magnetic Nanoparticles and their Biomedical Applications. *Curr. Med. Chem.* **2010,** *17*, 3120-3141.

16. Archakov, A. I.; Ivanov, Y. D., Analytical nanobiotechnology for medicine diagnostics. *Mol. BioSyst.* **2007,** *3*, 336-342.

17. Salaita, K.; Wang, Y. H.; Mirkin, C. A., Applications of dip-pen nanolithography. *Nat. Nanotechnol.* **2007,** *2*, 145-155.

18. Zotti, G.; Vercelli, B.; Berlin, A., Monolayers and multilayers of conjugated polymers as nanosized electronic components. *Acc. Chem. Res.* **2008,** *41*, 1098-1109.

19. Muller, D. J.; Dufrene, Y. F., Atomic force microscopy as a multifunctional molecular toolbox in nanobiotechnology. *Nat. Nanotechnol.* **2008,** *3*, 261-269.

20. Reineke, F.; Kammer, S.; Gehring, S., Operating modes in scanning probe microscopy. In *Defect Recognition and Image Processing in Semiconductors and Devices*, Jimenez, J., Ed. Iop Publishing Ltd: Bristol, 1994; 61-64.

21. Zhong, Q.; Inniss, D.; Kjoller, K.; Elings, V. B., Fractured polymer silica fiber surface studied by tapping mode atomic-force microscopy. *Surf. Sci.* **1993,** *290*, L688-L692.

22. Dougherty, W. M.; Bruland, K. J.; Garbini, J. L.; Sidles, J. A., Detection of AC magnetic signals by parametric mode coupling in a mechanical oscillator. *Meas. Sci. Technol.* **1996,** *7*, 1733-1739.

23. Martin, Y.; Williams, C. C.; Wickramasinghe, H. K., Atomic force microscope force mapping and profiling on a sub 100-A scale *J. Appl. Phys.* **1987,** *61*, 4723-4729.

24. Martin, Y.; Wickramasinghe, H. K., Magnetic imaging by force microscopy with 1000-A resolution. *Appl. Phys. Lett.* **1987,** *50*, 1455-1457.

25. Kelley, T. W.; Granstrom, E. L.; Frisbie, C. D., Conducting probe atomic force microscopy: A characterization tool for molecular electronics. *Adv. Mater.* **1999,** *11*, 261.

26. Martin, Y.; Abraham, D. W.; Wickramasinghe, H. K., High-resolution capacitance measurement and potentiometry by force microscopy *Appl. Phys. Lett.* **1988,** *52*, 1103-1105.

27. Nonnenmacher, M.; Oboyle, M. P.; Wickramasinghe, H. K., Kelvin probe force microscopy. *Appl. Phys. Lett.* **1991,** *58*, 2921-2923.

28. Li, J.-R.; Lewandowski, B. R.; Xu, S.; Garno, J. C., Detecting the Magnetic Response of Iron Oxide Capped Organosilane Nanostructures Using Magnetic Sample Modulation and Atomic Force Microscopy. *Anal. Chem.* **2009,** *81*, 4792-4802.

29. Bracco, G.; Holst, B.; Lyles, V.; Serem, W.; Yu, J.-J.; Garno, J., Surface Characterization Using Atomic Force Microscopy (AFM) in Liquid Environments. In *Surface Science Techniques*, Springer Berlin Heidelberg: Vol. 51, pp 599-620.

30. Ebner, A.; Wildling, L.; Zhu, R.; Rankl, C.; Haselgrubler, T.; Hinterdorfer, P.; Gruber, H. J., Functionalization of probe tips and supports for single-molecule recognition force Microscopy. In *Stm and Afm Studies On*, Samori, P., Ed. Springer-Verlag Berlin: Berlin, 2008; Vol. 285, pp 29-76.

31. Jalili, N.; Laxminarayana, K., A review of atomic force microscopy imaging systems: application to molecular metrology and biological sciences. *Mechatronics* **2004,** *14*, 907-945.

32. Riet, J. T.; Smit, T.; Gerritsen, J. W.; Cambi, A.; Elemans, J.; Figdor, C. G.; Speller, S., Molecular Friction as a Tool to Identify Functionalized Alkanethiols. *Langmuir* **2010,** *26*, 6357-6366.

33. Lauritsen, J. V.; Reichling, M., Atomic resolution non-contact atomic force microscopy of clean metal oxide surfaces. *J. Phys.-Condes. Matter 22*, 23.

34. Garcia, R.; Perez, R., Dynamic atomic force microscopy methods. *Surf. Sci. Rep.* **2002,** *47*, 197-301.

35. Axford, D. N.; Davis, J. J., Electron flux through apo- and holoferritin. *Nanotechnology* **2007,** *18*.

36. Slaughter, G. E.; Bieberich, E.; Wnek, G. E.; Wynne, K. J.; Guiseppi-Elei, A., Improving neuron-to-electrode surface attachment via alkanethiol self-assembly: An alternating current impedance study. *Langmuir* **2004,** *20*, 7189-7200.

37. Liu, Z. F.; Shen, Z. Y.; Zhu, T.; Hou, S. F.; Ying, L. Z.; Shi, Z. J.; Gu, Z. N., Organizing single-walled carbon nanotubes on gold using a wet chemical self-assembling technique. *Langmuir* **2000,** *16*, 3569-3573.

38. Rezek, B.; Ukraintsev, E.; Kromka, A., Optimizing atomic force microscopy for characterization of diamond-protein interfaces. *Nanoscale Res. Lett.* **2011,** *6*.

39. Li, L. Y.; Chen, S. F.; Jiang, S. Y., Protein adsorption on alkanethiolate self-assembled monolayers: Nanoscale surface structural and chemical effects. *Langmuir* **2003,** *19*, 2974-2982.

40. Mechler, A.; Kopniczky, J.; Kokavecz, J.; Hoel, A.; Granqvist, C. G.; Heszler, P., Anomalies in nanostructure size measurements by AFM. *Phys. Rev. B* **2005,** *72*.

41. Sode, A.; Musgrove, A.; Bizzotto, D., Stability of PtZn Nanoparticles Supported on Carbon in Acidic Electrochemical Environments. *J. Phys. Chem. C* **2009,** *114*, 546-553.

42. Tanabe, I.; Tatsuma, T., Size- and Shape-Controlled Electrochemical Deposition of Metal Nanoparticles by Tapping Mode Atomic Force Microscopy. *Chem. Phys. Chem. C* **2012,** *116*, 3995-3999.

43. Blunt, M. O.; Martin, C. P.; Ahola-Tuomi, M.; Pauliac-Vaujour, E.; Sharp, P.; Nativo, P.; Brust, M.; Moriarty, P. J., Coerced mechanical coarsening of nanoparticle assemblies. *Nat. Nanotechnol.* **2007,** *2*, 167-170.

44. Schnippering, M.; Powell, H. V.; Mackenzie, S. R.; Unwin, P. R., Real-Time Monitoring of Polyaniline Nanoparticle Formation on Surfaces. *J. Phys. Chem. C* **2009,** *113*, 20221-20227.

45. Li, H.; Pfefferkorn, D.; Binder, W. H.; Kressler, J., Phospholipid Langmuir Film as Template for in Situ Silica Nanoparticle Formation at the Air/Water Interface. *Langmuir* **2009,** *25*, 13328-13331.

46. Li, H.; Sachsenhofer, R.; Binder, W. H.; Henze, T.; Thurn-Albrecht, T.; Busse, K.; Kressler, J., Hierarchical Organization of Poly(ethylene oxide)-block-poly(isobutylene) and Hydrophobically Modified Fe2O3 Nanoparticles at the Air/Water Interface and on Solid Supports. *Langmuir* **2009,** *25*, 8320-8329.

47. Csete, M.; Kohazi-Kis, A.; Vass, C.; Sipos, A.; Szekeres, G.; Deli, M.; Osvay, K.; Bor, Z., Atomic force microscopical and surface plasmon resonance spectroscopical investigation of sub-micrometer metal gratings generated by UV laser-based two-beam interference in Au-Ag bimetallic layers. *Appl. Surf. Sci.* **2007,** *253*, 7662-7671.

48. Porter, L. A.; Choi, H. C.; Ribbe, A. E.; Buriak, J. M., Controlled electroless deposition of noble metal nanoparticle films on germanium surfaces. *Nano Lett.* **2002,** *2*, 1067-1071.

49. Smith, E. L.; Barron, J. C.; Abbott, A. P.; Ryder, K. S., Time Resolved in Situ Liquid Atomic Force Microscopy and Simultaneous Acoustic Impedance Electrochemical Quartz Crystal Microbalance Measurements: A Study of Zn Deposition. *Anal. Chem.* **2009,** *81*, 8466-8471.

50. Li, Y.; Dong, M.; Otzen, D. E.; Yao, Y.; Liu, B.; Besenbacher, F.; Mamdouh, W., Influence of Tunable External Stimuli on the Self-Assembly of Guanosine

Supramolecular Nanostructures Studied By Atomic Force Microscope. *Langmuir* **2009,** *25*, 13432-13437.

51. Takahashi, H.; Numao, S.; Bandow, S.; Iijima, S., AFM imaging of wrapped multiwall carbon nanotube in DNA. *Chem. Phys. Lett.* **2006,** *418*, 535-539.

52. Choi, Y. S.; Mecke, A.; Orr, B. G.; Holl, M. M. B.; Baker, J. R., DNA-directed synthesis of generation 7 and 5 PAMAM dendrimer nanoclusters. *Nano Lett.* **2004,** *4*, 391-397.

53. Empie, N.; Edwards, D., Atomic force microscopy study of the interaction of DNA and nanostructured beta-gallia rutile. *Langmuir* **2006,** *22*, 7658-7663.

54. Xia, Y. N.; Whitesides, G. M., Soft lithography. *Annu. Rev. Mater. Sci.* **1998,** *28*, 153-184.

55. Tour, J. M., Molecular electronics. Synthesis and testing of components. *Acc. Chem. Res.* **2000,** *33*, 791-804.

56. Samanta, D.; Sarkar, A., Immobilization of bio-macromolecules on self-assembled monolayers: methods and sensor applications. *Chem. Soc. Rev.* **2011,** *40*, 2567-2592.

57. Cheng, H.; Hu, Y., Influence of chain ordering on frictional properties of self-assembled monolayers (SAMs) in nano-lubrication. *Adv. Colloid Interface Sci.* **2012,** *171*, 53-65.

58. Dubois, L. H.; Nuzzo, R. G., Synthesis, structure, and properties of model organic-surfaces. *Annu. Rev. Phys. Chem.* **1992,** *43*, 437-463.

59. Schreiber, F., Structure and growth of self-assembling monolayers. *Prog. Surf. Sci.* **2000,** *65*, 151-256.

60. Smith, R. K.; Lewis, P. A.; Weiss, P. S., Patterning self-assembled monolayers. *Prog. Surf. Sci.* **2004,** *75*, 1-68.

61. Schlenoff, J. B.; Li, M.; Ly, H., Stability and self-exchange in alkanethiol monolayers. *J. Am. Chem. Soc.* **1995,** *117*, 12528-12536.

62. Xu, S.; Cruchon-Dupeyrat, S. J. N.; Garno, J. C.; Liu, G. Y.; Jennings, G. K.; Yong, T. H.; Laibinis, P. E., In situ studies of thiol self-assembly on gold from solution using atomic force microscopy. *J. Chem. Phys.* **1998,** *108*, 5002-5012.

63. Barth, C.; Foster, A. S.; Henry, C. R.; Shluger, A. L., Recent Trends in Surface Characterization and Chemistry with High-Resolution Scanning Force Methods. *Adv. Mater.* **2011,** *23*, 477-501.

64. Sagiv, J., Organized monolayers by adsorption.1. Formation and structure of oleophobic mixed monolayers on solid-surfaces *J. Am. Chem. Soc.* **1980,** *102*, 92-98.

65. Saner, C. K.; Lusker, K. L.; LeJeune, Z. M.; Serem, W. K.; Garno, J. C., Self-assembly of octadecyltrichlorosilane: Surface structures formed using different protocols of particle lithography. *Beilstein J. Nanotechnol.* **2012,** *3*, 114-122.

66. Lee, M. V.; Nelson, K. A.; Hutchins, L.; Becerril, H. A.; Cosby, S. T.; Blood, J. C.; Wheeler, D. R.; Davis, R. C.; Woolley, A. T.; Harb, J. N.; Linford, M. R., Nanografting of silanes on silicon dioxide with applications to DNA localization and copper electroless deposition. *Chem. Mater.* **2007,** *19*, 5052-5054.

67. Headrick, J. E.; Armstrong, M.; Cratty, J.; Hammond, S.; Sheriff, B. A.; Berrie, C. L., Nanoscale patterning of alkyl monolayers on silicon using the atomic force microscope. *Langmuir* **2005,** *21*, 4117-4122.

68. Rosa, L. G.; Liang, J., Atomic force microscope nanolithography: dip-pen, nanoshaving, nanografting, tapping mode, electrochemical and thermal nanolithography. *J. Phys.-Condes. Matter* **2009,** *21*, 18.

69. Haynes, C. L.; Van Duyne, R. P., Nanosphere lithography: A versatile nanofabrication tool for studies of size-dependent nanoparticle optics. *J. Phys. Chem. B* **2001,** *105*, 5599-5611.

70. Hulteen, J. C.; Vanduyne, R. P., Nanosphere lithography - A materials general fabrication process for periodic particle array surfaces. *J. Vac. Sci. Technol., A* **1995,** *13*, 1553-1558.

71. Denis, F. A.; Hanarp, P.; Sutherland, D. S.; Gold, J.; Mustin, C.; Rouxhet, P. G.; Dufrene, Y. F., Protein adsorption on model surfaces with controlled nanotopography and chemistry. *Langmuir* **2002,** *18*, 819-828.

72. Yang, S. M.; Jang, S. G.; Choi, D. G.; Kim, S.; Yu, H. K., Nanomachining by colloidal lithography. *Small* **2006,** *2*, 458-475.

73. Deckman, H. W.; Dunsmuir, J. H., Natural lithography. *Appl. Phys. Lett.* **1982,** *41*, 377-379.

74. Chen, X.; Chen, Z. M.; Fu, N.; Lu, G.; Yang, B., Versatile nanopatterned surfaces generated via three-dimensional colloidal crystals. *Adv. Mater.* **2003,** *15*, 1413-1417.

75. Wang, Y.; Han, S. B.; Briseno, A. L.; Sanedrin, R. J. G.; Zhou, F. M., A modified nanosphere lithography for the fabrication of aminosilane/polystyrene nanoring arrays and the subsequent attachment of gold or DNA-capped gold nanoparticles. *J. Mater. Chem.* **2004,** *14*, 3488-3494.

76. Frey, W.; Woods, C. K.; Chilkoti, A., Ultraflat nanosphere lithography: A new method to fabricate flat nanostructures. *Adv. Mater.* **2000,** *12*, 1515-1519.

77. Xu, D. W.; Graugnard, E.; King, J. S.; Zhong, L. W.; Summers, C. J., Large-scale fabrication of ordered nanobowl arrays. *Nano Lett.* **2004,** *4*, 2223-2226.

78. Liu, J. F.; Cruchon-Dupeyrat, S.; Garno, J. C.; Frommer, J.; Liu, G. Y., Three-dimensional nanostructure construction via nanografting: Positive and negative pattern transfer. *Nano Lett.* **2002,** *2*, 937-940.

79. Xu, S.; Miller, S.; Laibinis, P. E.; Liu, G. Y., Fabrication of nanometer scale patterns within self-assembled monolayers by nanografting. *Langmuir* **1999,** *15*, 7244-7251.

80. Xu, S.; Laibinis, P. E.; Liu, G. Y., Accelerating the kinetics of thiol self-assembly on gold - A spatial confinement effect. *J. Am. Chem. Soc.* **1998,** *120*, 9356-9361.

81. Liu, M.; Amro, N. A.; Liu, G. Y., Nanografting for surface physical chemistry. *Annu. Rev. Phys. Chem.* **2008,** *59*, 367-386.

82. Li, J. R.; Garno, J. C., Nanostructures of Octadecyltrisiloxane Self-Assembled Monolayers Produced on Au(111) Using Particle Lithography. *ACS Appl. Mater. Interfaces* **2009,** *1*, 969-976.

83. Li, J. R.; Garno, J. C., Elucidating the role of surface hydrolysis in preparing organosilane nanostructures via particle lithography. *Nano Lett.* **2008,** *8*, 1916-1922.

84. Tian, T.; LeJeune, Z.; Serem, W.; Yu, J.-J.; Garno, J., Nanografting: A Method for Bottom-up Fabrication of Designed Nanostructures. In *Tip-Based Nanofabrication*, Springer New York: 2011; pp 167-205.

85. Hansma, P. K.; Cleveland, J. P.; Radmacher, M.; Walters, D. A.; Hillner, P. E.; Bezanilla, M.; Fritz, M.; Vie, D.; Hansma, H. G.; Prater, C. B.; Massie, J.; Fukunaga, L.; Gurley, J.; Elings, V., Tapping mode atomic-force microscopy in liquids. *Appl. Phys. Lett.* **1994,** *64*, 1738-1740.

86. Chwang, A. B.; Granstrom, E. L.; Frisbie, C. D., Fabrication of a Sexithiophene Semiconducting Wire: Nanoshaving with an Atomic Force Microscope Tip. *Adv. Mater.* **2000,** *12*, 285-288.

87. Shi, J.; Chen, J.; Cremer, P. S., Sub-100 nm patterning of supported bilayers by nanoshaving lithography. *J. Am. Chem. Soc.* **2008,** *130*, 2718-2719.

88. Zhou, D.; Bruckbauer, A.; Ying, L.; Abell, C.; Klenerman, D., Building three-dimensional surface biological assemblies on the nanometer scale. *Nano Lett.* **2003,** *3*, 1517-1520.

89. Rosa, L. G.; Jiang, J.; Lima, O. V.; Xiao, J.; Utreras, E.; Dowben, P. A.; Tan, L., Selective nanoshaving of self-assembled monolayers of 2-(4-pyridylethyl)triethoxysilane. *Materials Letters* **2009,** *63*, 961-964.

90. Headrick, J. E.; Armstrong, M.; Cratty, J.; Hammond, S.; Sheriff, B. A.; Berrie, C. L., Nanoscale patterning of alkyl monolayers on silicon using the atomic force microscope. *Langmuir* **2005,** *21*, 4117-4122.

91. Garno, J. C.; Batteas, J. D., Nanofabrication with Self-Assembled Monolayers by Scanned Probe Lithography. In *Applied Scanning Probe Methods, Vol IV, Industrial Applications*, Bhushan, B., Ed. Springer-Verlag: Berlin Heidelberg New York, 2006.

92. LeJeune, Z. M.; Serem, W.; Kelley, A. T.; Ngunjiri, J. N.; Garno, J. C., AFM-based Nanofabrication with Self-Assembled Monolayers. In *Encyclopedia of Nanoscience and Technology, (2nd edition)*, Nalwa, H. S., Ed. American Scientific Publishers Stevenson Ranch, CA, 2010.

93. Xu, S.; Liu, G. Y., Nanometer-scale fabrication by simultaneous nanoshaving and molecular self-assembly. *Langmuir* **1997,** *13*, 127-129.

94. Ginger, D. S.; Zhang, H.; Mirkin, C. A., The evolution of dip-pen nanolithography. *Angew. Chem.-Int. Edit.* **2004,** *43*, 30-45.

95. Kelley, A. T.; Ngunjiri, J. N.; Serem, W. K.; Yu, J.-J.; Lawrence, S.; Crowe, S.; Garno, J. C., Applying AFM-based nanofabrication for measuring the thickness of nanopatterns: The role of headgroups in the vertical self-assembly of ω-functionalized *n*-alkanethiols. *Langmuir* **2010,** *26*, 3040-3049.

96. Hacker, C. A.; Batteas, J. D.; Garno, J. C.; Marquez, M.; Richter, C. A.; Richter, L. J.; vanZee, R. D.; Zangmeister, C. D., Structural and Chemical Characterization of Monofluoro-Substituted Oligo(phenylene-ethynylene) Thiolate Self-Assembled Monolayers on Gold. *Langmuir* **2004,** *20*, 6195-6205.

97. Amro, N. A.; Xu, S.; Liu, G.-Y., Patterning surfaces using tip-directed displacement and self-assembly. *Langmuir* **2000,** *16*, 3006-3009.

98. Muller, W. T.; Klein, D. L.; Lee, T.; Clarke, J.; McEuen, P. L.; Schultz, P. G., A strategy for the chemical synthesis of nanostructures. *Science* **1995,** *268*, 272-273.

99. Davis, J. J.; Bagshaw, C. B.; Busuttil, K. L.; Hanyu, Y.; Coleman, K. S., Spatially Controlled Suzuki and Heck Catalytic Molecular Coupling. *J. Am. Chem. Soc.* **2006,** *128*, 14135-14141.

100. Davis, J. J.; Coleman, K. S.; Busuttil, K. L.; Bagshaw, C. B., Spatially Resolved Suzuki Coupling Reaction Initiated and Controlled Using a Catalytic AFM Probe. *J. Am. Chem. Soc.* **2005,** *127*, 13082-13083.

101. Lee, H.; Kim, S. A.; Ahn, S. J.; Lee, H., Positive and negative patterning on a palmitic acid Languir–Blodgett monolayer on Si surface using bias-dependent atomic force microscopy lithography. *Applied Physics Letters* **2002,** *81*, 138-140.

102. Gu, J.; Yam, C. M.; Li, S.; Cai, C., Nanometric Protein Arrays on Protein-Resistant Monolayers on Silicon Surfaces. *J. Am. Chem. Soc.* **2004,** *126*, 8098-8099.

103. Hansma, H. G.; Vesenka, J.; Siegerist, C.; Kelderman, G.; Morrett, H.; Sinsheimer, R. l.; Elings, V.; Bustamante, C.; Hansma, P. K., Reproducible imaging and dissection of plasmid DNA under liquid with the atomic force microscope. *Science* **1992,** *256*, 1180-1184.

104. Weisenhorn, A. L.; Maivald, P.; Butt, H. J.; Hansma, P. K., Measuring adhesion, attraction, and repulsion between surfaces in liquids with an atomic-force microscope. *Phys. Rev. B* **1992,** *45*, 11226-11232.

105. Ngunjiri, J. N.; Kelley, A. T.; LeJeune, Z. M.; Li, J.-R.; Lewandowski, B.; Serem, W. K.; Daniels, S. L.; Lusker, K. L.; Garno, J. C., Achieving precision and reproducibility for writing patterns of n-alkanethiol SAMs with automated nanografting. *Scanning* **2008,** *30*, 123-136.

106. Cruchon-Dupeyrat, S.; Porthun, S.; Liu, G. Y., Nanofabrication using computer-assisted design and automated vector-scanning probe lithography. *Appl. Surf. Sci.* **2001,** *175*, 636-642.

107. Liu, G.-Y.; Amro, N. A., Positioning protein molecules on surfaces: A nanoengineering approach to supramolecular chemistry. *Proc. Natl. Acad. Sci. U.S.A.* **2002,** *99*, 5165-5170.

108. Liu, M.; Amro, N. A.; Liu, G.-Y., Nanografting for surface physical chemistry. *Ann. Rev. Phys. Chem.* **2008,** *59*, 367-386.

109. Garno, J. C.; Yang, Y. Y.; Amro, N. A.; Cruchon-Dupeyrat, S.; Chen, S. W.; Liu, G. Y., Precise positioning of nanoparticles on surfaces using scanning probe lithography. *Nano Letters* **2003,** *3*, 389-395.

110. LeJeune, Z. M.; McKenzie, M.; Hao, E.; Vicente, M. G. H.; Chen, B.; Garno, J. C., Surface assembly of pyridyl-substituted porphyrins on Au(111) investigated in situ using scanning probe lithography. *SPIE Proceedings* **2010,** *7593*, 759311.

111. Ngunjiri, J. N.; Garno, J. C., AFM-Based Lithography for Nanoscale Protein Assays. *Anal. Chem.* **2008,** *80*, 1361-1369.

112. Wadu-Mesthrige, K.; Amro, N. A.; Garno, J. C.; Xu, S.; Liu, G. Y., Fabrication of nanometer-sized protein patterns using atomic force microscopy and selective immobilization. *Biophys. J.* **2001,** *80*, 1891-1899.

113. Wadu-Mesthrige, K.; Xu, S.; Amro, N. A.; Liu, G. Y., Fabrication and imaging of nanometer-sized protein patterns. *Langmuir* **1999,** *15*, 8580-8583.

114. Tan, Y. H.; Liu, M.; Nolting, B.; Go, J. G.; Gervay-Hague, J.; Liu, G. Y., A Nanoengineering Approach for Investigation and Regulation of Protein Immobilization. *ACS Nano* **2008,** *2*, 2374-2384.

115. Liu, M.; Amro, N. A.; Chow, C. S.; Liu, G. Y., Production of nanostructures of DNA on surfaces. *Nano Letters* **2002,** *2*, 863-867.

116. Watson, S. M. D.; Coleman, K. S.; Chakraborty, A. K., A new route to the production and nanoscale patterning of highly smooth, ultrathin zirconium films. *ACS Nano* **2008,** *2*, 643-650.

117. Chan, Y.-H.; Schuckman, A. E.; Perez, L. M.; Vinodu, M.; Drain, C. M.; Batteas, J. D., Synthesis and characterization of a thiol-tethered tripyridyl porphyrin on Au(111). *J. Phys. Chem. C* **2008,** *112*, 6110-6118.

118. Case, M. A.; McLendon, G. L.; Hu, Y.; Vanderlick, T. K.; Scoles, G., Using nanografting to achieve directed assembly of de novo designed metalloproteins on gold *Nano Lett.* **2003,** *3*, 425-429.

119. Hu, J.; Das, A.; Hecht, M. H.; Scoles, G., Nanografting de novo proteins onto gold surfaces. *Langmuir* **2005,** *21*, 9103-9109.

120. Xu, S.; Cruchon-Dupeyrat, S. J. N.; Garno, J. C.; Liu, G. Y.; Jennings, G. K.; Yong, T. H.; Laibinis, P. E., In situ studies of thiol self-assembly on gold from solution using atomic force microscopy. *J. Chem. Phys.* **1998,** *108*, 5002-5012.

121. Poirier, G. E.; Pylant, E. D., The self-assembly mechanism of alkanethiols on Au(111). *Science* **1996,** *272*, 1145-1148.

122. Poirier, G. E., Mechanism of formation of Au vacancy islands in alkanethiol monolayers on Au(111). *Langmuir* **1997,** *13*, 2019-2026.

123. Liang, J.; Rosa, L. G.; Scoles, G., Nanostructuring, Imaging and molecular manipulation of dithiol monolayers on au(111) surfaces by atomic force Microscopy. *J. Phys. Chem. C* **2007,** *111*, 17275-17284.

124. Yu, J. H.; Ngunjiri, J. N.; Kelley, A. T.; Gano, J. C., Nanografting versus Solution Self-Assembly of alpha,omega-Alkanedithiols on Au(111) Investigated by AFM. *Langmuir* **2008,** *24*, 11661-11668.

125. Zhou, D. J.; Wang, X. Z.; Birch, L.; Rayment, T.; Abell, C., AFM study on protein immobilization on charged surfaces at the nanoscale: Toward the fabrication of three-dimensional protein nanostructures. *Langmuir* **2003,** *19*, 10557-10562.

126. Ngunjiri, J.; Garno, J. C., AFM-based lithography for nanoscale protein assays. *Anal. Chem.* **2008,** *80*, 1361-1369.

127. Price, W. J.; Kuo, P. K.; Lee, T. R.; Colorado, R.; Ying, Z. C.; Liu, G. Y., Probing the local structure and mechanical response of nanostructures using force modulation and nanofabrication. *Langmuir* **2005,** *21*, 8422-8428.

128. Price, W. J.; Leigh, S. A.; Hsu, S. M.; Patten, T. E.; Liu, G. Y., Measuring the size dependence of Young's modulus using force modulation atomic force microscopy. *J. Phys. Chem. A* **2006,** *110*, 1382-1388.

129. Brown, T. T.; LeJeune, Z. M.; Liu, K.; Hardin, S.; Li, J.-R.; Rupnik, K.; Garno, J. C., Automated Scanning Probe Lithography with n-Alkanethiol Self-Assembled Monolayers on Au(111): Application for Teaching Undergraduate Laboratories. *Journal of American Lab Automation* **2010,** *published on-line 10/8/2010*.

130. Xu, S.; Amro, N. A.; Liu, G. Y., Characterization of AFM tips using nanografting. *Appl. Surf. Sci.* **2001,** *175*, 649-655.

131. Duwez, A.-S., Exploiting electron spectroscopies to probe the structure and organization of self-assembled monolayers: a review. *Journal of Electron Spectroscopy and Related Phenomena* **2004,** *134*, 97-138.

132. Fenter, P.; Eisenberger, P.; Liang, K. S., Chain-length dependence of the structures and phases of CH3(CH2)n-1SH self-assembled on Au(111). *Phys. Rev. Lett.* **1993,** *70*, 2447-2450.

133. Nuzzo, R. G.; Korenic, E. M.; Dubois, L. H., Studies of the temperature-dependent phase-behavior of long-chain normal-alkyl thiol monolayers on gold. *J. Chem. Phys.* **1990,** *93*, 767-773.

134. Porter, M. D.; Bright, T. B.; Allara, D. L.; Chidsey, C. E. D., Spontaneously organized molecular assemblies .4. Structural characterization of normal-alkyl thiol monolayers on gold by optical ellipsometry, infrared-spectroscopy, and electrochemistry. *J. Am. Chem. Soc.* **1987,** *109*, 3559-3568.

135. Nuzzo, R. G.; Zegarski, B. R.; Dubois, L. H., Fundamental-studies of the chemisorption of organosulfur compounds on Au(111) - implications for molecular self-assembly on gold surfaces. *J. Am. Chem. Soc.* **1987,** *109*, 733-740.

136. Brower, T. L.; Garno, J. C.; Ulman, A.; Liu, G. Y.; Yan, C.; Golzhauser, A.; Grunze, M., Self-assembled multilayers of 4,4 '-dimercaptobiphenyl formed by Cu(II)-catalyzed oxidation. *Langmuir* **2002,** *18*, 6207-6216.

137. Kadalbajoo, M.; Park, J.-H.; Opdahl, A.; Suda, H.; Garno, J. C.; Batteas, J. D.; Tarlov, M. J.; DeShong, P., Synthesis and structural characterization of glucopyranosylamide films on gold. *Langmuir* **2007,** *23*, 700-707.

138. Liu, D.; Bruckbauer, A.; Abell, C.; Balasubramanian, S.; Kang, D.-J.; Klenerman, D.; Zhou, D., A Reversible pH-Driven DNA Nanoswitch Array. *J. Am. Chem. Soc.* **2006,** *128*, 2067-2071.

139. Riet, J. t.; Smit, T.; Coenen, M. J. J.; Gerritsen, J. W.; Cambi, A.; Elemans, J. A. A. W.; Speller, S.; Figdor, C. G., AFM topography and friction studies of hydrogen-bonded bilayers of functionalized alkanethiols. *Soft Matter* **2010,** *6*, 3450-3454.

140. Price, W. J.; Kuo, P. K.; Lee, T. R.; Colorado, R.; Ying, Z. C.; Liu, G.-Y., Probing the Local Structure and Mechanical Response of Nanostructures Using Force Modulation and Nanofabrication. *Langmuir* **2005,** *21*, 8422-8428.

141. Price, W. J.; Leigh, S. A.; Hsu, S. M.; Patten, T. E.; Liu, G.-Y., Measuring the Size Dependence of Young's Modulus Using Force Modulation Atomic Force Microscopy. *J. Phys. Chem. A* **2006,** *110*, 1382-1388.

142. Scaini, D.; Castronovo, M.; Casalis, L.; Scoles, G., Electron Transfer Mediating Properties of Hydrocarbons as a Function of Chain Length: A Differential Scanning Conductive Tip Atomic Force Microscopy Investigation. *ACS Nano* **2008,** *2*, 507-515.

143. Xu, S.; Laibinis, P. E.; Liu, G. Y., Accelerating the kinetics of thiol self-assembly on gold - A spatial confinement effect. *Journal of the American Chemical Society* **1998,** *120*, 9356-9361.

144. Yu, J. J.; Tan, Y. H.; Li, X.; Kuo, P. K.; Liu, G. Y., A nanoengineering approach to regulate the lateral heterogeneity of self-assembled monolayers. *J. Am. Chem. Soc.* **2006,** *128*, 11574-11581.

145. Chen, S. F.; Li, L. Y.; Boozer, C. L.; Jiang, S. Y., Controlled Chemical and Structural Properties of Mixed Self-Assembled Monolayers of Alkanethiols on Au(111). *Langmuir* **2000,** *16*, 9287-9293.

146. Hobara, D.; Kakiuchi, T., Domain structure of binary self-assembled monolayers composed of 3-mercapto-1-propanol and 1-tetradecanethiol on Au(111) prepared by coadsorption *Electrochem. Commun.* **2001,** *3*, 154-157.

147. Ryu, S.; Schatz, G. C., Nanografting: Modeling and Simulation. *J. Am. Chem. Soc.* **2006,** *128*, 11563-11573.

148. Yu, J. J.; Tan, Y. H.; Li, X.; Kuo, P. K.; Liu, G. Y., A nanoengineering approach to regulate the lateral heterogeneity of self-assembled monolayers. *J. Am. Chem. Soc.* **2006,** *128*, 11574-11581.

149. Liang, J.; Rosa, L. G.; Scoles, G., Nanostructuring, Imaging and molecular manipulation of dithiol monolayers on Au(111) surfaces by atomic force Microscopy. *J. Phys. Chem C* **2007,** *111*, 17275-17284

150. Lim, J. M.; Yoon, Z. S.; Shin, J. Y.; Kim, K. S.; Yoon, M. C.; Kim, D., The photophysical properties of expanded porphyrins: relationships between aromaticity, molecular geometry and non-linear optical properties. *Chemical Communications* **2009,** *3*, 261-273.

151. Hasobe, T., Supramolecular nanoarchitectures for light energy conversion. *Phys. Chem. Chem. Phys.* **2010,** *12*, 44-57.

152. LeJeune, Z. M.; McKenzie, M.; Daniels, S. L.; Hao, E.; Chen, B.; Vicente, M. G. H.; Garno, J. C., Controlling the Organization of Porphyrins on Surfaces using Nanolithography. *ACS Nano* **2010,** *in submission*.

153. Chapman, R. G.; Ostuni, E.; Takayama, S.; Holmlin, R. E.; Yan, L.; Whitesides, G. M., Surveying for Surfaces that Resist the Adsorption of Proteins. *J. Am. Chem. Soc.* **2000,** *122*, 8303-8304.

154. Ostuni, E.; Chapman, R. G.; Liang, M. N.; Meluleni, G.; Pier, G.; Ingber, D. E.; Whitesides, G. M., Self-Assembled Monolayers That Resist the Adsorption of Proteins and the Adhesion of Bacterial and Mammalian Cells. *Langmuir* **2001,** *17*, 6336-6343.

155. Holmlin, R. E.; Chen, X.; Chapman, R. G.; Takayama, S.; Whitesides, G. M., Zwitterionic SAMs that Resist Nonspecific Adsorption of Protein from Aqueous Buffer. *Langmuir* **2001,** *17*, 2841-2850.

156. Ostuni, E.; Chapman, R. G.; Holmlin, R. E.; Takayama, S.; Whitesides, G. M., A Survey of Structure-Property Relationships of Surfaces that Resist the Adsorption of Protein. *Langmuir* **2001,** *17*, 5605-5620.

157. Luk, Y.-Y.; Kato, M.; Mrksich, M., Self-Assembled Monolayers of Alkanethiolates Presenting Mannitol Groups are Inert to Protein Adsorption and Cell Attachment. *Langmuir* **2000,** *16*, 9604-9608.

158. Herrwerth, S.; Eck, W.; Reinhardt, S.; Grunze, M., Factors that Determine the Protein Resistance of Oligoether Self-Assembled monolayers - Internal Hydrophilicity, Terminal Hydrophilicity, and Lateral packing Density. *J. Am. Chem. Soc.* **2003,** *125*, 9359-9366.

159. Hu, Y.; Das, A.; Hecht, M. H.; Scoles, G., Nanografting de novo proteins onto gold surfaces. *Langmuir* **2005,** *21*, 9103-9109.

160. Case, M. A.; McLendon, G. L.; Hu, Y.; Vanderlick, T. K.; Scoles, G., Using nanografting to achieve directed assembly of de novo designed metalloproteins on gold. *Nano Lett.* **2003,** *3*, 425-429.

161. Kenseth, J. R.; Harnisch, J. A.; Jones, V. W.; Porter, M. D., Investigation of approaches for the fabrication of protein patterns by scanning probe lithography. *Langmuir* **2001,** *17*, 4105-4112.

162. Wadu-Mesthrige, K.; Amro, N. A.; Garno, J. C.; Xu, S.; Liu, G. Y., Fabrication of nanometer-sized protein patterns using atomic force microscopy and selective immobilization. *Biophys. J.* **2001,** *80*, 1891-1899.

163. Liu, G. Y.; Amro, N. A., Positioning protein molecules on surfaces: A nanoengineering approach to supramolecular chemistry. *Proc. Natl. Acad. Sci. U. S. A.* **2002,** *99*, 5165-5170.

164. Jang, C. H.; Stevens, B. D.; Phillips, R.; Calter, M. A.; Ducker, W. A., A strategy for the sequential patterning of proteins: Catalytically active multiprotein nanofabrication. *Nano Lett.* **2003,** *3*, 691-694.

165. Nuraje, N.; Banerjee, I. A.; MacCuspie, R. I.; Yu, L. T.; Matsui, H., Biological bottom-up assembly of antibody nanotubes on patterned antigen arrays. *J. Am. Chem. Soc.* **2004,** *126*, 8088-8089.

166. Staii, C.; Wood, D. W.; Scoles, G., Ligand-induced structural changes in maltose binding proteins measured by atomic force microscopy. *Nano Lett.* **2008,** *8*, 2503-2509.

167. Liu, G. Y.; Amro, N. A., Positioning protein molecules on surfaces: A nanoengineering approach to supramolecular chemistry. *Proc. Natl. Acad. Sci. U. S. A.* **2002,** *99*, 5165-5170.

168. Grabarek, Z.; Gergely, J., Zero-Length Crosslinking Procedure with the use of Active Esters. *Anal. Biochem* **1990,** *185*, 131-135.

169. Jang, C.-H.; Stevens, B. D.; Phillips, R.; Calter, M. A.; Ducker, W. A., A Strategy for the Sequential Patterning of Proteins: Catalytically Active Multiprotein Nanofabrication. *Nano Lett.* **2003,** *3*, 691-694.

170. Staii, C.; Wood, D. W.; Scoles, G., Verification of Biochemical Activity for Proteins Nanografted on Gold Surfaces. *J. Am. Chem. Soc.* **2007,** *130*, 640-646.

171. Castronovo, M.; Radovic, S.; Grunwald, C.; Casalis, L.; Morgante, M.; Scoles, G., Control of Steric Hindrance on Restriction Enzyme Reactions with Surface-Bound DNA Nanostructures. *Nano Lett.* **2008,** *8*, 4140-4145.

172. Liu, M.; Liu, G.-Y., Hybridization with Nanostructures of Single-Stranded DNA. *Langmuir* **2005,** *21*, 1972-1978.

173. Schwartz, P. V., Meniscus force nanografting: Nanoscopic patterning of DNA. *Langmuir* **2001,** *17*, 5971-5977.

174. Mirmomtaz, E.; Castronovo, M.; Grunwald, C.; Bano, F.; Scaini, D.; Ensafi, A. A.; Scoles, G.; Casalis, L., Quantitative Study of the Effect of Coverage on the Hybridization Efficiency of Surface-Bound DNA Nanostructures. *Nano Lett.* **2008,** *8*, 4134-4139.

175. Bano, F.; Fruk, L.; Sanavio, B.; Glettenberg, M.; Casalis, L.; Niemeyer, C. M.; Scoles, G., Toward Multiprotein Nanoarrays Using Nanografting and DNA Directed Immobilization of Proteins. *Nano Lett.* **2009,** *9*, 2614-2618.

176. Liu, M. Z.; Amro, N. A.; Chow, C. S.; Liu, G. Y., Production of nanostructures of DNA on surfaces. *Nano Lett.* **2002,** *2*, 863-867.

177. Liu, M. Z.; Liu, G. Y., Hybridization with nanostructures of single-stranded DNA. *Langmuir* **2005,** *21*, 1972-1978.

178. Liu, D. S.; Bruckbauer, A.; Abell, C.; Balasubramanian, S.; Kang, D. J.; Klenerman, D.; Zhou, D. J., A reversible pH-driven DNA nanoswitch array. *J. Am. Chem. Soc.* **2006,** *128* (6), 2067-2071.

179. Mirmomtaz, E.; Castronovo, M.; Grunwald, C.; Bano, F.; Scaini, D.; Ensafi, A. A.; Scoles, G.; Casalis, L., Quantitative Study of the Effect of Coverage on the Hybridization Efficiency of Surface-Bound DNA Nanostructures. *Nano Lett.* **2008,** *8*, 4134-4139.

180. Castronovo, M.; Radovic, S.; Grunwald, C.; Casalis, L.; Morgante, M.; Scoles, G., Control of Steric Hindrance on Restriction Enzyme Reactions with Surface-Bound DNA Nanostructures. *Nano Lett.* **2008,** *8*, 4140-4145.

181. Bano, F.; Fruk, L.; Sanavio, B.; Glettenberg, M.; Casalls, L.; Niemeyer, C. M.; Scoles, G., Toward Multiprotein Nanoarrays Using Nanografting and DNA Directed Immobilization of Proteins. *Nano Lett.* **2009,** *9*, 2614-2618.

182. Josephs, E. A.; Ye, T., Nanoscale Positioning of Individual DNA Molecules by an Atomic Force Microscope. *J. Am. Chem. Soc.* **2010,** *132*, 10236-10238.

183. Kopf, I.; Grunwald, C.; Bruendermann, E.; Casalis, L.; Scoles, G.; Havenith, M., Detection of Hybridization on Nanografted Oligonucleotides Using Scanning Near-Field Infrared Microscopy. *J. Phys. Chem. C 114*, 1306-1311.

184. Josephs, E. A.; Ye, T., Nanoscale Positioning of Individual DNA Molecules by an Atomic Force Microscope. *J. Am. Chem. Soc.* **2010,** *132*, 10236-10238.

185. Lee, M. V.; Nelson, K. A.; Hutchins, L.; Becerril, H. A.; Cosby, S. T.; Blood, J. C.; Wheeler, D. R.; Davis, R. C.; Woolley, A. T.; Harb, J. N.; Linford, M. R., Nanografting of Silanes on Silicon Dioxide with Applications to DNA Localization and Copper Electroless Deposition. *Chem. Mater.* **2007,** *19*, 5052-5054.

186. Despont, M.; Drechsler, U.; Durig, U.; Haberle, W.; Lutwyche, M. I.; Rothuizen, H. E.; Stutz, R.; Widmer, R.; Binnig, G., The "Millipede" - More than one thousand tips for future AFM data storage. *IBM Journal of Research and Development* **2000,** *44*, 323-340.

187. Salaita, K.; Wang, Y.; Fragala, J.; Vega, R. A.; Liu, C.; Mirkin, C. A., Massively Parallel Dip-Pen Nanolithography with 55000-Pen Two-Dimensional Arrays. *Angew. Chem. Int. Ed.* **2007,** *45*, 7220-7223.

188. Schreiber, F., Structure and growth of self-assembling monolayers. *Prog. Surf. Sci.* **2000,** *65*, 151-256.

189. Sagiv, J., Organized Monolayers by Adsorption. 1. Formation and Structure of Oleophobic Mixed Monolayers on Solid Surfaces *J. Am. Chem. Soc.* **1980,** *102*, 92-98.

190. Wen, K.; Maoz, R.; Cohen, H.; Sagiv, J.; Gibaud, A.; Desert, A.; Ocko, B. M., Postassembly chemical modification of a highly ordered organosilane multilayer: New insights into the structure, bonding, and dynamics of self-assembling silane monolayers. *ACS Nano* **2008,** *2*, 579-599.

191. Brandow, S. L.; Chen, M.-S.; Aggarwal, R.; Dulcey, C. S.; Calvert, J. M.; Dressick, W. J., Fabrication of Patterned Amine Reactivity Templates Using 4-Chloromethylphenylsiloxane Self-Assembled Monolayer Films. *Langmuir* **1999,** *15*, 5429-5432.

192. Kim, S.-J.; Ryu, K.; Chang, S. W., Solution-processed organic field-effect transistors patterned by self-assembled monolayers of octadecyltrichlorosilane and phenyltrichlorosilane. *J. Mater. Sci.* **2010,** *45*, 566-569.

193. Dulcey, C. S.; Georger, J. H.; Krauthamer, V.; Stenger, D. A.; Fare, T. L.; Calvert, J. M., Deep UV Photochemistry of Chemisorbed Monolayers - Patterned Coplanar Molecular Assemblies *Science* **1991,** *252*, 551-554.

194. Chen, M.-S.; Dulcey, C. S.; Chrisey, L. A.; Dressick, W. J., Deep-UV Photochemistry and Patterning of (Aminoethylaminomethyl)phenethylsiloxane Self-Assembled Monolayers. *Adv. Funct. Mater.* **2006,** *16*, 774-783.

195. Sun, S. Q.; Montague, M.; Critchley, K.; Chen, M. S.; Dressick, W. J.; Evans, S. D.; Leggett, G. J., Fabrication of biological nanostructures by scanning near-field photolithography of chloromethylphenyisiloxane monolayers. *Nano Lett.* **2006,** *6*, 29-33.

196. Brandow, S. L.; Schull, T. L.; Martin, B. D.; Guerin, D. C.; Dressick, W. J., Use of low-temperature thermal alkylation to eliminate ink migration in microcontact printed patterns. *Chem.-Eur. J.* **2002,** *8*, 5363-5367.

197. Perkins, F. K.; Dobisz, E. A.; Brandow, S. L.; Calvert, J. M.; Kosakowski, J. E.; Marrian, C. R. K., Fabrication of 15 nm wide trenches in Si by vacuum scanning tunneling microscope lithography of an organosilane self-assembled film and reactive ion etching *Appl. Phys. Lett.* **1996,** *68*, 550-552.

198. Marrian, C. R. K.; Perkins, F. K.; Brandow, S. L.; Koloski, T. S.; Dobisz, E. A.; Calvert, J. M., Low voltage electron beam lithography in selfassembled ultrathin films with the scanning tunneling microscope. *Appl. Phys. Lett.* **1994,** *64*, 390-392.

199. Dressick, W. J.; Dulcey, C. S.; Brandow, S. L.; Witschi, H.; Neeley, P. F., Proximity x-ray lithography of siloxane and polymer films containing benzyl chloride functional groups. *J. Vac. Sci. technol. A* **1999,** *17*, 1432-1440.

200. Koloski, T. S.; Dulcey, C. S.; Haralson, Q. J.; Calvert, J. M., Nucleophilic Displacement Reactions at Benzyl Halide Self-Assembled Monolayer Film Surfaces. *Langmuir* **1994,** *10*, 3122-3133.

201. Mineo, P.; Motta, A.; Lupo, F.; Renna, L.; Gulino, A., Si(111) Surface Engineered with Ordered Nanostructures by an Atom Transfer Radical Polymerization. *J. Phys. Chem.C* **2011,** *115*, 12293-12298.

202. Kimmerlin, T.; Seebach, D., '100 years of peptide synthesis': ligation methods for peptide and protein synthesis with applications to beta-peptide assemblies. *J. Pept. Res.* **2005,** *65*, 229-260.

203. Lu, C. H.; Zhou, W. H.; Han, B.; Yang, H. H.; Chen, X.; Wang, X. R., Surface-imprinted core-shell nanoparticles for sorbent assays. *Anal. Chem.* **2007,** *79*, 5457-5461.

204. Facchetti, A.; van der Boom, M. E.; Abbotto, A.; Beverina, L.; Marks, T. J.; Pagani, G. A., Design and preparation of zwitterionic organic thin films: self-assembled siloxane-based, thiophene-spaced N-benzylpyridinium dicyanomethanides as nonlinear optical materials. *Langmuir* **2001,** *17*, 5939-5942.

205. Gu, J. H.; Yam, C. M.; Li, S.; Cai, C. Z., Nanometric protein arrays on protein-resistant monolayers on silicon surfaces. *J. Am. Chem. Soc.* **2004,** *126*, 8098-8099.

206. Lee, M. V.; Nelson, K. A.; Hutchins, L.; Becerril, H. A.; Cosby, S. T.; Blood, J. C.; Wheeler, D. R.; Davis, R. C.; Woolley, A. T.; Harb, J. N.; Linford, M. R., Nanografting of silanes on silicon dioxide with applications to DNA localization and copper electroless deposition. *Chem. Mat.* **2007,** *19*, 5052-5054.

207. Jung, H.; Kulkarni, R.; Collier, C. P., Dip-pen nanolithography of reactive alkoxysilanes on glass. *J. Am. Chem. Soc.* **2003,** *125*, 12096-12097.

208. Maoz, R.; Frydman, E.; Cohen, S. R.; Sagiv, J., "Constructive nanolithography": Inert monolayers as patternable templates for in-situ nanofabrication of metal-semiconductor-organic surface structures - A generic approach. *Adv. Mater.* **2000,** *12*, 725.

209. Wei, X., Recent Developments in the Fabrication of Ordered Nanostructure Arrays Based on Nanosphere Lithography. *Recent Patents on Nanotechnology* **2010,** *4*, 194-204.

210. Li, J. R.; Henry, G. C.; Garno, J. C., Fabrication of nanopatterned films of bovine serum albumin and staphylococcal protein A using latex particle lithography. *Analyst* **2006,** *131*, 244-250.

211. Winzer, M.; Kleiber, M.; Dix, N.; Wiesendanger, R., Fabrication of nano-dot- and nano-ring-arrays by nanosphere lithography. *Appl. Phys. A-Mater. Sci. Process.* **1996,** *63*, 617-619.

212. Jiang, P.; Hwang, K. S.; Mittleman, D. M.; Bertone, J. F.; Colvin, V. L., Template-directed preparation of macroporous polymers with oriented and crystalline arrays of voids. *J. Am. Chem. Soc.* **1999,** *121*, 11630-11637.

213. Kuo, C. W.; Shiu, J. Y.; Chen, P. L.; Somorjai, G. A., Fabrication of size-tunable large-area periodic silicon nanopillar arrays with sub-10-nm resolution. *J. Phys. Chem. B* **2003,** *107*, 9950-9953.

214. Holland, B. T.; Blanford, C. F.; Do, T.; Stein, A., Synthesis of highly ordered, three-dimensional, macroporous structures of amorphous or crystalline inorganic oxides, phosphates, and hybrid composites. *Chem. Mat.* **1999,** *11*, 795-805.

215. McLellan, J. M.; Geissler, M.; Xia, Y., Self-assembly of hexadecanethiol molecules on gold from the vapour phase as directed by a two-dimensional array of silica beads. *Chem. Phys. Lett.* **2005,** *408*, 80-83.

216. McLellan, J. M.; Geissler, M.; Xia, Y. N., Edge Spreading Lithography and Its Application to the Fabrication of Mesoscopic Gold and Silver Rings. *J. Am. Chem. Soc.* **2004,** *126*, 10830-10831.

217. Geissler, M.; McLellan, J. M.; Chen, J.; Xia, Y. N., Side-by-Side Patterning of Multiple Alkanethiolate Monolayers on Gold by Edge-Spreading Lithography. *Angew. Chem. int. Ed.* **2005,** *44*, 3596-3600.

218. Geissler, M.; McLellan, J. M.; Xia, Y. N., Edge-Spreading Lithography: Use of Patterned Photoresist Structures to Direct the Spreading of Alkanethiols on Gold. *Nano Lett.* **2005,** *5*, 31-36.

219. Li, J. R.; Garno, J. C., Elucidating the role of surface hydrolysis in preparing organosilane nanostructures via particle lithography. *Nano Lett.* **2008,** *8*, 1916-1922.

220. Li, J.-R.; Lusker, K. L.; Yu, J. J.; Garno, J. C., Engineering the spatial selectivity of surfaces at the nanoscale by patterning organosilane self-assembled monolayers via particle lithography. *ACS Nano* **2009,** *3*, 2023-2035.

221. Lusker, K. L.; Yu, J.-J.; Garno, J. C., Particle Lithography with vapor deposition of organosilanes: A molecular toolkit for studying confined surface reactions in nanoscale liquid volumes. *Thin Solid Films* **2011,** *7*, 5223-5229.

222. Saner, C. K.; Lusker, K. L.; LeJeune, Z. M.; Serem, W. K.; Garno, J. C., Self-assembly of octadecyltrichlorosilane: Surface structures formed using different protocols of particle lithography. *Beilstein J. Nanotechnol.* **2012,** *3*, 114-122.

223. Nečas, D.; Klapetek, P., Gwyddion: an open-source software for SPM data analysis (http://gwyddion.net/). *Cent. Eur. J. Phys.* **2012,** *10*, 181-188.

224. Liu, G. Y.; Xu, S.; Qian, Y. L., Nanofabrication of self-assembled monolayers using scanning probe lithography. *Acc. Chem. Res.* **2000,** *33*, 457-466.

225. Rozlosnik, N.; Gerstenberg, M. C.; Larsen, N. B., Effect of Solvents and Concentration on the Formation of a Self-Assembled Monolayer of Octadecylsiloxane on Silicon (001). *Langmuir* **2003,** *19*, 1182-1188.

226. Vallant, T.; Brunner, H.; Mayer, U.; Hoffmann, H.; Leitner, T.; Resch, R.; Friedbacher, G., Formation of Self-Assembled Octadecylsiloxane Monolayers on Mica and Silicon Surfaces Studied by Atomic Force Microscopy and Infrared Spectroscopy. *J. Phys. Chem. B* **1998,** *102*, 7190-7197.

227. Jeon, N. L. F., K.; Branshaw, K.; Nuzzo, R. G. Langmuir 1997, 13(13), 3382–3391., Structure and Stability of Patterned Self-Assembled Films of Octadecyltrichlorosilane Formed by Contact Printing. *Langmuir* **1997,** *13*, 3382-3391.

228. Brandow, S. L.; Chen, M.-S.; Dulcey, C., S.; Dressick, W. J., Formation of Aromatic Siloxane Self-Assembled Monolayers. *Langmuir* **2008,** *24*, 3888-3896.

229. Wen, K.; Maoz, R.; Cohen, H.; Sagiv, J.; Gibaud, A.; Desert, A.; Ocko, B. M., Postassembly chemical modification of a highly ordered organosilane multilayer: New insights into the structure, bonding, and dynamics of self-assembling silane monolayers *ACS Nano* **2008,** *2*, 579-599.

230. Chinwangso, P.; Jamison, A. C.; Lee, T. R., Multidentate Adsorbates for Self-Assembled Monolayer Films. *Acc. Chem. Res.* **2011,** *44*, 511-519.

231. Carbonell, L.; Whelan, C. M.; Kinsella, M.; Maex, K., A thermal stability study of alkane and aromatic thiolate self-assembled monolayers on copper surfaces. *Superlattices Microstruct.* **2004,** *36*, 149-160.

232. Ebbens, S.; Hutt, D.; Liu, C., The Thermal Stability of Alkanethiol Self-Assembled Monolayers on Copper for Fluxless Soldering Applications. *IEEE Trans. Compon. Packag. Technol.* **2010,** *33*, 251-259.

233. Hakamada, M.; Takahashi, M.; Furukawa, T.; Tajima, K.; Yoshimura, K.; Chino, Y.; Mabuchi, M., Electrochemical stability of self-assembled monolayers on nanoporous Au. *Phys. Chem. Chem. Phys.* **2011,** *13*, 12277-12284.

234. Ito, E.; Kang, H.; Lee, D.; Park, J. B.; Hara, M.; Noh, J., Spontaneous desorption and phase transitions of self-assembled alkanethiol and alicyclic thiol monolayers chemisorbed on Au(1 1 1) in ultrahigh vacuum at room temperature. *J. Colloid Interface Sci.* **2013,** *394*, 522-529.

235. Li, J.; Ang, X. F.; Lee, K. H.; Romanato, F.; Wong, C. C., In-Situ Monitoring of the Thermal Desorption of Alkanethiols with Surface Plasmon Resonance Spectroscopy (SPRS). *J. Nanosci. Nanotechnol.* **2010,** *10*, 4624-4628.

236. Ramin, L.; Jabbarzadeh, A., Odd-Even Effects on the Structure, Stability, and Phase Transition of Alkanethiol Self-Assembled Monolayers. *Langmuir* **2011,** *27*, 9748-9759.

237. Rodriguez, L. M.; Cristina, L. J.; Alarcon, L. S.; Blum, B.; Salvarezza, R. C.; Xi, L.; Lau, W. M.; Sanchez, E. A.; Gayone, J. E.; Grizzi, O., Adsorption and thermal stability of alkanethiol films on GaAs(110): A comparative study by TOF-DRS and TOF-SIMS. *Nucl. Instrum. Meth. B* **2011,** *269*, 924-931.

238. Srisombat, L.-o.; Zhang, S.; Lee, T. R., Thermal Stability of Mono-, Bis-, and Tris-Chelating Alkanethiol Films Assembled on Gold Nanoparticles and Evaporated "Flat" Gold. *Langmuir* **2010,** *26*, 41-46.

239. Stettner, J.; Winkler, A., Characterization of Alkanethiol Self-Assembled Monolayers on Gold by Thermal Desorption Spectroscopy. *Langmuir* **2010,** *26*, 9659-9665.

240. Subramanian, S.; Sampath, S., Enhanced thermal stability and structural ordering in short chain n-alkanethiol monolayers on gold probed by vibrational spectroscopy and EQCM. *Anal. Bioanal. Chem.* **2007,** *388*, 135-145.

241. Tam-Chang, S.-W.; Biebuyck, H. A.; Whitesides, G. M.; Jeon, N.; Nuzzo, R. G., Self-Assembled Monolayers on Gold Generated from Alkanethiols with the Structure $RNHCOCH_2SH$. *Langmuir* **1995,** *11*, 4371-4382.

242. Bain, C. D.; Troughton, E. B.; Tao, Y. T.; Evall, J.; Whitesides, G. M.; Nuzzo, R. G., Formation of monolayer films by the spontaneous assembly of organic thiols from solution onto gold. *J. Am. Chem. Soc.* **1989,** *111*, 321-335.

243. Porter, M. D.; Bright, T. B.; Allara, D. L.; Chidsey, C. E. D., Spontaneously organized molecular assemblies. 4. Structural characterization of normal-alkyl thiol monolayers on gold by optical ellipsometry, infrared-spectroscopy, and electrochemistry. *J. Am. Chem. Soc.* **1987,** *109*, 3559-3568.

244. Poirier, G. E.; Tarlov, M. J.; Rushmeier, H. E., Two-Dimensional Liquid Phase and the px.sqroot.3 Phase of Alkanethiol Self-Assembled Monolayers on Au(111). *Langmuir* **1994,** *10*, 3383-3386.

245. Zhang, S. S.; Leem, G.; Srisombat, L. O.; Lee, T. R., Rationally designed ligands that inhibit the aggregation of large gold nanoparticles in solution. *J. Am. Chem. Soc.* **2008,** *130*, 113-120.

246. Srisombat, L.; Jamison, A. C.; Lee, T. R., Stability: A key issue for self-assembled monolayers on gold as thin-film coatings and nanoparticle protectants. *Colloids Surf. A* **2011,** *390*, 1-19.

247. Srisombat, L. O.; Park, J. S.; Zhang, S.; Lee, T. R., Preparation, characterization, and chemical stability of gold nanoparticles coated with mono-, bis-, and tris-chelating alkanethiols. *Langmuir* **2008,** *24*, 7750-7754.

248. Park, J. S.; Vo, A. N.; Barriet, D.; Shon, Y. S.; Lee, T. R., Systematic control of the packing density of self-assembled monolayers using bidentate and tridentate chelating alkanethiols. *Langmuir* **2005,** *21*, 2902-2911.

249. Park, J. S.; Smith, A. C.; Lee, T. R., Loosely packed self-assembled monolayers on gold generated from 2-alkyl-2-methylpropane-1,3-dithiols. *Langmuir* **2004,** *20*, 5829-5836.

250. Wagner, P.; Hegner, M.; Guntherodt, H.-J.; Semenza, G., Formation and in Situ Modification of Monolayers Chemisorbed on Ultraflat Template-Stripped Gold Surfaces. *Langmuir* **1995,** *11*, 3867-3875.

251. Necas, D.; Klapetek, P., Gwyddion: an open-source software for SPM data analysis. *Cent. Eur. J. Phys.* **2012,** *10*, 181-188.

252. Lyles, V. D.; Serem, W. K.; Garno, J. C., Surface characterization using atomic force microscopy in liquid environments. In *Surface Analytical Techniques*, Bracco, G.; Holst, B., Eds. Springer, in press: 2013.

253. Hansma, P. K.; Cleveland, J. P.; Radmacher, M.; Walters, D. A.; Hillner, P. E.; Bezanilla, M.; Fritz, M.; Vie, D.; Hansma, H. G.; Prater, C. B.; Massie, J.; Fukunaga, L.; Gurley, J.; Elings, V., Tapping Mode Atomic-Force Microscopy In Liquids. *Appl. Phys. Lett.* **1994,** *64*, 1738-1740.

254. Xu, S.; Cruchon-Dupeyrat, S.; Garno, J. C.; Jennings, G. K.; Yong, T.-H.; Laibinis, P. E.; Liu, G.-Y., In-situ Studies of Thiol Self -Assembly on Gold from Solution using Atomic Force Microscopy. *J. Chem. Phys.* **1998,** *108*, 5002-5012.

255. Liu, G.-Y.; Xu, S.; Qian, Y., Nanofabrication of Self-Assembled Monolayers Using Scanning Probe Lithography. *Acc. Chem. Res.* **1998,** *33*, 457-466.

256. Yang, G.; Garno, J. C.; Liu, G.-Y. i. E. B. V., Amsterdam, Scanning Probe-Based Lithography for Production of Biological and Organic Nanostructures on Surfaces. In *Comprehensive Nanoscience and Technology*, Andrews, D.; Scholes, G.; Wiederrecht, G., Eds. Elsevier, B. V.: Amsterdam, 2010.

257. Brower, T. L.; Garno, J. C.; Ulman, A.; Liu, G.-Y.; Yan, C.; Golzhauser, A.; Grunze, M., Self-Assembled Multilayers of 4,4'-Dimercaptobiphenyl Formed by Cu(II) Oxidation. *Langmuir* **2002,** *18*, 6207-6216.

258. Kelley, A. T.; Ngunjiri, J. N.; Serem, W. K.; Yu, J.-J.; Lawrence, S.; Crowe, S.; Garno, J. C., Applying AFM-based nanofabrication for measuring the thickness of nanopatterns: The role of headgroups in the vertical self-assembly of ω-functionalized *n*-alkanethiols. *Langmuir* **2010,** *26*, 3040-3049.

APPENDIX A. CLEANING PROCEDURE TO GOLD SUBSTRATES

Cleaning procedure for FTIR studies

1. Rinse the gold surfaces with deionized water.

2. Place the gold substrates into the UV-ozone generator for 30 min.

Preparing Template-Stripped Ultraflat Gold from Recycled Substrates

1. Rinse the gold substrates (on Mica) and glass slides with deionized water.

2. Place the gold substrates and circular (1 cm) glass cover slides into the UV-ozone generator for 30 min.

3. Mix Epoxy (EPO-TEK, Billerica, MA) kit part A and B (1:1) in a small weigh boat using a metal spatula.

4. Add 1-2 μL mixed Epoxy to each glass slide.

5. Place the glass slide onto the gold substrate so that the epoxy spreads out between the gold layer and glass slide without any air bubbles. The amount of glue should barely fill the space between the glass and gold, without spilling of between the edges.

6. Heat samples in oven at 150 °C for 2 h to anneal the epoxy.

7. Remove the samples and cool to room temperature. Samples can be stored for 6 months before using, provided that the mica is not stripped.

8. To prepare SAMs, carefully peel the mica and glass pieces apart using tweezers and immediately submerge the surface in SAM solutions.

APPENDIX B: LETTER OF PERMISSION

Tian Tian <ttian2@tigers.lsu.edu>

RE: TN116926 FW: Permission request to Springer's book chapter

1 message

Permissions Europe/NL <Permissions.Dordrecht@springer.com> Tue, Feb 12, 2013 at 6:53 AM

To: "ttian2@tigers.lsu.edu" <ttian2@tigers.lsu.edu>

Dear Sir/Madam,

Thank you for your request.

With reference to your request to reprint material in which Springer Science and Business Media control the copyright, our permission is granted free of charge and at the following conditions:

Springer material

- represents original material which does not carry references to other sources (if material in question refers with a credit to another source, authorization from that source is required as well);
- requires full credit [Springer and the original publisher/journal title, volume, year of publication, page, chapter/article title, name(s) of author(s), figure number(s), original copyright notice] to the publication in which the material was originally published, by adding; with kind permission from Springer Science+Business Media B.V.;
- may not be altered in any manner. Abbreviations, additions, deletions and/or any other alterations shall be made only with prior written authorization of the author and/or Springer Science + Business Media.
- may not be republished in Electronic Open Access.

This permission

a. is non-exclusive.

https://mail.google.com/mail/u/0/?ui=2&ik=424f04136f&view=pt&search=... 2/18/2013

b. includes use in an electronic form: provided it's password protected, or on intranet or university's repository, including UMI (according to the definition at the Sherpa website: http://www.sherpa.ac.uk/romeo/), or CD-Rom/E-book,
c. is subject to a courtesy information to the author (address is given with the article/chapter).
d. is personal to you and may not be sublicensed, assigned, or transferred by you to any other person without Springer's written permission.
e. is valid only when the conditions noted above are met.

Permission free of charge on this occasion does not prejudice any rights we might have to charge for reproduction of our copyrighted material in the future.

Kind regards,

Maaike Duine

From: Tian Tian [mailto:ttian2@tigers.lsu.edu]
Sent: Tuesday, February 05, 2013 9:11 PM
To: Onlineservice, SCSC
Subject: Permission request to Springer's book chapter

Dear Sir/Madam,

I would like to ask for a letter of permission to reprint from Springer "Tip-based Nanofabrication: Fundamentals and Applications" on the chapter I have written with authors Zorabel M. LeJeune, Wilson K. Serem, Jing-Jiang Yu, and Jayne C. Garno, The chapter is entitled "Nanografting: A Method for Bottom-up Fabrication of Designed Nanostructures". (http://link.springer.com/chapter/10.1007/978-1-4419-9899-6_5) I would like to include the chapter on my dissertation to be submitted to Louisiana State University.

Thank you for your time.

Best regards,

Tian Tian

PhD. Candidate

APPENDIX C: SUPPLEMENTAL INFORMATION FOR CHAPTER 5

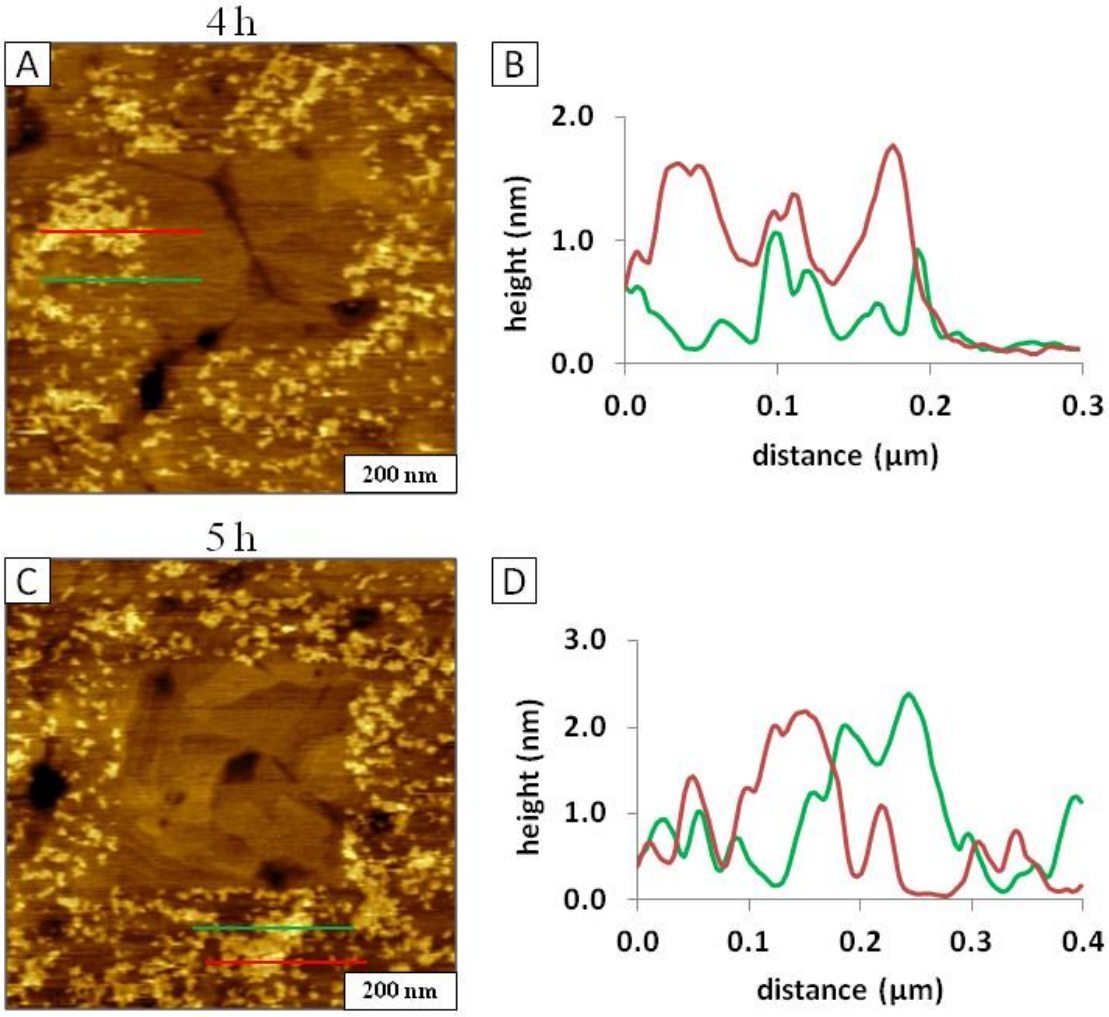

Supplemental Figure 1 Later timepoints during solution self-assembly of TMMH for areas of gold with nanoshaved reference sites. Contact mode AFM topographs acquired after [A] 4 h; and [B] 5 h of immersion in a 0.01 mM solution of TMMH in ethanol.

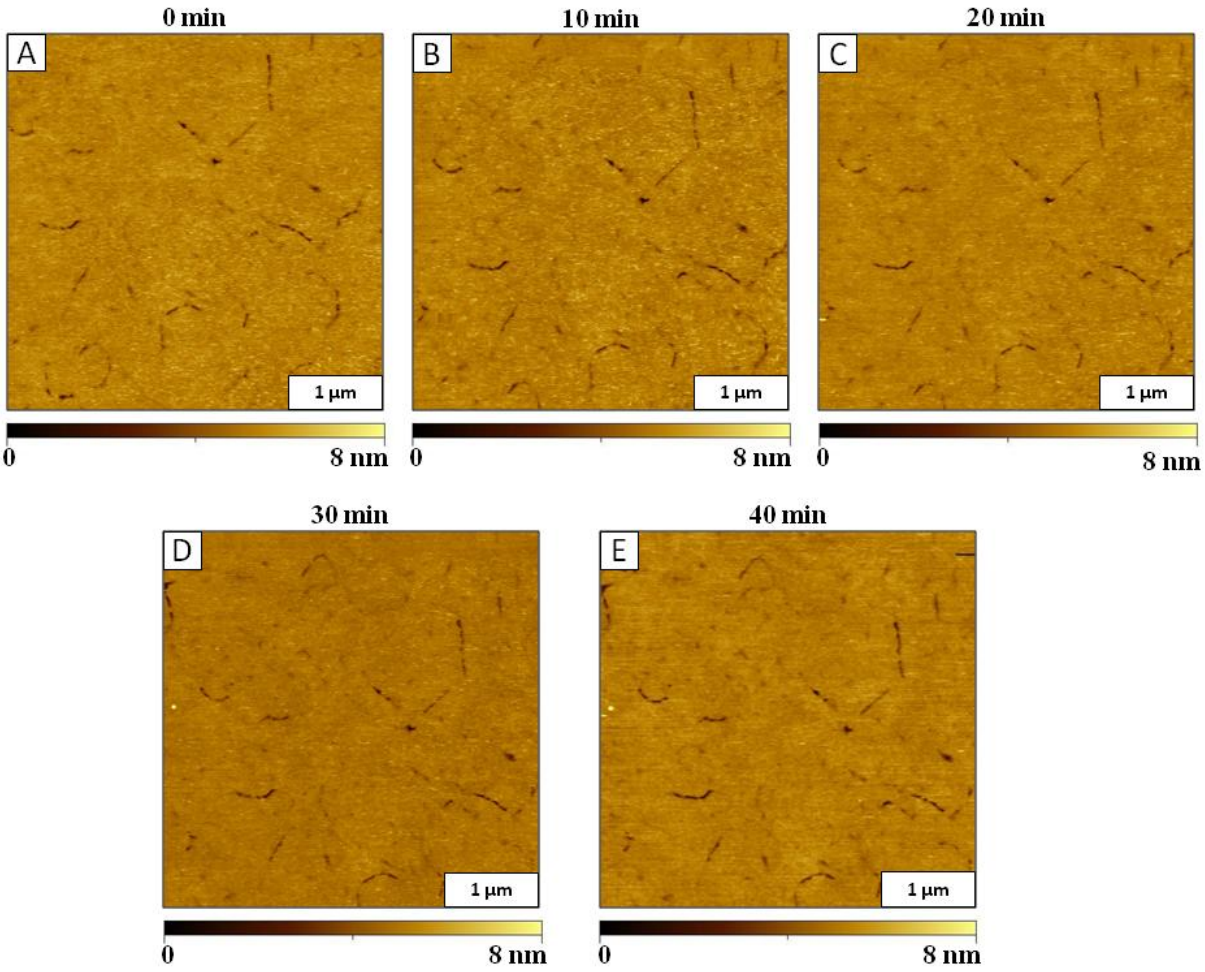

Supplemental Figure 2 Early snapshots of the gold surface after introducing TMMH solution. (0.01 mM TMMH in ethanol) [A] Topography at 0 min [B] 10 min; [C] 20 min; [D] 30 min; [E] 40 min of exposure to TMMH solution.

Vita

Tian Tian was born in Beijing, China to Youlong Qi and Mei Wang. She received her Bachelor of Science degree in Pharmacy from Peking University and Master of Science in Integrated Science and Technology from Southeastern Louisiana University. In fall 2009, she joined Louisiana State University and started her Doctoral Program in Analytical Chemistry under the guidance of Dr. Jayne Garno.

Tian has participated in regional, national and international conferences presenting her research in oral and poster presentations. During her graduate years, she received Outstanding Teaching Award in Analytical Chemistry and Coates Travel Award.